UNITED STATES DEPARTMENT OF COMMERCE
JESSE H. JONES, Secretary
NATIONAL BUREAU OF STANDARDS
Lyman J. Briggs, Director

✦

Journal of Research

of the

National Bureau of Standards

✦

Volume 28, Number 5

May 1942

[Published with approval of the Director of the Budget]

UNITED STATES
GOVERNMENT PRINTING OFFICE
WASHINGTON : 1942

For sale by the Superintendent of Documents, Washington, D. C. - - - - - - Price 30 cents
$3.50 per year on subscription

The prices of the separate Research Papers appearing in this JOURNAL are given on the front cover page. If 100 or more copies of any separate are ordered, a discount of 25 percent is allowed. Those who desire copies of separate Research Papers should send their orders and remittances without delay to the Superintendent of Documents, U. S. Government Printing Office, Washington, D. C. This will aid him to determine the number of copies to be printed for sale. Research Papers are not printed from electrotypes, and usually no more reprints can be had when the first and only printing is exhausted.

MATHEMATICAL TABLES

A list of the mathematical tables now obtainable from the National Bureau of Standards is printed on page 3 of the Journal cover. New tables will be announced from time to time as they become available.

U. S. DEPARTMENT OF COMMERCE NATIONAL BUREAU OF STANDARDS

RESEARCH PAPER RP1468

Part of Journal of Research of the National Bureau of Standards, Volume 28, May 1942

ELIMINATION OF OXIDE FILMS ON FERROUS MATERIALS BY HEATING IN VACUUM

By Vernon C. F. Holm

ABSTRACT

An investigation of the mechanism by which lightly oxidized specimens of ferrous materials were brightened when heated in vacuum showed that the presence of carbon was essential. Oxidized specimens of iron containing small amounts of carbon were brightened in 15 to 20 minutes at 800° C, and the elimination of the oxide film was accompanied by decreases in the carbon content. Clean-up of oxide films on stainless steel occurred also when the specimens were heated to about 1,050° C. Oxidized high-purity iron which contained less than 0.001 percent of carbon could not be brightened by vacuum heating at temperatures up to 1,250° C. Vacuum heating of lightly oxidized specimens of high-purity iron sometimes caused the oxide film to agglomerate, forming distinct, geometric patterns that could be observed under the microscope.

CONTENTS

	Page
I. Introduction	569
II. Materials and method	570
III. Possible explanations for the elimination of oxide films	572
1. Dissociation of oxides	572
2. Volatilization of oxides	573
3. Absorption of oxide films	574
4. The role of carbon	575
IV. Structures of oxide films on high-purity iron	578
V. Summary	579
VI. References	579

I. INTRODUCTION

In the manufacture of certain metal products where shaping is accomplished by cold-forming operations, it is often necessary to relieve the stresses by annealing. In some processes the products may be heated at specified temperatures for developing desirable physical properties, as in aging and hardening treatments. However, most metals when heated in air form oxide films or scale that are often unsightly and may interfere with subsequent manufacturing operations. In many instances the final product must have a bright surface finish. In such cases it is a decided advantage if surface oxidation can be avoided and costly pickling and polishing operations eliminated. On the other hand, the heat treatment of metals without surface oxidation is not always a simple matter, as it involves both the selection and the careful maintenance of suitable atmospheres in which

the concentrations of oxygen are held below the required limits. The amount of oxygen that can be tolerated varies greatly with different metals and even for plain carbon steels the atmospheres are sometimes adjusted to compensate for differences in carbon content. Since oxidation may occur through the action of gaseous oxides, as well as elemental oxygen, the partial pressures of water vapor, carbon dioxide, and even carbon monoxide, require close control. The harmful action of water vapor was particularly emphasized in a recent paper by Gillett and Gonser [1].[1]

In the bright annealing of stainless steels, extreme precautions are necessary and the partial pressure of oxygen must be kept at a very low value. This has been accomplished, in some cases, by the use of atmospheres formed by cracking anhydrous ammonia. Such atmospheres obviously have a high percentage of hydrogen and would tend to cause decarburization at the temperatures necessary for annealing. However, recent work [2] on the effect of hydrogen in iron and steel has demonstrated that heating a metal in the gas may have other harmful effects. The use of some chemically inert gas would be the ideal solution of the problem except that the removal of the last traces of oxygen presents difficulties. Utilization of vacuum furnaces as a means of obtaining inert environments for annealing has been suggested, but for practical reasons these appear applicable only in relatively few instances. However, because vacuum heating[2] offers a means of investigating the changes that occur during bright annealing without the effect of the usual gas-metal equilibria, it was felt that such a study might provide some pertinent information regarding the behavior of metals in inert atmospheres at high temperatures.

Some preliminary experiments on vacuum bright annealing were reported in an earlier paper [3]. It was shown that bright specimens of stainless steels became tarnished when heated in vacuum at 800° C, whereas specimens of plain steels remained bright. In the temperature range 950° to 1,250° C, stainless steels could be heated without tarnishing. Further, it was shown that tarnished specimens of plain carbon steels were brightened by heating at 800° C, whereas tarnished stainless steels generally were brightened only at temperatures above 1,000° C. In the subsequent discussion of the paper several possible explanations for the brightening were suggested, as follows:

1. The oxide dissociates into metal and oxygen.
2. The oxide volatilizes.
3. The oxide is absorbed or dissolved in the body of the metal.
4. The oxide combines with the carbon of the metal and is eliminated as carbon monoxide.

The earlier experiments have been extended to ascertain which of these suggested mechanisms was responsible for the elimination of the oxide films.

II. MATERIALS AND METHOD

In the present work a study was made of changes in weight of specimens during oxidation and in subsequent vacuum heating. In some instances the changes in weight were correlated with changes in oxygen content as determined by vacuum fusion. Carbon determinations were made on some of the specimens to indicate the possible

[1] Figures in brackets indicate the literature references at the end of this paper.
[2] The term "vacuum heating" refers to the heating of a specimen or specimens in vacuum.

role of this element. It was desirable to use specimens of large surface area and at the same time not to exceed certain space limitations, both in the vacuum-heating furnace and in the vacuum-fusion apparatus. This was accomplished by the use of thin strip specimens in the form of coils. It was necessary, in many instances, to subject the coiled specimens to several cycles, each consisting in oxidation in air at a suitable temperature followed by heating in vacuum. In the subsequent discussion these cycles are referred to as "oxidation and vacuum-heating cycles." The materials that were used are listed in table 1.

TABLE 1.—*Materials used in studying the effect of vacuum heating on oxidized specimens*

Specimen	Material	Thickness	Oxygen	Carbon	Remarks
		mm	*Percent*	*Percent*	
1	High-purity iron [1]	0.06	0.006	0.001	
2	High-purity iron [1]	.10	.003	.001	
3	Electrolytic iron	.15	.002	.013	Cathode iron melted in Arsem furnace, forged, and cold-rolled to 0.15 mm.
4	Electrolytic iron	.15	.002	.039	Cathode iron melted in Arsem furnace with small carbon additions, forged, and cold-rolled to 0.15 mm.
5	Open-hearth iron	.09	.10	.02	Total impurities about 0.3%.
6	Stainless steel	.22	.014	.07	18.5% Cr; 8.2% Ni.

[1] Prepared by Thompson and Cleaves [4]; total impurities, about 0.01 percent.

Specimens 2 to 2.5 cm wide and 15 to 20 cm long were cut from cold-rolled strip material and were cleaned by swabbing with ether, then rinsing consecutively with carbon tetrachloride, alcohol, and ether. They were dried in an oven at about 60° C for a few minutes and were cooled in a desiccator. Before weighing, the strips were loosely coiled on a clean $\frac{3}{16}$-in. steel rod, so that the diameter of the entire coil did not exceed 1 cm. During oxidation the specimens were suspended in a vertical silica tube heated in a resistance furnace. Since the ends of the tube were not tightly closed, an ample supply of air was available for oxidation. Temperatures of about 400° C were used for the irons and about 800° C for the stainless steel. The progress of oxidation was determined by periodic inspections, and the specimens were removed from the furnace when a blue temper color had developed. Oxidation was usually completed in from 5 to 15 minutes under these conditions, but occasionally more time was required for the stainless steel. The oxidized specimens were cooled in a desiccator before weighing.

The vacuum heating was performed in the vacuum furnace previously described [3]. This consisted of a vacuum-tight silica tube mounted vertically within a high-frequency induction coil. Low pressures were obtained by means of a mercury diffusion pump used in conjunction with a rotary oil pump. The coiled specimen was held in a suspended iron thimble that was heated by induction and maintained at the desired temperature for 15 to 20 minutes. After cooling in the vacuum furnace, the specimen was reweighed. Sometimes when a specimen was treated through several oxidation and vacuum-heating cycles, a sample coupon was clipped from the outer coil at each stage so that the progressive changes in the appearance of the specimen could be observed with greater ease. Some of the

coils were opened after oxidation or after vacuum heating to ascertain the uniformity of the treatment. In no case was any significant difference observed in different portions of the coil.

III. POSSIBLE EXPLANATIONS FOR THE ELIMINATION OF OXIDE FILMS

1. DISSOCIATION OF OXIDES

Although dissociation of the oxide under these conditions of low pressure and high temperature appears, at first glance, to offer the simplest explanation for the elimination of the oxide film on an oxidized specimen, this mechanism is not in line with either theoretical considerations or observed facts. In the case of a more noble metal, like copper, the dissociation pressure of the oxide at temperatures comparable to those used is great enough so that an oxide film would decompose in a vacuum. However, according to Mellor [5] the dissociation pressure of FeO is of the order of 10^{-9} mm of mercury at 1,400° C and only 10^{-14} mm at 1,000° C. At present, no devices are known by which a vacuum of even 10^{-9} mm of mercury can be produced or measured. It is theoretically possible that vapors of metals whose oxides have lower dissociation pressures, for example chromium, might combine with oxygen and reduce the pressure sufficiently so that even iron oxide could dissociate. However, this would require ideal conditions, and in an apparatus that has not been especially conditioned for extremely low pressure work, it is not probable that the pressure would be reduced by this means below the limits obtainable with a mercury diffusion pump. In the present experiments, "clean-up" of films on iron specimens took place without the presence of any chromium in the furnace, which indicates that the mechanism of clean-up did not involve any function of this element.

Some experiments on specimens of the materials listed in table 1 illustrated the changes in weight that occurred during oxidation and subsequent vacuum heating. Oxidized specimens of electrolytic and open-hearth iron were vacuum-heated at 800° C, and the stainless steels were heated at 1,000° to 1,050° C, just as in the experiments described in the previous paper. These temperatures were found to permit satisfactory clean-up of the oxide films in 15 to 20 minutes. The high-purity irons were also vacuum-heated at 1,000 to 1,050° C; but in no case did the high-purity materials brighten completely with this treatment, although the blue temper color gave way to a gray metallic appearance. The error in the preliminary experiments of mistaking this for true brightening was indicated when microscopic inspection showed that the oxide had not been eliminated.

As a rule, the gain in weight during oxidation was about 0.0005 g for each specimen of iron. The losses in vacuum heating were slightly higher, averaging about 0.0008 g, except for the high-purity materials, which showed no appreciable decrease. Some of the specimens of stainless steel gained as much as 0.0015 g in oxidation and lost about twice this amount when heated in vacuum; other specimens behaved like the irons. These data are noteworthy in that they show that materials which were brightened during vacuum heating lost more weight in this treatment than had been gained in oxidation. Although the difference was not great, the results were consistent. If simple

dissociation could account for the elimination of the oxide film, the losses in weight should have been approximately equal to the gains during oxidation. The most important observation, however, was that the oxide film on high-purity iron could not, in any instance, be removed by vacuum heating. If dissociation of oxides could account for the clean-up of oxide films on ferrous specimens, the same effect should have been obtained on high-purity iron as on less pure ferrous materials during vacuum heating. However, the behavior of the high-purity iron was strikingly different. In view of these observations and by consideration of the extremely low dissociation pressure of iron oxide, it appears that the dissociation of oxides could not have been a significant factor in the brightening of oxidized specimens during vacuum heating.

2. VOLATILIZATION OF OXIDES

The possibility that volatilization of an oxide film may be responsible for its removal during vacuum heating was pointed out by Gonser [6] on the basis of experiments at the Battelle Memorial Institute. In his experiments, lightly oxidized strips of stainless steel were heated by the passage of a heavy electric current to a temperature estimated at 1,250° to 1,350° C in a vacuum produced by a mechanical pump. The hottest portions of the specimens were brightened during the heating, and the accompanying loss was stated to be three or more times the gain in weight during oxidation. As the oxide film disappeared from the specimen, a dark deposit appeared on the walls on the enclosing glass tube. In the light of these observations, Gonser made the logical assumption that the oxide film had been eliminated by volatilization.

In the present experiments on stainless steel, which were performed at somewhat lower temperatures, about 1,050° C, although a dark film on the inner walls of the furnace was sometimes observed, the losses in weight during vacuum heating were not great enough to account for the elimination of the oxide film in the form of a metallic oxide. Furthermore, in repeated experiments involving alternate oxidation and vacuum heating of the same specimen, a stage was reached when the specimen would no longer brighten. If volatilization were the correct explanation for the removal of the oxide film on stainless steel, it should be possible to carry the process through numerous cycles and not be hindered, as was the case, by the apparent depletion of some element in the material. The black deposit on the furnace walls was probably formed from volatilized metal that subsequently may or may not have oxidized. In the present investigation, considerable deposition of condensed iron was observed on the inner walls of the furnace tube when specimens of high-purity iron were heated above 1,200° C.

Specimens of high-purity iron could not be brightened by heating at 1,250° C, under the same conditions which resulted in the brightening of stainless steels; and one specimen that was heated at 1,250° C for 20 minutes did not clean up, although it lost 2 percent of its weight through vaporization.

The inability of stainless steel specimens to clean up after a few cycles of oxidation and vacuum heating and the fact that in no case could specimens of high-purity iron be completely brightened, even

at 1,250° C, suggests that some other factor, and not volatilization, was responsible for the elimination of the oxide film on a ferrous specimen. It is not denied that some volatilization of oxide may have occurred, but the evidence obtained indicates that this cause alone was not adequate to account for complete brightening in any one of the specimens.

3. ABSORPTION OF OXIDE FILMS

Because iron can form a solid solution with oxygen, there is some reason for assuming that the observed brightening of oxidized specimens may have resulted, at least partially, from simple absorption of the surface oxides by the underlying metal. Rhines [7] stated that in bright annealing operations on certain copper alloys, internal oxidation may occur when sufficient oxygen is present in the atmosphere, even though the surface remains clear and bright. In a recent investigation by Rogers and Stamm [8] on the determination of the A_3 point in high-purity iron, it is reported that a small specimen that had been slightly oxidized while it was being sealed into an evacuated silica bulb regained its bright appearance after being held at temperatures near the A_3 point for about 4 hours. In this case the weight of oxygen involved amounted to about 0.003 percent, and the authors concluded that the clean-up was probably due to absorption of oxide in the metal.

The data in the literature on the solid solubility of oxygen in iron are rather scanty and somewhat inconsistent, and do not afford definite information concerning the solubility at various temperatures. However, experiments were carried out to show whether or not sufficient oxide could be absorbed to account for the brightening of oxidized specimens under the conditions of vacuum heating that have been considered here. The experiments already described have shown that oxidized specimens of high-purity iron could not be completely brightened by vacuum heating and that no significant loss in weight occurred. Furthermore, vacuum-fusion determinations of oxygen in specimens of high-purity iron that had been oxidized and vacuum-heated at 800°, 940°, and at 1,020° C definitely indicated that the oxygen acquired during oxidation was not lost during subsequent vacuum heating. It is evident that absorption of the oxide films in the underlying metal would not affect the weight or oxygen content of the specimen.

In order to investigate the possibility that, in spite of the incomplete brightening, some of the oxide may have dissolved in the iron, it was decided to make oxygen determinations on high-purity iron specimens that had been oxidized and vacuum-heated, and also to ascertain the amount of oxygen that remained after such specimens had been pickled for removal of the oxides on the surface. The difference in oxygen content of the pickled specimen and the original material would represent the amount of oxygen absorbed during vacuum heating.

In order to provide favorable conditions for solution of oxygen in high-purity iron, specimens were subjected to several cycles of oxidation at 400° and vacuum heating at 1,050° C. A specimen of high-purity iron No. 1 (table 1) was uncoiled and cut in halves after three cycles. One half was pickled for 1 minute in hydrochloric acid

containing a commercial inhibitor, preceding the vacuum-fusion determination. The unpickled portion was found to contain 0.120 percent of oxygen, whereas the value for the pickled portion, 0.010 percent, was only slightly greater than the oxygen content of the original material, 0.006 percent. A determination on a pickled specimen of high-purity iron No. 2 (table 1) after six cycles indicated an oxygen content of 0.003 percent, which was comparable to the value obtained on an untreated specimen of this sample. These results indicate that an insignificant amount of oxygen dissolved in the high-purity iron under conditions which brightened other ferrous materials.

Some additional vacuum-fusion determinations are of interest in this connection because they illustrate the differences in behavior of ordinary iron and high-purity iron during vacuum heating. The oxygen content of a specimen of electrolytic iron No. 3 (table 1) increased from 0.004 to 0.016 percent during light oxidation, and after vacuum heating, only 0.005 percent of oxygen remained. Likewise, the oxygen content of a specimen of electrolytic iron No. 4 (table 1) increased from 0.002 to 0.007 percent in a light oxidizing treatment, but after vacuum heating, the specimen contained only 0.003 percent. In both instances, complete brightening occurred during vacuum heating, practically all of the oxygen picked up in the oxidizing treatment was eliminated during vacuum heating, and the increase in oxygen content above the original value was negligible. According to these experiments the elimination of oxide films was not dependent upon the absorption of oxide by the underlying metal, and in the case of high-purity iron, the amount absorbed was far too minute to cause any significant brightening.

4. THE ROLE OF CARBON

The experiments up to this point have shown that the three suggested causes—dissociation, volatilization, and absorption of oxides—played an insignificant part in the elimination of oxide films on ferrous specimens during vacuum heating. It remained now to investigate the fourth suggested mechanism, the role of carbon in the vacuum brightening of oxidized specimens. In the previous paper [3] it was suggested that carbon might be involved in the reaction that caused brightening, but no direct experimental evidence to that effect was shown. In his discussion of the paper, Gonser reported that stainless steel which after vacuum heating for removal of oxide film was cooled slowly to facilitate precipitation of carbides contained fewer carbide particles than the original material. This was an indication that carbon had taken part in the elimination of the oxide films.

In the present experiments, specimens of three materials of known carbon contents were subjected to numerous cycles of oxidation and vacuum heating. The electrolytic irons were vacuum-heated, as usual, at 800° C, and the stainless steel at about 1,050° C. Each specimen consisted of a coiled strip weighing about 6 g. After treatment, the carbon contents were redetermined. The results are presented in table 2.

TABLE 2.—*Changes in carbon content of electrolytic iron and a stainless steel during oxidation and vacuum heating treatments*

[For the electrolytic iron each cycle consisted in oxidation at 400° C and vacuum heating at 800° C. Oxidation of the stainless steel was accomplished at about 800° C and vacuum heating at approximately 1,050° C.]

Material	Number of cycles	Original carbon content	Final carbon content
		Percent	*Percent*
Electrolytic iron No. 3	3	0.013	0.005
Electrolytic iron No. 4	3	.039	.012
Electrolytic iron No. 4	6	.039	.004
Stainless steel No. 6	5	.07	.01

It is evident that in each case the vacuum heating was associated with a definite decrease in carbon content. Of the four specimens, each carried an oxide coating after the last vacuum heating, except one specimen of electrolytic iron No. 4, which had been subjected to only three cycles of oxidation and vacuum heating. At this stage, the specimen still retained 0.012 percent of carbon, which apparently was sufficient to effect complete brightening. When the carbon content had reached a level of only 0.004 or 0.005 percent, however, as in electrolytic iron No. 3 after three cycles, and electrolytic iron No. 4 after six cycles, brightening no longer occurred. The stainless steel brightened satisfactorily in the first one or two cycles, but as the carbon content dropped from 0.07 to 0.01 percent in the course of the treatment, the ability to eliminate the oxide film was lost.

The results of these experiments support the conclusion that the oxide films were eliminated through reaction with the carbon in the specimens, apparently to form carbon monoxide. The necessary supply of carbon at the surface was presumably maintained by diffusion from beneath, until the carbon content became so low that the rate of the reaction was negligible. This was shown in a run on electrolytic iron No. 4 in which a sample coupon was clipped from the specimen at each stage in the treatment. Figure 1 is a photograph of these coupons, which are representative of the changes in surface appearance of this material during six successive cycles of oxidation and vacuum heating. It is evident that the material after the first three cycles was quite bright but subsequently became darker with each treatment, and, after the last one, showed definite evidence of oxide. The dark streaks which appear on some of the specimens are due to surface irregularities that developed during coiling and uncoiling, and these should not be confused with the changes in general appearance that occurred during the thermal treatments. The untreated specimen, which had not been coiled, appears smooth and bright over its entire surface. The carbon content of the original material was 0.039 percent, and in the final vacuum heating this was presumably reduced to 0.004 or 0.005 percent.

The change in appearance of a specimen of high-purity iron in a similar run is shown in figure 2. In this case the vacuum heating was at 1,050° C. The vacuum-heated specimen at the left, which had not been oxidized, is the only one that is completely bright, and after each oxidation the vacuum-heated specimens showed increasing evidence of the oxide film. In the third cycle there is very little difference between the appearance of the oxidized specimen and that of the

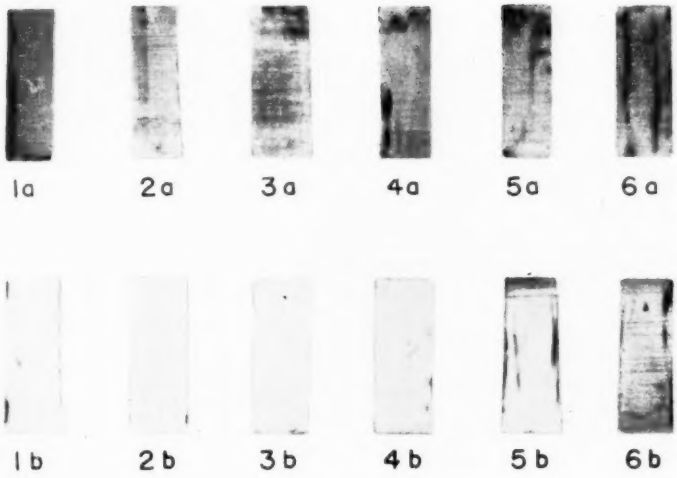

FIGURE 1.—*Changes in the appearance of electrolytic iron during six successive cycles of oxidation at 400° C. and vacuum heating at 800° C.*

1a represents the appearance of the specimen after the first oxidation, whereas *1b* illustrates the appearance of the oxidized specimen after vacuum heating in the first cycle. The coupon at the extreme left shows the appearance of the untreated material.

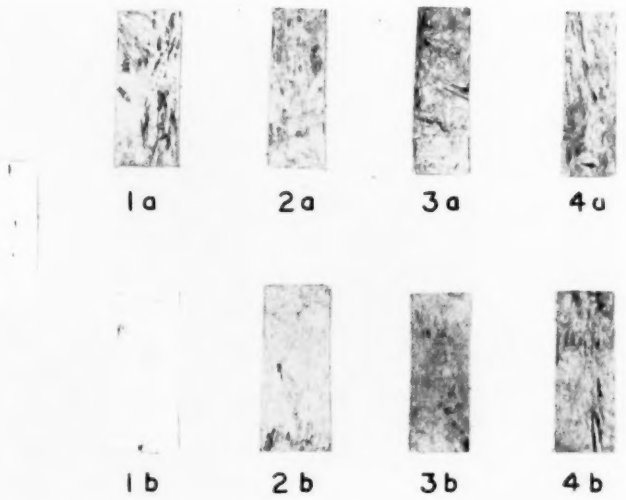

FIGURE 2.—*Changes in the appearance of high-purity iron during four sucessive cycles of oxidation at 400° C. and vacuum heating at 1,050° C.*

The specimen at the extreme left illustrates the appearance of the specimen after heating in vacuum *without* prior oxidation. *1a* represents the appearance of the specimen after the first oxidation, whereas *1b* represents the appearance of the oxidized specimen after vacuum heating in the first cycle.

UNIV. OF MICH.

vacuum-heated specimen. A comparison of figure 1 and figure 2 serves to illustrate the effect of carbon in the elimination of oxide films. It should be kept in mind that the electrolytic iron was heated at only 800° C, whereas the high-purity iron was heated at 1,050° C.

The manner in which the behavior of the different ferrous materials varied with the initial carbon content is shown graphically in figure 3. Curve *A*, for high-purity iron, indicates a gradual net gain in weight for the specimen, due to the fact that the losses during vacuum heating were negligible. Curve *B*, for electrolytic iron with 0.039 percent of carbon, shows a slight decrease in weight for the first four cycles. In subsequent cycles the carbon content was apparently too low to effect any significant loss of oxygen during the heating in vacuum, and the specimen gained in weight in the same manner as the high-purity iron. The final carbon content was 0.004 percent.

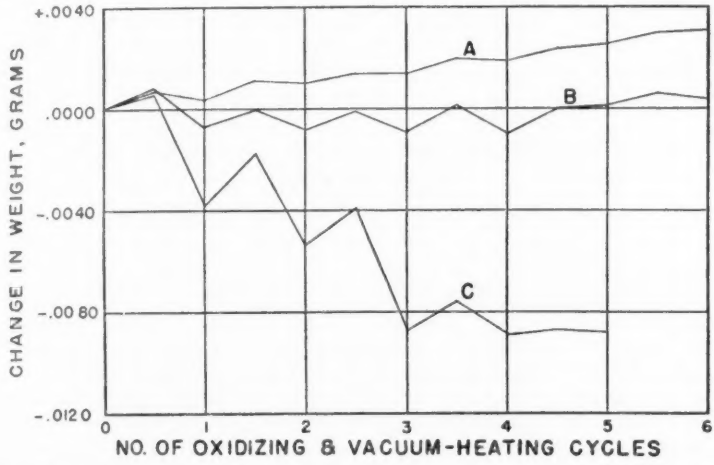

FIGURE 3.—*Change in weight during repeated oxidation and vacuum-heating cycles for specimens of high-purity iron No. 2 (A), electrolytic iron No. 4 (B), and stainless steel No. 6 (C).*

Oxidation was at 400° C for the high-purity and electrolytic irons and at 800° C for the stainless steel. The electrolytic iron was vacuum heated at 800° C, whereas temperatures of 1,050° C were used for the high-purity iron and the stainless steel.
Each curve is defined by two points for each cycle; the first point defines the change in weight during oxidation, the second, during vacuum heating.

The curve, *C*, for the stainless steel indicates distinctly greater changes in each cycle and a larger net loss in weight than that which occurred for electrolytic iron. This difference may be due partly to the fact that the stainless steel specimen underwent a greater change in carbon content, from 0.07 to 0.01 percent. It might be proposed that part of the loss was due to volatilization of oxide, but if this were true the specimen should have lost weight during the last cycle. However, the final vacuum heating did not cause any significant elimination of the oxide film. It is possible that some volatilization of metal may have occurred, although the experiments showed that the high-purity iron did not lose weight when vacuum-heated at the same temperature. Since complete clean-up occurred only in the first cycles, when the carbon content was sufficiently high, and because

the specimen did not brighten or lose weight in the last cycle, when the carbon had been reduced to 0.01 percent, it appeared logical to assume that carbon was the essential agent in the brightening of the stainless steel just as in the case of electrolytic iron.

In all the experiments in this investigation, it appeared that the presence of carbon was necessary for the elimination of oxide films in vacuum heating. In all cases brightening could be associated with definite decreases in carbon content. Oxidized specimens of high-purity iron, which contained 0.001 percent or less of carbon, could not be brightened by heating in vacuum for the usual periods at temperatures up to 1,250° C. The weight changes which were observed during oxidation and vacuum heating were generally of the correct magnitude to indicate that brightening occurred with the loss of oxygen as carbon monoxide. It is concluded, therefore, that the presence of carbon was the essential condition that made possible the elimination of oxide films on ferrous specimens during vacuum heating. It is possible that small amounts of oxide may have been volatilized or absorbed by the specimens, but brightening by these causes was insignificant in comparison with that effected by carbon..

IV. STRUCTURES OF OXIDE FILMS ON HIGH-PURITY IRON

In the course of the experiments a number of vacuum-heated specimens were examined under the microscope. Specimens which brightened satisfactorily did not show any unusual features except that the surface became somewhat irregular during the vacuum heating at high temperatures. However, the oxidized specimens of high-purity iron which could not be brightened by being heated in vacuum at 1,050° C presented an unusual appearance at high magnification. When heated in vacuum, the continuity of the initial oxide film shown in figure 4 was broken up and agglomeration into small isolated masses occurred, these being arranged according to definite geometric patterns. The area shown in figure 5 (*A*) illustrates the tendency of the agglomerated film to form square figures, as most of the lines intersect at right angles. In figure 5 (*B*), the lines intersect at approximately 60-degree angles, with the result that the figures are triangular. Since the type and orientation of these patterns vary from grain to grain, it appears probable that they are related to the orientation in the underlying metal. Figure 5 (*C*) shows an area at the junction of several grains. The tendency of some grains to oxidize to a greater degree than others, as indicated by the ratio of light to dark areas, is evident, and the orientation and nature of the pattern formed by the agglomerated oxide are different for different grains. The light areas between the globules indicate the background of bright metal. This bright metal would be capable of reoxidation, and in the oxidizing experiments this fact was verified. A blue color was developed during oxidation after each vacuum heating.

Figure 5 (*D*) shows the appearance of one of the vacuum-heated specimens of high-purity iron that was polished on a cross section to show the thickness of the oxide globules.

When specimens of high-purity iron similar to those shown in figure 5 were heated to 1,250° C in vacuo, the oxide globules gathered into still larger masses, and the distinctness of the initial geometric patterns was lost. Some of the globules were located in the grain boundaries,

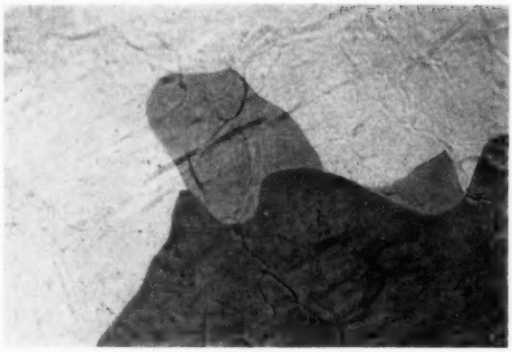

FIGURE 4.—*Oxidized surface of high-purity iron; ×500.*

Oxidation at 400° C occurred in varying degree for different grains, as indicated by differences in interference colors. The light-gray areas in the micrograph represent a straw color in the specimen, whereas the darkest areas are dark brown. The blue areas, which photographed to give the intermediate-gray tone, represent the highest degree of oxidation.

UNIV. OF MICH.

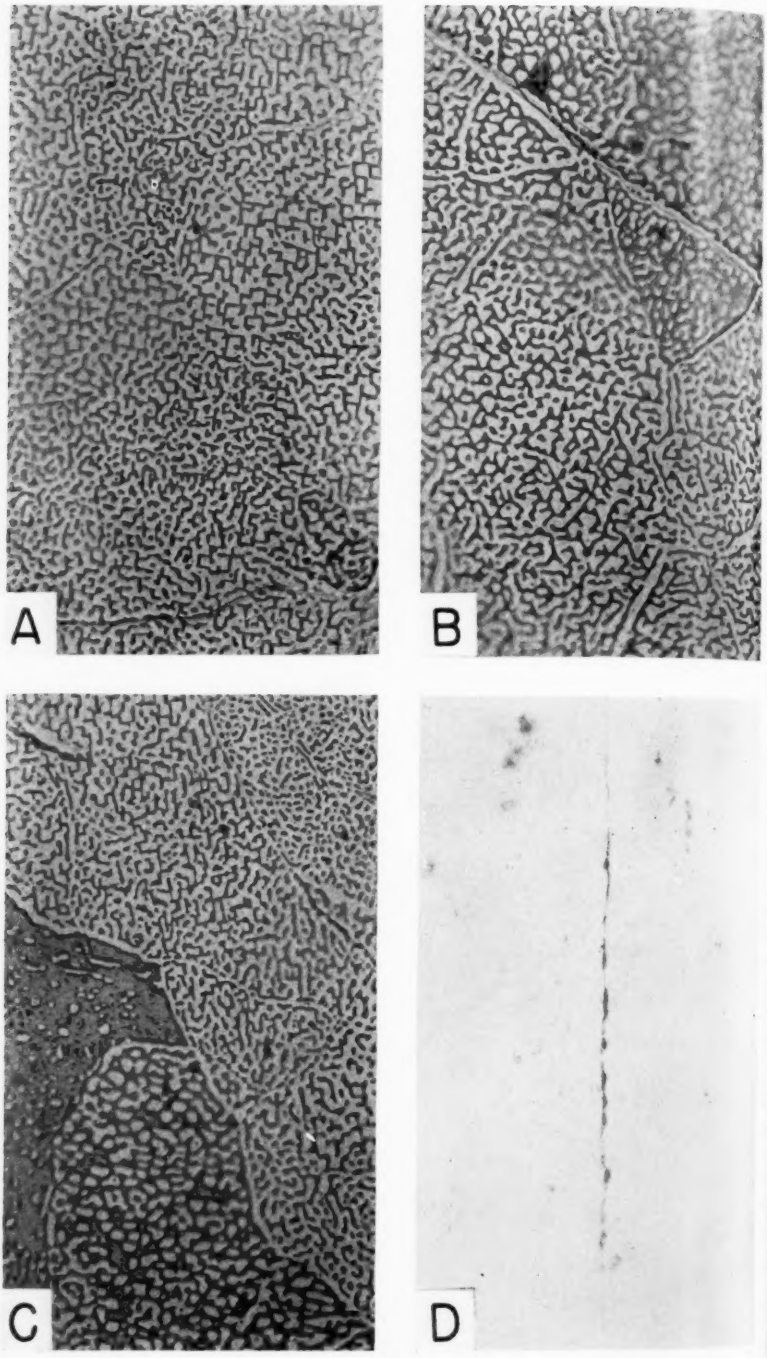

FIGURE 5.—*Oxidized specimens of high-purity iron, vacuum-heated at 1,050° C.*

A, *B*, and *C* illustrate the surface appearance of specimens after vacuum heating. Note the geometric patterns outlined by the globules. ×500.

D is a micrograph of the polished cross section of the surface of one of the above specimens, showing the thickness of the oxide globules. The surface was protected by a layer of electrodeposited copper during polishing. ×1000

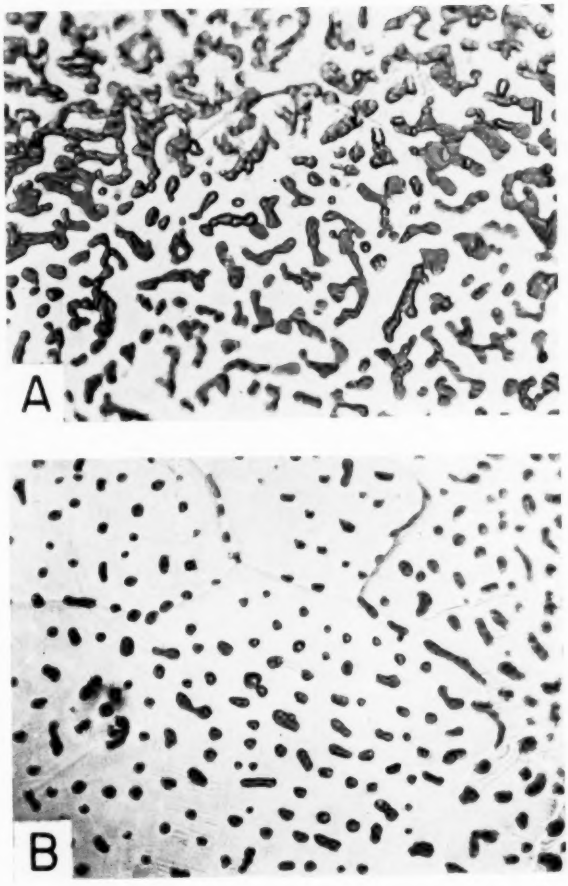

FIGURE 6.—*Oxidized specimens of high-purity iron, vacuum heated at 1,250° C.; ×500.*

A, coarse, globular structures formed at the higher temperature.
B, globules partly covered by condensed iron from the heating thimble. Note the globules in the grain boundaries.

whereas others lay directly across the boundaries, extending from one grain to another. The appearance of two different areas of a specimen is shown in figure 6. During the heating at 1,250° C, some iron vaporized from the heating thimble used as the container, and was condensed on the specimen. This was indicated by the partial brightening of the oxidized specimens through the deposition of a film of iron and by weight changes. The smaller number of globules in the area shown in figure 6 (*B*) than in figure 6 (*A*) perhaps can be attributed to the presence in this region of a thicker film of condensed iron in which many of the globules are embedded and hidden.

V. SUMMARY

Oxide films on ferrous materials—such as carbon steel, stainless steel, open-hearth iron, or electrolytic iron—that contain carbon may be removed by heating to suitable temperatures in a high vacuum. When oxide films are removed from such materials, there is an accompanying decrease in carbon content.

The clean-up of oxide films by vacuum heating can occur only if the carbon content is above a certain minimum value. For the conditions of heating that were used, this minimum was about 0.005 percent for iron and approximately 0.01 percent for stainless steel.

Oxide films on ferrous materials low in carbon, like high-purity iron, could not be removed by heating in vacuum for the period of time used for the carbon-bearing materials at temperatures up to 1,250° C. This has been interpreted as showing that no significant brightening occurs either by thermal dissociation of oxides, volatilization of oxides, or by absorption of oxide films in the underlying metal.

When lightly oxidized specimens of high-purity iron were heated at about 1,050° C in vacuum, agglomeration of the initially continuous oxide film occurred, the small isolated masses being distributed on a background of bright metal. Sometimes the agglomerated oxide masses were arranged according to a geometric pattern which varied from one grain to another.

VI. REFERENCES

[1] H. W. Gillett and B. W. Gonser, Fundamental Features of Controlled Atmospheres, Particularly for the Heat Treatment of Steel, Am. Soc. Metals Preprint (October 1941).

[2] C. A. Zapffe and C. E. Sims, *Hydrogen, flakes and shatter cracks, a correlated abstract, Part II*, Metals & Alloys **12,** 44 (1940).

[3] V. C. F. Holm, *Observations on the tarnishing of stainless steels on heating in vacuo*, Surface Treatment of Metals, p. 379 (American Society for Metals, 7301 Euclid Avenue, Cleveland, Ohio, 1941).

[4] J. G. Thompson and H. E. Cleaves, *Preparation of high-purity iron*, J. Research NBS **23,** 163 (1939) RP1226.

[5] J. W. Mellor, A Comprehensive Treatise on Inorganic and Theoretical Chemistry, **13,** 713 (Longmans, Green and Co., New York and London, 1934).

[6] B. W. Gonser, Discussion of paper by V. C. F. Holm (see reference 3), Surface Treatment of Metals, p. 389 (American Society for Metals, 7301 Euclid Avenue, Cleveland, Ohio, 1941).

[7] F. N. Rhines, *A metallographic study of internal oxidation in the alpha solid solutions of copper*, Trans. Am. Inst. Mining Met. Engrs., Institute of Metals Division, **137,** 246 (1940).

[8] B. A. Rogers and K. O. Stamm, *A magnetic determination of the A_3 transformation point in iron*, Metals Tech. **8,** TP1388 (1941).

WASHINGTON, January 30, 1942.

U. S. Department of Commerce National Bureau of Standards

RESEARCH PAPER RP1469

Part of Journal of Research of the National Bureau of Standards, Volume 28, May 1942

MEASUREMENTS OF ULTRAVIOLET SOLAR- AND SKY-RADIATION INTENSITIES IN HIGH LATITUDES

By W. W. Coblentz, F. R. Gracely, and R. Stair

ABSTRACT

Data are given on the intensity of the biologically effective ultraviolet radiation, of wavelengths 3200 A and shorter, from the sun and the entire sky, incident on a horizontal plane, under various meteorological conditions, in high latitudes. These data were secured by means of a photoelectric cell and automatic recording apparatus, whereby a continuous record of ultraviolet intensities, in absolute value, was obtained during the voyage of the Louise A. Boyd Arctic Expedition, up the west coast of Greenland to Etah (lat. 78.3° N) and down the coast of Baffin Land and Labrador.

The outstanding results of this survey are, that, for the same solar heights, in the highest latitudes visited (78° N) the ultraviolet intensities appear to be somewhat higher than in latitude 62° N, but somewhat lower than in latitude 39° N (Washington), in agreement with expectation, taking into consideration the distribution of ozone in the stratosphere with latitude and the season. In the highest latitudes, at the noon hour, on the clearest days, in mid-summer, the intensity of the ultraviolet solar and sky radiation ranged from 30 to 40 $\mu W/cm^2$, which is a significant value biologically, of especial interest to the medical profession in connection with the question of the incidence of rickets.

CONTENTS

	Page
I. Introduction	581
II. Instruments and methods	583
III. Discussions of ultraviolet-intensity data	586
IV. References and notes	590

I. INTRODUCTION

Although the principal purpose of the Louise A. Boyd Arctic Expedition [1] [1] was to secure data on radio-wave propagation, the voyage presented an excellent opportunity for the Radiometry Section of the Bureau to extend its survey of intensities of ultraviolet solar radiation incident in different localities [7, 8, 9].

By installing simple automatic measuring and recording apparatus [2, 3], for the first time a continuous record was obtained, in absolute value, of the intensity of the biologically effective ultraviolet radiation from the sun and from the entire sky incident on a horizontal plane, under various meteorological conditions, in the polar regions. The information thus obtained is novel and is of considerable biological interest, particularly to the medical profession.[2]

[1] Numbers in brackets indicate the literature references and notes at the end of this paper.

[2] Acknowledgment is made to the Council on Physical Therapy of the American Medical Association for two grants in aid to develop this type of ultraviolet meter [2] for use in heliotherapy. In an unforeseen manner the first practical application of these instruments has been to the securing of quantitative data on ultraviolet intensities in the polar regions.

The voyage was up the west coast of Greenland to Etah (lat. 78.3° N) and down the coast of Baffin Land and Labrador. The herein-described ultraviolet measurements were secured by F. R. Gracely, member of the expedition from the Radio Section of this Bureau.

In connection with the present survey of ultraviolet intensities in the polar regions, practically only three previous sets of measurements are available for comparison; and these are not on a strictly quantitative basis.

The first set of measurements, by Dannmeyer [4], were made in the summer of 1927, at a sea-level station in Iceland (lat. 64° to 66° N), using a *Cd*-photoelectric cell. No description was given of the photoelectric cell; but presumably it was of the type then in common use, consisting of a spherical bulb of Uviol (or quartz) glass having one-half of the interior covered with a thin layer of *Cd*-alloy, which is photosensitive to wavelengths shorter than 3200 A.

In the absence of a primary standard, in absolute units, Dannmeyer compared his photoelectric cell with the *Cd*-photocell used earlier by Dorno (and designated the Dorno Standard) on the "volt-second" basis, as measured with an electrometer.

The outstanding results of Dannmeyer's measurements, of interest in the present work, are: (a) for the same solar height (say 30°; air mass, $m=2$) the total intensity of the ultraviolet radiation from the sun and the sky was not markedly higher than that of similar sea-level stations in lower latitudes (except Hamburg, lat. 55.5° N; air probably polluted by smoke); and (b) when the solar altitude was low (30° down to 10°; $m=2$ to 6), the intensity of the ultraviolet radiation from the sun, incident on a horizontal plane, was only one-third to one-seventh of that from the whole sky.

The biological significance of the large amount of ultraviolet sky radiation is discussed by Dannmeyer, who comments on the fact that in Iceland, in the early spring, long before the sun can shine into the deep fjords, the faces of the inhabitants take on a ruddy color that develops into a dark-brown tan in midsummer, when exposed to both sun and sky radiation.

The second set of ultraviolet solar radiation measurements of interest in the present work were made by Kestner [6] in 1926 and in 1927 on the Lofoten islands, latitude 67.3° N. Weather conditions were never perfect; but considering days of the same degree of haziness (as it appeared to the eye) in the suburbs of Hamburg, and in higher latitudes, from his measurements he concluded that, for the same solar heights, the intensity of ultraviolet radiation north of the Arctic circle is greater than in mid-Europe. Referring to figure 1, which will be more fully described on a subsequent page, if the amount of ozone is less in latitude 70° N than in latitude 55° to 60° N, as indicated in the two lower curves, then, aside from differences in atmospheric pollution by dust and smoke, the intensity of ultraviolet radiation should be greater in the higher latitude, as reported by Kestner [6].

The third set of ultraviolet measurements of interest in the present work were made by Götz [5] in the summer of 1929, at Kingsbay, Spitzbergen (lat. 78.9°), in connection with the determination of the amount of ozone in the stratosphere.

For this purpose he measured the relative intensities of certain ultraviolet wavelengths as determined from the densities of spectro-

grams obtained at various solar heights. No measurements were made on the total intensity of ultraviolet solar and sky radiation incident on a horizontal plane.

In connection with the present work, the chief interest in Götz's measurements is his summary of data on the variation of ozone in the stratosphere with latitude and time of the year. This is illus-

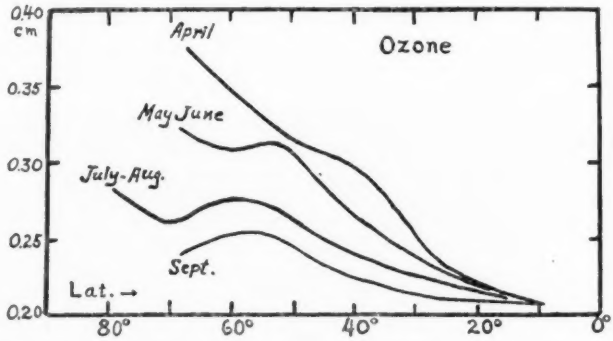

FIGURE 1.—*Curves showing the variation of ozone in the stratosphere with latitude and season (Dobson, Götz).*

trated in figure 1, which is a reproduction of Götz's figure 6 [5] showing the variation in the total amount of ozone with geographic latitude and the season. The scale of ordinates is in centimeters of ozone, reduced to normal temperature and pressure.

Since the amount of ultraviolet solar and sky radiation incident upon the earth's surface depends upon the amount of ozone in the stratosphere, and since, as above noted, this amount varies with the geographic latitude and the season, the data on ultraviolet solar and sky intensities obtained during the present cruise are too meager for extensive correlation with latitude and season; but they are useful in showing what was available to the crew, during this expedition, and in demonstrating a simple method of obtaining such measurements in future ocean voyages.

In view of the fact that Götz [5, p. 148] seemed to doubt the accuracy of Dannmeyer's measurements showing a relatively large amount of ultraviolet radiation incident from the whole sky, at a sea-level station in Iceland, it is relevant to note (from unpublished observations made by W. W. C. and R. S.) that, with a low sun (height 30° down to 15°; approximate air masses $m=2$ to 4), the intensity of the ultraviolet radiation from the whole sky, incident upon a horizontal surface, even during the clearest days, at a sea-level station (Washington) is 3 to 15 times that of direct sunlight, in agreement with the measurements made by Dannmeyer, in Iceland.

II. INSTRUMENTS AND METHODS

The apparatus used in measuring the intensity of ultraviolet solar and sky radiation incident on a horizontal plane was composed of three parts: (a) an electronic integrating device consisting of an *Mg*-phototube, condenser, and grid-glow-tube [10] enclosed in an evacuated glass chamber which was mounted in a metal box that was

attached to the top of the mainmast of the boat; (b) a metal box, below deck, containing the relay, rectifier tubes, and an impulse counter ("message counter"; see fig. 4 of reference [2]) made by R. J. Cashman; and (c) an automatic impulse recorder (modified commercial traffic recorder) which registered the impulses received from the photoelectric integrator and, at the expiration of every hour, printed the day, the hour, and the total number of impulses on a strip of paper [3]. In this manner, in addition to the reading on the impulse ("message") counter, a permanent, printed record was obtained of the amount of ultraviolet solar and sky radiation incident during different hours of the day.

In the operation of the device, the photoelectric cell, on exposure to ultraviolet radiation, charges a condenser to a critical voltage at which it is discharged through the impulse-counting mechanism; and this charging of the condenser is repeated at a rate that is proportional to the intensity of the incident ultraviolet radiation, which varies with the solar altitude and with the ever-changing weather conditions.

Unable to obtain delivery of a photoelectric cell in which the photosensitive receiver, the condenser, and the grid-glow-tube were enclosed in a single evacuated glass tube, one of the *Mg*–photoelectric cells illustrated in figure 3 of reference [2], with a condenser and grid-glow-tube, was enclosed in an evacuated glass tube and mounted in a metal box, illustrated in figure 2. Unfortunately the manufacturer placed an opaque ring around the inner tube, at such a height that it shadowed the receiver for solar heights less than about 15°. Hence, although at these low elevations the sun contributed but little relative to the ultraviolet incident from the whole sky, no attempt was made to work out the data obtained at low elevations of the sun.

Moreover, to prevent shadowing by the ship's sails, it was necessary to mount the photoelectric cell (fig. 2) in a metal box that was attached to the top of the mainmast, at a height of about 60 ft above the deck. Consequently the swaying of the mast prevented a continuous exposure of the photoelectric receiver in a horizontal position. Hence, only when the ship was in quiet water can the herein-recorded ultraviolet intensities be considered close to the true values for incidence on a horizontal surface. The records show that from August 10 to September 1 the voyage was through waters quieted by the presence of ice. When in port at Etah (August 15 to 19) and in Frobisher Bay (September 21 to 22), the water was quiet. However, since the ultraviolet radiation from the sky was no doubt four to five times [4] that of the sun, the variation in incidence by swaying of the photoelectric cell probably has not greatly affected the intensity measurements. This conclusion seems to be substantiated by the close agreement of the measurements obtained on the clearest days during the cruise with similar measurements made in Washington, taking into consideration solar height and the seasonal amount of ozone in the stratosphere. In fact, the daily totals of the impulses recorded in August were closely the same as observed on the clearest days in December 1941, in Washington, when the solar heights were closely the same as obtained during the voyage in the highest latitudes.

The calibration of a meter of this type (*Mg–3*, which includes a condenser and an electron-discharge tube [2]) to obtain intensities of biologically effective ultraviolet radiation of wavelengths 3200 A and shorter in absolute units is a relatively simple process.

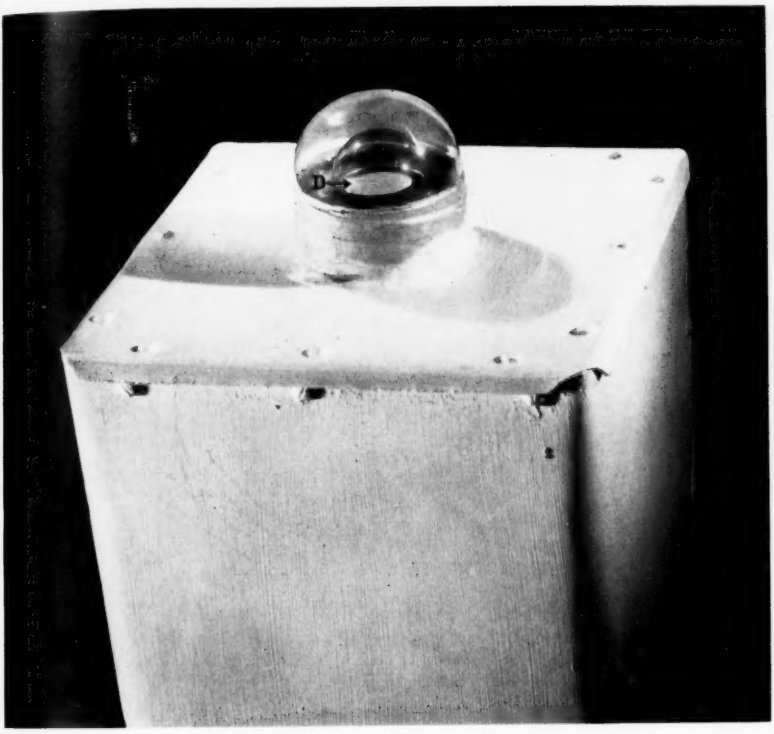

FIGURE 2.—*Photoelectric cell enclosed in a metal box that was attached to the top of the mainmast of the boat.*

The photosensitive, flat-disk receiver, *D*, measures the ultraviolet solar and sky radiation incident on a horizontal plane. The bright spots are unavoidable reflections of the light sources used in making the photograph.

UNIV. OF MICH.

The procedure consists in exposing the uncalibrated meter and the primary standard (*Mg 41–1*), side by side, to the sun and to the whole sky, and noting the relative number of impulses registered in a given time. Such a comparison was made before the voyage; and a more thorough comparison was made (by W. W. C.) in November and December, after the return, when the noon-hour solar heights were comparable with those that obtained at the highest latitudes (Etah; 78.3°). The comparison was made under various cloudless, cloudy, overcast, smoky, and hazy sky conditions; but no systematic difference in the ratios was observed. As shown in curve *A* of figure 3, the ratio of impulses (*Mg 41–1: Mg–3*) was uniform for air masses less

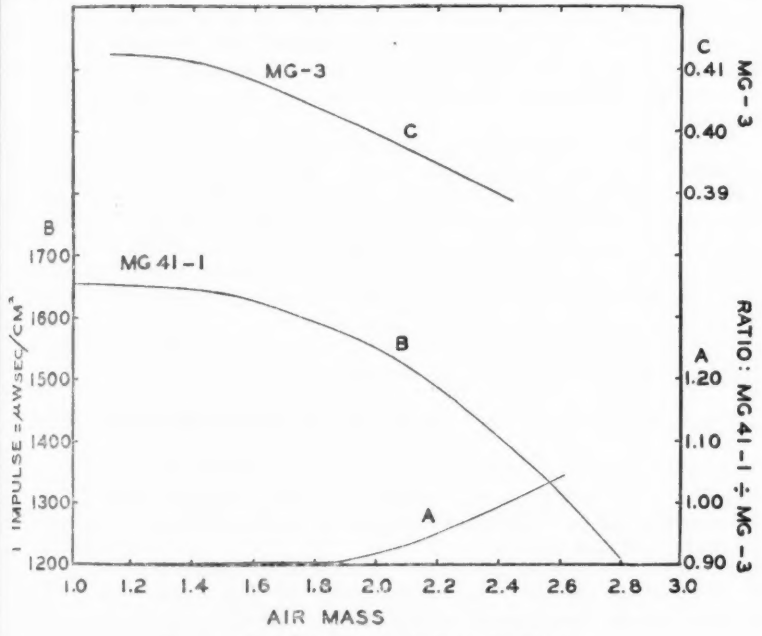

FIGURE 3.—*Calibration of phototube Mg–3.*

Curve *A*, ratio of impulses of phototubes *Mg 41–1* to *Mg–3*; curve *B*, factors for reducing impulses of *Mg 41–1* to ultraviolet intensities, μw sec/cm ²; curve *C*, factors for reducing the total impulses per hour to intensities in μw/cm ², using photoelectric cell *Mg–3*.

than $m=1.8$; but for air masses greater than $m=2$ the double-walled glass enclosure of the phototube, *Mg–3*, reduced the ultraviolet intensities, so that for air masses greater than $m=2.4$ the standard ultraviolet meter (*Mg 41–1*) functioned more rapidly than *Mg–3*.

The primary standard (*Mg 41–1*) is being standardized by two of the writers (W. W. C and R. S.) to measure intensities of ultraviolet solar and sky radiation of wavelengths 3200A and shorter, in absolute value, on a horizontal plane, using two methods: (a) by calibration against a standard of ultraviolet radiation [14]; and (b) by calibration against an ultraviolet-intensity meter [2, 13] that measures radiation incident normal on the photoelectric receiver. The latter was calibrated against a standard of ultraviolet radiation [14], and gave ultraviolet solar-radiation intensities (of wavelengths shorter than

3132A) in close agreement with measurements made with a balanced thermopile [11, 12, 15] which was calibrated, in absolute value, against a standard of thermal radiation. This ultraviolet-intensity meter has been in use, during the past 7 years, in measuring ultraviolet solar intensities. Although the calibration of this primary standard is incomplete, the degree of accuracy attained appears to be sufficient for evaluating the ultraviolet solar and sky intensities reported in the present paper.

In figure 3, curve *B* gives the factors for converting the impulses produced by the primary standard, *Mg 41–1*, to ultraviolet intensities (sun+sky) of wavelengths 3200A and shorter. The ordinates are in microwatt seconds per square centimeter (μw sec/cm^2). The reduction of the data is simple. Suppose that at a certain solar height (say 30°; $m=2$) the impulses were recorded at a rate of 1 impulse in 10 seconds (i. e., 90 impulses in 15 minutes on the recorder [3]), then the average ultraviolet intensity during that interval was ($1{,}550 \div 10 =$) 155 μw/cm^2.

The recorder used during the voyage printed the total number of impulses received during each hour. In figure 3, curve *C* gives the factors (deduced from curves *A* and *B*) for determining the average intensity of ultraviolet solar and sky radiation from the total number of impulses recorded during the hour, using ultraviolet meter *Mg-3*. For example, on August 21, during the noon hour, in latitude 77.8° N (solar height 24.3°; $m=2.42$) the recorder registered 108 impulses. The average intensity of the ultraviolet solar and sky radiation was therefore ($108 \times 0.389 =$) 42 μw/cm^2. The total energy incident during the hour was ($42 \times 3{,}600$) 151,200 μw sec/cm^2.

III. DISCUSSION OF ULTRAVIOLET-INTENSITY DATA

As already noted, the intensity of the ultraviolet solar radiation reaching the earth's surface depends upon the amount of ozone in the stratosphere; and as shown in figure 1, this amount varies with the latitude and the season.

In figure 4, curves are given showing the number of impulses per hour recorded on two clear days (July 23 and August 21) and on a partly cloudy day (August 19, 1941). In this connection it is of interest to note that in August, in the highest latitudes, during the clearest weather, with the midnight sun at an altitude of 3° to 5°, the ultraviolet radiation (practically all from the sky) was sufficiently intense to activate the photoelectric integrator during 22 hours of the day.

For example, while stationed at Etah (78.3° N), hence operating under the most favorable conditions as regards freedom from rolling of the boat, between 7 and 8 hours G. M. T. (solar height about 3°; $m=14$) the counter registered 3 impulses, and between 8 and 9 hours (S. H.$=5°$; $m=10$) it registered 5 impulses per hour, as compared with 108 impulses per hour at the noon hour (S. H.$=24.4°$; $m=2.41$).

This relatively high ultraviolet intensity when the sun was low on the horizon is not to be considered remarkable, however, in view of the fact that in the same latitude, at Kingsbay, Spitzbergen, in August 1929, Götz [5] observed intensities of total solar radiation (normal incidence) ranging from 0.35 to 0.42 (g cal/cm^2)/min at midnight (solar height, S.H.$=3°$ to $4°$) to 1.15 (g cal/cm^2)/min. at noon

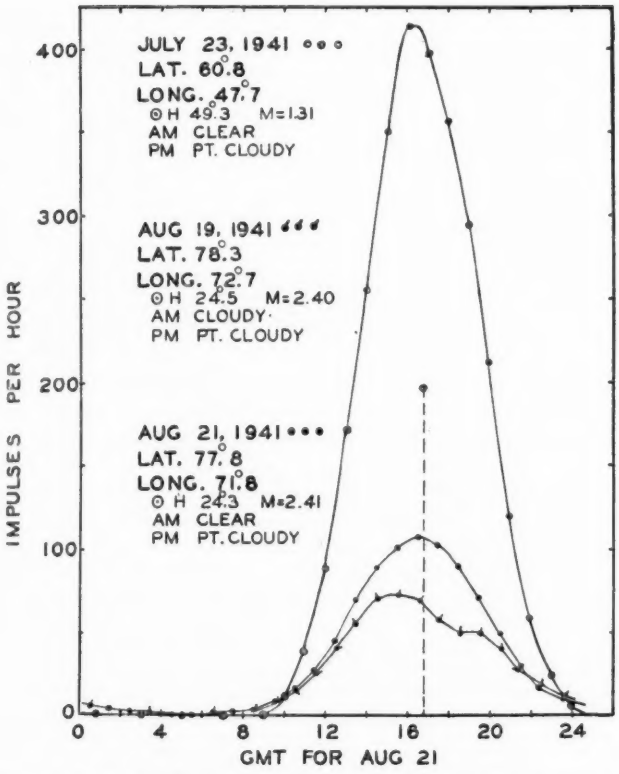

FIGURE 4.—*Graphs showing the impulses per hour received on several of the clearest days of the voyage in high latitudes.*

(S. H.=25°). He comments on the fact that the transparency of the atmosphere for total solar radiation at Kingsbay is but slightly higher than for similar solar heights (air masses traversed) in continental Europe.

In this connection it is relevant to cite unpublished records [3], repeatedly obtained in Washington, D. C., showing sufficient ultraviolet sky radiation to produce one impulse 15 minutes after sunset.

As noted above, the 108 impulses observed on the clearest day in high latitudes (August 21; lat. 77.8°; S. H. 24.4°; $m=2.41$) represent an average noon-hour intensity of 42 μw/cm^2. For similar solar heights in Washington the following ultraviolet solar and sky intensities were recorded [3]: October 8=46; November 17=52; December 6=44; and December 19=42 μw/cm^2. The average ratio of sky to sun radiation was 4.5 for $m=2.4$.

To simplify the exposition of the data on the integrated ultraviolet intensities as measured by the impulses recorded, in figure 5 are depicted the total number of impulses recorded daily (with only three interruptions indicated by broken lines) throughout the voyage in high latitudes, which are also indicated in this illustration.

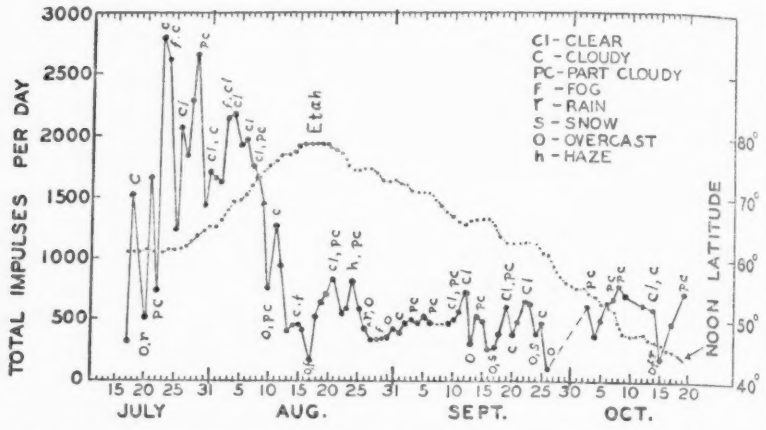

FIGURE 5.—*Graph showing the total impulses per day recorded during the voyage.*

A conspicuous feature of this illustration is the few days of clear weather recorded. The three-fold larger number of impulses recorded on the clearest days in July as compared with those recorded in the highest latitudes (Aug. 21 and 24) is to be ascribed to differences in solar height. The daily totals of August 21 and 24 may perhaps be somewhat higher than observed on the clearest days in December in Washington; but this might be due to greater freedom from atmospheric pollution by dust and smoke.

In figure 6 are depicted the ultraviolet intensities, in $\mu w/cm^2$, observed daily during the voyage. The values were computed by means of the factors given in curve *C* of figure 3 and the number of impulses recorded at the noon hour. In general, the noon hour intensities are indicative of the total number of impulses (and, hence, of the total amount of ultraviolet solar and sky radiation) received per day. Because of the above-mentioned shortcomings of this ultraviolet meter for low solar altitudes, no attempt is made to reduce the daily total impulses to total microwatt hours. Obviously, using the average intensity and the number of impulses recorded each hour, it would be a simple matter to deduce the total daily amount of ultraviolet received.

From figure 6 it may be noted that on numerous days during the voyage in August and September the intensity of the ultraviolet solar and sky radiation ranged from 30 to 40 $\mu w/cm^2$, which is a significant value biologically [12]. For example, if the erythematogenic efficiency of ultraviolet solar radiation in high latitudes is one-half that of Washington sunlight, then an exposure of 1.5 to 2 hours would produce an erythema.

In figure 7 is illustrated the variation in intensity of ultraviolet solar and sky radiation on three of the clearest days—namely, July 23, August 21, and September 22, 1941. The most conspicuous feature in this illustration is the much higher intensities in the highest latitudes (air mass $m=2.4$ to 2.8). Part of this difference may be ascribed to the seasonal change in ozone in the stratosphere, which is very marked in latitude 61° to 62° N (fig. 1), where the observations

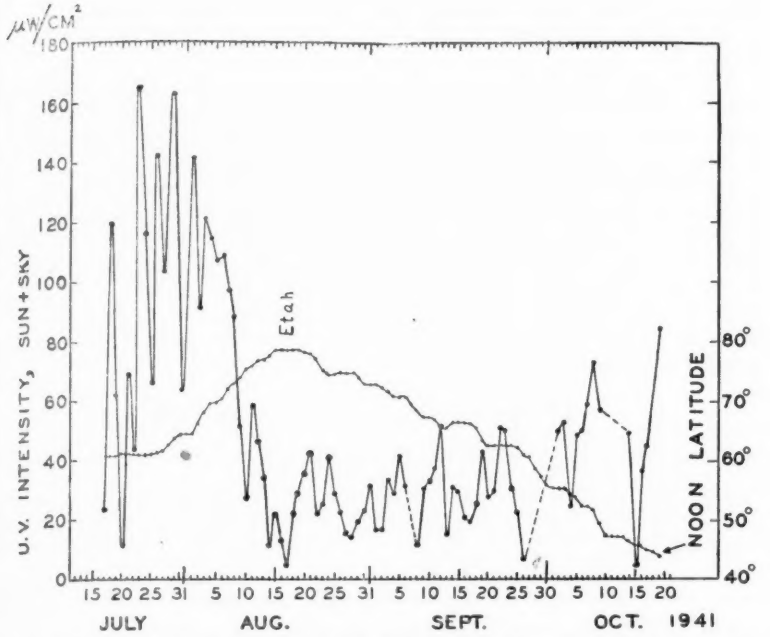

FIGURE 6.—*Graph showing the intensity of ultraviolet solar and sky radiation at the noon hour during the voyage.*

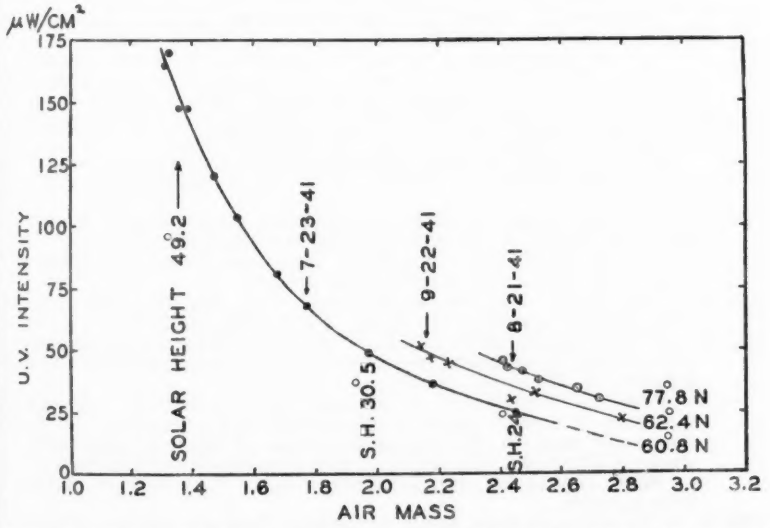

FIGURE 7.—*Curves showing the variation in intensity of ultraviolet radiation with solar height on three of the clearest days during the voyage.*

were made on July 23 and September 22, 1941. The ultraviolet intensities in September should be higher than in July, as recorded in figure 7.

The high ultraviolet intensities observed in the highest latitudes (fig. 7, August 21, 77.8°; $m=2.4$ to 2.8) substantiate previous, more qualitative, measurements [4, 5, 6], indicating an apparently lower amount of atmospheric ozone than in lower latitudes.

In conclusion it is of interest to note that, for similar solar heights (fig. 7, air masses $m=1.3$ to 1.4), the intensities of ultraviolet solar and sky radiation observed on the clearest days in July in Washington (lat. 38.9° N) were closely the same as recorded July 23 in latitude 60.8° N. This may be owing to the fact that at the land station greater atmospheric pollution by dust compensated for the lower amount of ozone (hence, increased transparency to ultraviolet radiation; fig. 1) in the lower latitude.

IV. REFERENCES AND NOTES

[1] The Louise A. Boyd Arctic Expedition, Tech. News Bul. NBS **291,** 57 (July 1941); **296,** 103 (December 1941).

[2] W. W. Coblentz and R. J. Cashman, *A photoelectric cell for measuring ultraviolet solar and sky radiation on a horizontal plane,* Bul. Am. Meteorol. Soc. **21,** 149 (1940). W. W. Coblentz, Bul. Am. Meteorol. Soc. **22,** 316 (1941).

[3] Instruments and methods of radiometry. Tech. News Bul. NBS **289,** 41 (May 1941). Reference to the use of an automatic impulse ("traffic") counter.

[4] F. Dannmeyer, *Die ultraviolette Himmelsstrahlung in nördlichen Breiten,* Strahlentherapie **35,** 607 (1930).

[5] F. Götz, *Zum Strahlungsklima des Spitzbergensommers,* Gerlands Beitr. Geophys. **31,** 119 (1931).

[6] O. Kestner and W. Borchardt, *Strahlenmessungen nördlich des Polarkreises,* Pflügers Arch. ges. Physiol. **217,** 504 (1927); **218,** 469 (1928).

[7] W. W. Coblentz, R. Stair, and J. M. Hogue, *Measurements of ultraviolet solar radiation in various localities.* BS J. Research **10,** 79 (1933) RP517.
Data on ultraviolet solar and sky radiation at various altitudes in Switzerland, in Denmark, on the North Sea, and on the Atlantic Ocean; observed with a standardized photochemical ultraviolet-intensity meter.

[8] W. W. Coblentz and R. Stair, *Factors affecting ultra-violet solar-radation intensities,* J. Research NBS **15,** 123 (1935) RP816.
Data on ultraviolet solar radiation in the tropics (San Juan, P. R.), and at high altitudes in Arizona; also data on the effect of smoke, fog, snow, and sky.

[9] W. W. Coblentz and R. Stair, *Evaluation of ultraviolet solar radiation of short wave lengths,* J. Research NBS **16,** 315 (1936) RP877.
Data on ultraviolet solar-radiation intensities observed at Washington, D. C., San Juan, P. R., and Flagstaff, Ariz.

[10] H. C. Rentschler, *An ultraviolet light meter,* Proc. Am. Inst. Elec. Engs. **49,** 113 (1930); Trans. Illum. Engl. Soc. (N. Y.) **25,** 406 (1930).

[11] W. W. Coblentz, R. Stair, and J. M. Hogue, *A balanced thermocouple and filter method of ultraviolet radiometry, with practical applications,* BS J. Research **7,** 723 (1931) RP370.
A description is given of (a) the evaluation of ultraviolet solar radiation by means of a single thermocouple receiver and a balanced (differential) thermopile receiver, (b) physiological tests of the erythematogenic efficiency of ultraviolet solar radiation, and (c) calibration of a photoelectrically operated impulse counter, in absolute units, by means of radiometric filter methods.

[12] W. W. Coblentz, R. Stair, and J. M. Hogue , *Tests of a balanced thermocouple and filter radiometer as a standard ultraviolet dosage intensity meter,* BS J. Research **8,** 759 (1932) RP450.
Data are given on the erythematogenic efficiency of ultraviolet radiation from various artificial sources and from the sun.

[13] W. W. Coblentz and R. Stair, *A portable ultraviolet intensity meter, consisting of a balanced amplifier photoelectric cell and microammeter,* BS J. Research **12,** 231 (1934) RP647.

[14] W. W. Coblentz and R. Stair, *A standard source of ultraviolet radiation for calibrating photoelectric dosage intensity meters,* J. Research NBS **16,** 83 (1936) RP858.

[15] W. W. Coblentz and R. Stair, *Evaluation of ultraviolet solar radiation of short wave lengths,* J. Research NBS **16,** 315 (1936) RP877.

Data are given showing a close agreement in the evaluation of ultraviolet solar radiation by means of: (a) a balanced thermopile [11] calibrated in absolute units by means of a standard of thermal radiation; and (b) a *Ti*-photoelectric cell [13] calibrated in absolute value, against a standard of ultraviolet radiation [14].

WASHINGTON, D. C., February 1, 1942.

U. S. DEPARTMENT OF COMMERCE NATIONAL BUREAU OF STANDARDS

RESEARCH PAPER RP1470

Part of Journal of Research of the National Bureau of Standards, Volume 28, May 1942

RATE OF OXIDATION OF TYPICAL NONFERROUS METALS AS DETERMINED BY INTERFERENCE COLORS OF OXIDE FILMS

By Dunlap J. McAdam, Jr. and Glenn W. Geil

ABSTRACT

By means of interference colors the rates of oxidation were determined for 18 nonferrous metals and were compared with those for typical steels. The influence of temperature, oxidation time, and film thickness on the rate of oxidation is illustrated by projections of surface in three-dimensional diagrams. The diagrams for the nonferrous metals are similar to those for steels. For a constant film thickness, the relation between temperature and oxidation time is linear logarithmic. The variation of film thickness with either temperature or oxidation time, plotted logarithmically, is represented by a reversed curve. A discussion is given of the influence of the affinity of the metal for oxygen and of the rate of diffusion through the oxide film. The film behaves as if the specific resistance varies nonlinearly with the film thickness.

CONTENTS

	Page
I. Introduction	594
II. Electrochemical theory of the dry oxidation of metals	594
III. Materials and method	596
IV. Influence of temperature on oxidation time for constant film thickness	597
1. General description of diagrams	597
2. Diagrams for typical metals	597
3. Relative positions of the diagrams for typical nonferrous metals and three typical steels	598
V. Variation of the film thickness with time at constant temperature	599
1. Derivation of diagrams	599
2. General description of the diagrams	600
3. Form of the curve of variation of film thickness with time at constant temperature	601
VI. Variation of the film thickness with temperature, for constant oxidation time	602
1. General description of diagrams	602
2. Form of the curves of variation of film thickness with temperature, for constant oxidation time	603
VII. Factors affecting the form and position of the three-dimensional diagram representing the oxidation of a metal	604
1. Influence of the affinity of the metal for oxygen on the rate of diffusion through the oxide film	604
2. Influence of the affinity of the metal for oxygen on the initial rate of oxidation	606
3. Reasons for the complex variation of the rate of oxidation with the film thickness	608
VIII. Summary	612
IX. References	612

I. INTRODUCTION

In a previous paper [10],[1] the authors gave results of an investigation of the rate of formation of oxide films on steels at elevated temperatures. The thickness of these films was determined by means of interference colors, sometimes called "temper" colors or "heat" colors. These colors are caused by interference between rays of light reflected from the inner and outer surfaces of the oxide film. The coincidence of two waves differing in phase by 180° causes light of a certain wavelength to disappear; if the incident light is heterogeneous, therefore, the reflected light is of the corresponding complementary color. Interference occurs when the film thickness is an odd multiple of one-fourth the wavelength of a component of the incident light. Interference, however, is determined by the wavelength in the film, not by the wavelength in air. The index of refraction of the oxide, therefore, is a factor involved in the relations between wavelength, film thickness, and interference color. A knowledge of the wavelength of the light in the oxide film, corresponding to an interference color, would make it possible to estimate the film thickness.

By means of interference colors caused by oxide films, a study has been made of the rate of oxidation of typical nonferrous metals, as affected by composition, temperature, oxidation time, and film thickness. In this paper, as in the previous paper, two-dimensional diagrams of three types are presented as complementary views of three-dimensional diagrams, each showing the relation between temperature, oxidation time, and film thickness. The first type shows the relation between temperature and oxidation time, for constant interference colors (constant film thickness). The second type shows the relation between oxidation time and film thickness, for several constant temperatures. The third type shows the relation between temperature and film thickness, for constant oxidation time.

Figures of assembled graphs representing the nonferrous metals and typical steels are also presented. These diagrams show the relative resistance of these metals to oxidation and are used in a study of the relation between resistance to oxidation and the properties of the oxide film.

II. ELECTROCHEMICAL THEORY OF THE DRY OXIDATION OF METALS

A general résumé of the literature on the oxidation of metals has already been given [10], together with brief mention of the prevalent theories. A more detailed outline will now be given of the electrochemical theory of oxidation, based chiefly on the investigations of Wagner and his coworkers [1, 2, 3, 4, 18, 19, and 20].

This theory states that after the first adherent film of oxide has formed the reaction proceeds by movement of ions and electrons through the film. The film consists of a space lattice of electropositive metal ions and electronegative oxygen ions. During oxidation, metal ions and an equivalent number of electrons leave the metal, enter the film, and move outward toward the film-gas interface. The oxygen ions in the film, however, are too large to diffuse inward, because each oxygen atom has acquired two electrons on taking its place

[1] Figures in brackets indicate the literature references at the end of this paper.

in the film. The growth of the film, therefore, consists chiefly in the meeting of oxygen ions and outwardly diffused metal ions at the film-gas interface.

The elements in a metal oxide may not be in the stoichiometric proportions. In the oxides of zinc and cadmium (and possibly aluminum at very high temperatures), the metal is in slight excess. In FeO, Cu_2O, and NiO, oxygen is said to be in slight excess [3, 4], although there is a contrary report for Cu_2O [8]. Such an excess of oxygen is said to be characteristic of the lower oxides of metals; in CuO and in other higher oxides of metals, the elements are said to be in stoichiometric proportions.

In ZnO, and possibly in other oxides that have excess of metal, the excess ions of metal are believed to be in the interstices of the lattice, and are accompanied by an equivalent number of free electrons. In the oxidation of such a metal, the metal ions and electrons move outward through the interstices of the lattice. When the oxide has a slight deficiency of metal (as in FeO), however, some of the positions generally occupied by metal ions in the space lattice are vacant. The outward movement of metal ions through such an oxide consists of jumps of ions from occupied to unoccupied positions in the lattice. Even in some oxides that are of stoichiometric composition, there are said to be vacancies in the metal space lattice and an equivalent number of metal ions in the interstices of the lattice.

The outward movement of electrons, moreover, may consist in either the outward flow of quasi-free electrons or a series of jumps from occupied positions to electron vacancies, sometimes called positive holes. In Cu_2O, for example, nearly all the copper ions have one less electron than a copper atom. A few ions, however, have lost two electrons and thus are cupric ions. As the electrons move outward by jumps, the positions of these positive holes move inward until they are filled at the metal-oxide interface.

According to the theory, therefore, the process of diffusion of ions and electrons varies greatly with the composition of the oxide film. These variations probably are associated with considerable differences of the rate of diffusion, and hence with considerable differences of the rate of oxidation. Unfortunately for the application of this theory, however, detailed information about the diffusion process is available for only a few metal oxides, and some of even this meager information (as reported by different investigators) is contradictory.

The total process of oxidation of a metal consists in three individual processes [14]: (a) Transfer of metal across the metal-film interface; (b) diffusion of metal ions and electrons outward through the film; and (c) adsorption of oxygen at the film-gas interface, and transfer across the interface. The rate of oxidation is controlled by the process which is naturally the slowest of the three. Initially process (a) is the controlling factor, and for a while the rate of oxidation is practically independent of the partial pressure of the oxygen and of the film thickness. Process (c) may control when the oxygen pressure is very low. With increase in the film thickness, process (b) becomes increasingly important, and eventually the controlling factor is the rate of diffusion through the film.

As shown by Price [14], the system comprising metal, film, and oxygen may be viewed as a galvanic cell, whose electrodes are the metal and the oxygen gas. In this cell, the film substance acts both

as the electrolyte and as the external circuit. In its ionic conduction, the film plays the role of the electrolyte; in its electronic conduction, the film plays the role of the external circuit of a galvanic cell. The electromotive force of this cell is provided by the affinity of the metal for oxygen. If n_1, n_2, and n_3 ($n_1+n_2+n_3=1$) are the transport numbers of cations, anions, and electrons, respectively, the part of the total electromotive force E, required to drive electrons through the film is $(n_1+n_2)E$, and the part required to drive ions through the film is n_3E. For oxidation of metals, n_2 is negligible and n_1 is generally small in relation to n_3. Most of the energy, therefore, is expended in movement of the ions.

III. MATERIALS AND METHOD

The materials used in this investigation were as follows: electrolytic copper, lead, and zinc, aluminum of about 99.9 percent purity, and nickel of the commercial *A* grade. A typical percentage composition of the nickel is: Ni+Co, 99.40; C, 0.10; Si, 0.05; S, 0.005; Cu, 0.10; Fe, 0.15; Mn, 0.20. Ruthenium and rhodium (99.99 percent pure) were prepared at this Bureau. Cadmium, chromium, cobalt, columbium, manganese, silicon, tantalum, tungsten, vanadium, and zirconium were purchased as "pure" metals from A. D. Mackay, New York City.

The method of preparing the specimens for the investigations and the method of experiment were the same as that used for steels, as described in the previous paper [10]. Suitable specimens of each metal were prepared and one surface was polished and cleaned. The specimens, with polished surface upward, were placed in a small electric furnace which was automatically maintained within 0.5 percent of the desired absolute temperature. The oxidation time was counted as beginning with the insertion of the specimen into the furnace, with no allowance for the time required to heat the specimen to the temperature of the furnace, or for the effect of the brief lowering of the temperature each time the furnace was partly opened to facilitate observation of the colors. From previous work [10], however, it is known that such allowances are important for short oxidation times but usually unimportant for oxidation times greater than about 20 minutes.

The oxidation times were observed for the appearance of the most easily distinguishable of the interference colors—straw, brown, and blue. It was usually possible to observe the first- and second-order colors. For some metals the third-order brown and blue and even the fourth-order blue were observed. Complete diagrams representing the relation between temperature, oxidation time, and film thickness were obtained with eight of these metals: copper, lead, nickel, ruthenium, silicon, tungsten, vanadium, and zinc. Although only incomplete diagrams were obtained with the other metals, the diagrams (not shown) have been established well enough to indicate the approximate relative positions of the graphs representing first-order blue.

IV. INFLUENCE OF TEMPERATURE ON OXIDATION TIME FOR CONSTANT FILM THICKNESS

1. GENERAL DESCRIPTION OF DIAGRAMS

In studying the relation between temperature, time, and film thickness, consideration will be given first to the relation between temperature and time, for constant film thickness (constant interference color). Diagrams representing this relation for typical nonferrous metals are shown in figures 1 to 5.

Logarithmic coordinates are used in these diagrams. Abscissas represent oxidation time in minutes; at the top of each figure is an additional scale representing days. Ordinates, as in the previous paper [10], represent the tenth power of the absolute temperature; the slope (tangent of the angle) thus has been multiplied by 10. Each figure also contains a scale in degrees centigrade.

The graphs [2] in these figures represent the temperature-time relation for straw color, reddish brown, and blue, of the first and higher orders. Each graph is designated by a letter (X, Y, or Z) representing straw color, reddish brown, or blue, respectively. For colors of the second, third, or fourth order, this letter is followed by a numeral designating the order.

The solid-line graphs in figures 1 to 5 are based on the uncorrected positions of the experimental points. Each line is based not only on the experimental points belonging to that line, but also on the probable ideal relationship (in form and position) between all the lines of the diagram. In determining the form of such a diagram, moreover, consideration was given to the complementary diagrams of the two other types, discussed in sections V and VI. Each diagram of the type shown in figures 1 to 5 thus represents a plan view of a surface in a three-dimensional diagram.

2. DIAGRAMS FOR TYPICAL METALS

In figures 1 to 5, the solid lines representing the various interference colors are straight throughout most of their extent, but are curved throughout the portions representing short oxidation time. Correction to allow for the time required to heat the specimen to the temperature of the furnace, or for the brief decrease of temperature whenever the furnace was partly opened, probably would make the graphs straight throughout their entire extent, as indicated by the broken lines diverging from some of the solid lines. The graphs for these nonferrous metals, therefore, are similar to the graphs for steels, presented in the previous paper [10].

In figure 3 the diagrams for zinc and lead are plotted with the same coordinate scales. In figures 4 and 5 the two diagrams are plotted with the same abscissa scale, but with different ordinate scales, indicated at the left and right sides of the figure.

In the diagrams (figs. 1, 2, 3, and 5) for nickel, tungsten, zinc,[3] vanadium, and ruthenium, the slope of a graph varies with the interference color; the slope is greatest for the lowest line in each diagram

[1] The word "graph" is used to designate a single straight line or curve and the points on which it is based; the word "diagram" is used to designate a series or family of graphs.

[3] Vernon [17] was unable to obtain interference colors with zinc.

and is least for the highest line. The slope evidently decreases with increase in the corresponding film thickness. The difference in slope between two adjacent lines is greatest for straw color and reddish brown of the first order, and becomes less as the film thickness increases. These diagrams, therefore, are qualitatively similar to the diagrams for nearly all of the steels represented in the previous paper [10]. The diagrams for a few of the alloy steels show very little difference in slope between the lowest and highest lines. Similar to these are the diagrams for lead, silicon, and copper shown in figures 3 and 4 of the present paper.

The linear relation represented by the corrected graphs, as shown in the previous paper, may be represented by the equation

$$t_2/t_1=(T_1/T_2)^n \tag{1}$$

In this equation, t represents the oxidation time, T represents the absolute temperature, and n represents the reciprocal of the slope, allowance being made for the fact that the slope in these figures has been multiplied by 10. Equation 1, therefore, indicates that the oxidation time (for constant film thickness) varies inversely as the nth power of the absolute temperature, and that the mean rate of oxidation (the reciprocal of the oxidation time) varies *directly* as the same power of the temperature. Values of n for all the graphs shown in figures 1 to 5 and for three typical steels are listed in table 1.

In addition to the diagrams shown in figures 1 to 5, incomplete diagrams have been obtained for aluminum, cadmium, chromium, cobalt, columbium, manganese, molybdenum, rhodium, tantalum, and zirconium. For aluminum, cadmium, and rhodium, only the position of each line has been established; for the others, both the form and the position have been established. These diagrams are similar in form to those in figures 1 to 5. Lines for first-order blue for these metals have been assembled in figure 8.

3. RELATIVE POSITIONS OF THE DIAGRAMS FOR TYPICAL NONFERROUS METALS AND THREE TYPICAL STEELS

A qualitative study of the relative resistances to oxidation of the nonferrous metals and the typical steels may be made by comparing the graphs for the same interference color. Such a comparison is made in figures 6 to 9; the interference colors represented in these figures are the three first-order colors and third-order blue. The steels used in this comparison are electrolytic iron, 13.6-percent chromium steel, and 24.4-percent chromium steel. As shown in the previous paper [10], the diagrams for carbon steels and for steels containing no more than 3 percent of chromium differ little in position from the diagram for electrolytic iron.

In the diagram representing straw color (fig. 6), the lines representing silicon and ruthenium are far above the other lines, including the lines representing the two stainless steels. The lines for nickel, tungsten, and 24.4-percent chromium steel differ little in position. Not far below these are the lines for zinc, vanadium, and 13.5 percent chromium steel. Although lead and copper are less corrodible than iron when in contact with water, they evidently are much inferior to iron in resistance to oxidation at elevated temperatures in air. In the

diagram representing first-order brown (fig. 7), the lines for nickel, tungsten, and zinc are somewhat higher in relation to the lines for silicon, ruthenium, lead, and copper than they are in figure 6, and the lines for the two stainless steels (especially the 24.4-percent chromium steel) are much higher in relation to the lines for all the other metals.

In the diagram representing first-order blue (fig. 8), continuous lines are used to represent the graphs completely established, broken lines are used for the graphs whose form and position have been approximately established, and dotted lines are used for the graphs whose approximate positions alone have been established. The line for the 13.6-percent chromium steel is relatively much higher than in figure 7, and now nearly coincides with the lines for ruthenium, chromium, and 24.4-percent chromium steel. The relative positions of the other continuous lines (from graphs completely established) have changed little. In the diagram representing third-order blue (fig. 9), the relative position of the line for 24.4-percent chromium steel has improved slightly, and the relative positions of the other lines are practically unchanged. With increase in the film thickness, therefore, the most striking improvement in relative resistance to oxidation was obtained with the two stainless steels. Nickel, tungsten, zinc, and vanadium, however, improved somewhat. The greatest change in the relative positions of the lines occurred between the film thicknesses corresponding to straw color and brown of the first order.

V. VARIATION OF THE FILM THICKNESS WITH TIME AT CONSTANT TEMPERATURE

1. DERIVATION OF DIAGRAMS

Each diagram of figures 1 to 5 represents a plan view of a surface as seen in a three-dimensional diagram in which the vertical dimension (normal to the plane of the figure) represents film thickness. The graphs in each of these diagrams, therefore, may be viewed as contour lines. Because the film thickness corresponding to a contour line increases with the progression of the interference colors, a plan view gives qualitative information about the form of the surface in the three-dimensional diagram. For more definite information, both qualitative and quantitative, it is necessary to consider not only the plan view, but also the front view and the side elevation. The front view gives direct information about the variation of the film thickness with the time at constant temperature. Diagrams of front views, derived from six of the eight diagrams of figures 1 to 5, are shown in figures 13, 14, and 15.

The relation between film thickness (y), wavelength (λ), index of refraction (μ), and the order (b) of the interference color, is expressed by the equation

$$y=\frac{(2b-1)\lambda}{4\mu}. \tag{2}$$

The observed color depends not only on interference between the light reflected from the bottom of the oxide film and that reflected from the top, but also upon the selective absorption of light by the metal and the oxide film. This dependence was studied for nickel and

copper, the metals that would be expected to show the most prominent influence of selective absorption. For this investigation, specimens of these two metals, some with and some without oxide films, were examined by means of a recording spectrophotometer.[4]

The variation of the reflectance of the specimen with the wavelength of the incident light was determined, and from these measurements the reflectance ratio (the ratio of the reflectance of the oxidized surface to the reflectance of the unoxidized surface) was computed. The use of the reflectance ratio, rather than simply the reflectance of the oxidized specimen, permits the selective absorption of light in the oxide film to be evaluated independently of the selective absorption of light by the metal itself. Figures 11 and 12 show the variation of the reflectance ratio with the wavelength. Since the film thickness corresponding to an interference color is, according to eq 2, a function of the wavelength of the extinguished light, the significant part of a curve in these figures is the wavelength of the minimum reflectance ratio. From the curves for nickel (fig. 11) the wavelength for the minimum reflectance ratio may be readily estimated for brown of the first and second orders and for first-order blue. No minimum is found in the curve of reflectance ratio for first-order straw color, but the curve evidently is approaching a minimum which would be at a wavelength somewhat below the short-wave limit of the spectrophotometer used. An estimated value of 3500 A has been taken for this minimum. Similarly for copper all curves in figure 12 yield definite minima except that for second-order straw color, which is evidently approaching a minimum at a wavelength not far below the short-wave limit of the spectrophotometer used. The reflectance ratios for copper differ from those for nickel by being lower in the long-wave end of the spectrum. This difference must be ascribed to difference in selective absorption of light by the two oxide films, and not to interference effects. No attempt has been made to take this difference into account in estimating the wavelength corresponding to the light extinguished by interference. These wavelengths have been taken from figures 11 and 12 for determining oxide-film thickness by eq 2 for nickel and copper. For other metals the wavelengths of the light extinguished by interference have been taken as 3500, 4500, and 6300 A, corresponding to straw color, brown, and blue, respectively.

As indicated by eq 2, the absolute thickness of the oxide film cannot be determined without knowledge of its index of refraction, for light of wavelength equal to that of the extinguished component. For some of the nonferrous metals studied, neither the indices of refraction nor their variation with wavelength are known. It was therefore found convenient not to use any recorded values of the refractive index to obtain film thickness by eq 2. Instead, as in the previous paper [10], a value of 1.0 was used for μ. The thicknesses so obtained refer to the distance to which the two film faces would have to be separated by air in order to obtain the interference effects observed. These thicknesses have therefore been identified as "uncorrected air-equivalent values."

2. GENERAL DESCRIPTION OF THE DIAGRAMS

Abscissas in these front views (figs. 13, 14, and 15) of three-dimensional diagrams, like abscissas in the plan views (figures 1 to 5), repre-

[4] Acknowledgment is made to H. J. Keegan, of the Colorimetry and Spectrophotometry Section, for making the spectrophotometric measurements and for helpful suggestions in regard to assembling this information.

sent the logarithms of the first powers of the oxidation times. The scale of abscissas, however, is more condensed in the front views than in the plan views. The variations of slope of the curves have been magnified by using as ordinates the fifth powers of the film thickness (tenth powers are used in the corresponding diagrams of the previous paper). The letters used to designate the interference colors at the right of each figure have the same significance as in figures 1 to 5.

Each small open circle in figures 13, 14, and 15 corresponds to a point on each of the straight graphs of the plan view; each black circle corresponds to a point obtained by extrapolation of one of these straight graphs. Each curve is based not only on the corresponding small circles, but also on the interrelationship between all the curves of the diagram and on the interrelationship between the front view, plan view, and side elevation (figs. 16 and 17) of the three-dimensional diagram.

3. FORM OF THE CURVE OF VARIATION OF FILM THICKNESS WITH TIME AT CONSTANT TEMPERATURE

The curves in figures 13, 14, and 15, with the exception of those in the diagram for copper (fig. 15), are qualitatively similar to the corresponding curves for steels [10]. Each curve (with the exception of those for copper) increases in slope as it extends to the right, and all the curves evidently approach the same slope (indicated by the broken lines).[5] The tangent of the angle of this slope is 2.5, but would be 0.5 if the first powers of the film thickness were used as ordinates. A straight line having this slope, with logarithmic coordinates, represents a quadratic parabola. When this slope is reached, therefore, the film thickness is varying as the square root of the oxidation time [10]. The thickness at which the quadratic relationship is reached decreases with increase in the temperature, and also varies with the metal; it is less for tungsten,[6] lead, and silicon than for nickel and zinc.

The slope of a curve (figs. 13, 14, and 15) at any point may be represented by the equation

$$m=\frac{d \log y}{d \log t}=(t/y)(dy/dt). \tag{3}$$

In this equation, y and t have the same significance as in previous equations, and m represents the tangent of the angle of slope, when the coordinates represent the first powers of the two variables. The value of m for the asymptote approached by the curves is 0.5.

The curves in the diagram for copper (fig. 15) extend not only through the range of interference colors, but also to a point representing a much thinner film. The wider range of film thickness represented in this diagram is made possible by including evidence based on results obtained by Lustman and Mehl [9],[7] who used polarized light in an investigation of very thin films. Throughout the range of interference colors, the curves are less exactly established

[5] The downward convexity of these curves, as shown in the previous paper [10], does not mean that the curves would have this form if plotted with Cartesian coordinates. If so plotted, as illustrated in figure 20, the slope decreases continuously with increase in the oxidation time.

[6] The diagram for tungsten does not support Scheil's conclusion [15] that the thickness of the oxide film on this metal increases linearly with the oxidation time.

[7] Neither this diagram nor the diagrams for the other metals supports the conclusion by Lustman and Mehl [9] that the oxidation rate of metals at low temperatures changes discontinuously with the temperature.

than are the curves for the nonferrous metals previously considered. As shown in the plan view (fig. 4), the scatter of the experimental points is too great to permit exact location of the graphs from which the corresponding experimental points in figure 15 are derived. Nevertheless, the evidence based on this investigation and on the investigation by Lustman and Mehl is sufficient to establish the approximate form and position of these curves.

Throughout the range of interference colors on copper (fig. 15) the curvature is slight, and the approach to a quadratic relationship is much slower than in the diagrams for the other metals here considered. Even at a thickness corresponding to third-order blue, the slope of each curve is considerably less than that representing a quadratic parabola.

The reversal of curvature with extension of the curves into the field representing films too thin to exhibit interference colors is based on data presented by Lustman and Mehl [9]. Curves L representing these data have been corrected to allow for the fact that the data recorded by Lustman and Mehl represent estimated values of both the actual film thickness and the index of refraction, whereas film thicknesses in figure 15 are "air-equivalent" values. Correction has also been made by subtracting 35 seconds from the oxidation times recorded by these investigators. As their experiments involved removal of hydrogen and admission of a rapid stream of air (not preheated), some deduction apparently should be made from the recorded oxidation times. Moreover, their diagrams and a statement in their paper indicate that practically no film was formed during an initial period of about 35 seconds. The deduction of 35 seconds from the oxidation times has made the slope of the lower parts of curves L in figure 15 somewhat less steep than if the curves were uncorrected.

The curves based both on this investigation and on that of Lustman and Mehl, consequently, are less steep at the lower ends than curves based only on the latter investigation. For very thin films the curves (fig. 15) approach a tangent whose slope would be 1.0 if the first powers of the film thicknesses were used as ordinates; they thus indicate that thickness is proportional to oxidation time. The film thickness represented by the lower ends of the curves is only 10 A, and hence the number of atomic layers in the film is of the order of 10.

The diagram for copper (fig. 15) is the only diagram of this type, either in this paper or the preceding paper [10], in which there is experimental evidence of a reversal of curvature. In all the other diagrams, the curves at their lower ends turn rapidly to the left. If these curves could be extended further, however, they all probably would eventually show a reversal and an approach to a final steep slope. This surmise is illustrated by the assembled curves in figures 18 and 21, which are discussed in section VII.

VI. VARIATION OF THE FILM THICKNESS WITH TEMPERATURE, FOR CONSTANT OXIDATION TIME

1. GENERAL DESCRIPTION OF DIAGRAMS

Two views of each three-dimensional diagram representing the oxidation of these nonferrous metals have already been considered. The third view, a side elevation, represents the variation of the film

thickness with temperature, for constant oxidation time. Such views of six diagrams are shown in figures 16 and 17. For correct representation of the side elevations, abscissas read from right to left. Abscissas represent the logarithms of the tenth powers of the absolute temperatures, and ordinates represent the logarithms of the fifth powers of the film thicknesses. The scale dimension, however, is twice as large for abscissas as for ordinates. For each diagram except that for copper (fig. 17), the powers of the variables are the same as for the corresponding coordinates in the plan view and front view.

The side elevation can be derived from either the plan view or the front view. The small circles in figures 16 and 17 are derived from corresponding points on graphs of the plan views. The black circles represent results of some extrapolation. Each curve is based not only on the positions of the corresponding symbols, but also on the probable interrelationship between all the curves of the diagram, and on the proper relationship between the side elevation and the corresponding plan and front views.

2. FORM OF THE CURVES OF VARIATION OF FILM THICKNESS WITH TEMPERATURE, FOR CONSTANT OXIDATION TIME

The curves in the side elevations (figs. 16 and 17) are qualitatively similar to the curves in the front views (figs. 13, 14, and 15). The slope increases with the temperature, and each curve apparently approaches a steeply sloping asymptote. The slope of a curve at any point is represented by the equation

$$h=\frac{d \log y}{d \log T}=(T/y)(dy/dT). \tag{4}$$

In this equation, T represents the absolute temperature, and h represents the tangent of the angle of slope, if the coordinates represent the first powers of the two variables. In figures 16 and 17, the relation between the powers of the two variables and the scale dimensions are such that h is one-fourth the indicated slope.

With increase in the film thickness, the three-dimensional diagram approaches an inclined plane. The relation between the inclinations of this plane in the plan view, front view, and side elevation is represented by the following relation between the three indices of slope

$$h=mn. \tag{5}$$

An asymptotic value of h, therefore, can be obtained by the use of the asymptotic value of n and the asymptotic value 0.5 for m. The asymptotic value of h varies with the metal. For the metals represented in figures 16 and 17 and in table 1, the values of h range between about 11 and 22. For constant oxidation time, therefore, the film thickness varies as about the 11th to the 22d power of the absolute temperature.

With downward extension of the curves for nickel (fig. 16), they probably would cross the corresponding curves for lead. Similar evidence in figure 17, moreover, suggests that the curves for zinc would cross the corresponding curves for copper. In this respect, these pairs of diagrams are similar to the corresponding pairs of diagrams for carbon steels and high chromium steels shown in figures 27 and 28 of the previous paper [10]. Up to a certain film thickness, which varies

with the metal, high-chromium steels evidently oxidize more readily than carbon steels, nickel oxidizes more readily than lead, and zinc oxidizes more readily than copper. Above these thicknesses, the relative resistance to oxidation of the metals of each of these pairs is reversed. Reasons for this behavior will be discussed later.

VII. FACTORS AFFECTING THE FORM AND POSITION OF THE THREE-DIMENSIONAL DIAGRAM REPRESENTING THE OXIDATION OF A METAL

1. INFLUENCE OF THE AFFINITY OF THE METAL FOR OXYGEN ON THE RATE OF DIFFUSION THROUGH THE OXIDE FILM

The relative resistance of chromium steels and carbon steels to oxidation varies greatly with the film thickness. When the film is very thin, chromium steels oxidize more rapidly than carbon steels [10, 13, 16]. With increase in the film thickness, however, the relative resistance of chromium steels increases, and eventually becomes greater than that of carbon steels. The film thickness at which this inversion of relationship occurs decreases with increase in the chromium content, at least up to about 13 percent. As shown by Portevin, Prétet, and Jolivet [13], the tendency of the metal to cross the metal-film interface is greater for chromium than for iron, but the chromium ions diffuse outward more slowly than the iron ions. Oxide of chromium thus tends to become concentrated in a layer at the inner surface of the oxide film. Through this layer, the outward diffusion of ions of iron is less rapid than through oxide of iron. When enough chromium has been oxidized to build up a certain thickness of chromium oxide, therefore, a chromium steel oxidizes less rapidly than a carbon steel.

A similar effect [13, 16] is produced by other alloying elements whose affinity for oxygen is greater than that of iron (as shown by a greater heat of formation of the oxide). Among such elements are aluminum and silicon. An investigation by Scheil and Kiwit [16] led them to the conclusion that the oxidation-resistance of steel is improved by alloying with elements less noble, such as aluminum, chromium, silicon, vanadium, molybdenum, and beryllium. The oxides of these elements were found to be concentrated in the inner layer of the oxide film. For highest resistance to oxidation, they suggest also that the oxide of the alloying element should have a high melting point.

The effect of alloying elements on the oxidation of copper was studied by Fröhlich [8]. He investigated the effect of additions of aluminum, iron, lithium, magnesium, manganese, nickel, arsenic, boron, beryllium, chromium, calcium, cerium, cobalt, phosphorus, antimony, silicon, titanium, zinc, tin, and silver. Of all these elements, only silver is more noble than copper. In the oxidation of all these alloys except the copper-silver alloy, the oxide of the alloying element was found to be concentrated in the inner layer of the oxide film.

The evidence indicates that the ions of a less noble metal alloyed with either iron or copper diffuse outward less rapidly than the ions of the predominant metal, and thus form an inner layer of oxide with relatively high resistance to diffusion. It would be expected, therefore, that an unalloyed metal with high affinity for oxygen would tend to form quickly a thin protective film of oxide, and thus would acquire

high resistance to further oxidation. It might even be expected that the greater the affinity of the metal for oxygen, the more rapidly would the metal oxidize at first and the more slowly would it oxidize after this initial period. This would imply that the resistance of the film to outward diffusion of metal ions and electrons tends to increase with increase in the affinity of the metal for oxygen. It would imply further that, for a film of sufficient thickness, the resistances of metals to oxidation would be in the order of their chemical affinities. If this surmise were correct, the heights of the graphs representing first order (or a color of a higher order) for various metals would be in the order of their chemical affinities. The correctness of this implication will be tested by a comparison of the assembled graphs in figure 10 with the data in table 2.

The assembling of the graphs in figure 10 is not only for a comparison of the resistances of these metals to oxidation, but also for a comparison of these resistances with various physical properties of the oxides. The oxides are listed in table 2 in the order of decreasing heats of formation per gram atom of oxygen. For evaluation of the relative resistances to oxidation, the positions of the graphs in figure 10 have been corrected to allow for the differences in the indices of refraction of the oxides and in the volume of oxide per gram atom of oxygen (columns 11 and 12 of table 2). As shown in eq 2, the film thickness for a given interference color is inversely proportional to the index of refraction of the oxide. The higher the index of refraction and the greater the volume of oxide per gram atom of oxygen, therefore, the sooner will a given interference color appear. The factor used in correcting the position of each graph in figure 10, consequently, is the product of the factors listed in columns 11 and 12 of table 2; these products are listed in column 13. The amounts of the corrections may be seen by comparing the positions of corresponding graphs in figures 8 and 10. The greatest corrections are in the positions of the graphs for lead and copper.

The relative heights of the graphs at two positions in figure 10 are listed in columns 7 and 8 of table 2, and have been indicated by numbers adjacent to some of the graphs. Comparison of columns 2, 7, and 8 of table 2 shows some evidence of a correlation between the order of decreasing heats of formation of the oxides and the order of decreasing heights of the graphs. The graphs for aluminum, silicon, and chromum, whose oxides have high heats of formation, are near the top of the diagram; the graphs for lead and copper, whose oxides have relatively low heats of formation, are at the bottom of the diagram. Moreover, it is easy to account for the relatively high position of the graphs for rhodium and ruthenium, whose oxides have the lowest heats of formation. Parallelism between the order of decreasing heats of formation and the order of decreasing heights of the corresponding graphs could not continue below a certain value of the heat of formation. When the heat of formation is less than this value, the chemical affinity is so slight that the rate of oxidation is controlled throughout by the slow rate of transfer across the interface rather than by the resistance of the film to diffusion. It is not surprising, therefore, to find that the graphs for rhodium and ruthenium are much higher than the graph for copper.

The other graphs in figure 10 show no clear correlation between the heats of formation and the rate of oxidation. The graphs for man-

ganese, tantalum, vanadium, and zirconium, whose oxides have high heats of formation, are near the middle of the diagram. The graph for nickel, moreover, is much too high, and the graphs for iron and manganese are much too low, to be correlated with the order of the heats of formation. The graph for nickel is much higher than that for cobalt, although the oxides of these metals have about the same heat of formation.

The affinity of the metal for oxygen, however, is not measured exactly by the heat of formation, but is measured by the free energy at the temperature of the reaction. The free energies of oxidation at 25° and 427° C, for some of the metals, are listed in columns 4 and 5 of table 2[8]. Because the entropy values are not known for some of the oxides, the free energies for these metals could not be calculated. As the free-energy values in both columns are in the same order as the heats of formation, they give no better correlation with the relative positions of the graphs in figure 10. In column 6 of table 2 are listed values of free energy for the different indicated temperatures, which are approximately the temperatures represented by the middles of the corresponding graphs in figure 10. These values also are in the order of decreasing heats of formation of the oxides.

The lack of parallelism between the chemical affinities and the relative positions of the graphs cannot be attributed to differences in the melting points of either the metals or the oxides, or to differences in the boiling points of the metals. This is shown by a comparison of the data in columns 7, 8, 14, 15, and 16 of table 2.

No consistent relation, therefore, exists between the order of decreasing chemical affinity and the order of positions of the graphs in figure 10. This evidently means that the order of decreasing chemical affinity is not the order of decreasing resistance to diffusion through the oxide film. The resistance to diffusion through the film in most metals evidently is affected greatly by factors other than the chemical affinity of the metal for oxygen. As shown in section II, the mode of transfer of the ions and electrons through the oxide film varies greatly with the metal. This difference in the mode of transfer probably is associated with great differences in the resistance to diffusion.

2. INFLUENCE OF THE AFFINITY OF THE METAL FOR OXYGEN ON THE INITIAL RATE OF OXIDATION

If sufficient evidence were available, a correlation might be found between the affinity of a metal for oxygen and the initial rate of oxidation. The fact that the initial rate of oxidation is greater for an iron-chromium, iron-silicon, or iron-aluminum alloy than for iron suggests that the initial rate depends upon the affinity of the metal for oxygen. A similar suggestion is given by the evidence in figure 16 that the curves for nickel, if extended far enough downward, would cross the corresponding curves for lead, and by the evidence in figure 17 that the curves for zinc would cross the curves for copper. Additional evidence is revealed by a comparison of the assembled curves in figures 18 and 19.

The experimentally established portion of each curve in figures 18 and 19 is drawn as a continuous line. The curve for copper, because of

[8] Acknowledgment is made to F. D. Rossini, of this Bureau, for helpful suggestions in regard to assembling this information.

its experimental basis, is drawn as a continuous line throughout its entire extent. Each other curve is extended downward, as a broken line, far below the field representing the range of experimentally determined points. The lower limit of the diagram represents a film thickness of not much more than 100A, or about the same number of atomic layers. This downward extension of the curves is intended to indicate only qualitatively the forms and the probable interrelationship of the curves.

In a diagram of the type shown in figure 18, the assembled curves should, if possible, represent results obtained at the same temperature. Such an ideal representation, however, was not possible; five of the curves represent results obtained at two slightly different temperatures, and the curves for copper and iron represent results obtained at a much lower temperature. The diagram, however, makes it possible to deduce the approximate relative positions of the curves in an ideal diagram of this type.

If curves for copper and iron were obtained at a temperature of 600° C, they evidently would be far to the left of the curves for the same metals at 200° C, and probably would be beyond the boundary of the diagram. They, therefore, would not cross the curve for ruthenium, but probably would cross the curves for tungsten and nickel. The previously discussed evidence that the initial rate of oxidation is higher for a chromium steel than for a carbon steel [10, 13, 16] indicates that the curve for 24.4-percent chromium steel in figure 18 would eventually cross a curve obtained with electrolytic iron at the same temperature, 600° C. This evidence, together with the course of the established portion of the curve, indicates that the leftward extension of the curve for 24.4-percent chromium steel in figure 18 is approximately correct. The curve thus crosses the curves for tungsten and nickel. A curve for chromium (not shown) probably would take about the same course. Similar evidence [10, 13, 16] suggests that the curve for silicon should take the indicated approximate course and should eventually cross a curve obtained with iron at the same temperature, 600° C.

In figure 19, each curve represents the variation of film thickness with temperature, for a constant oxidation time of 1,000 minutes. This diagram, therefore, represents directly the relative resistance of the indicated metals to oxidation. The courses of the established parts of the curves for nickel, tungsten, zinc, iron, and 24.4-percent chromium steel, together with other evidence previously mentioned, show that the extrapolated portion of the curve for 24.4-percent chromium steel takes the indicated approximate course, thus crossing the curves for the other four metals. There is little doubt, moreover, that the curve for the 24.4-percent chromium steel should cross, as indicated, the curves for lead and copper. A similar course probably would be taken by a curve for chromium. The curve for silicon, in view of the previously mentioned evidence that the initial rate of oxidation is higher for silicon steels than for iron, should extend rapidly to the right, as in figure 19, thus crossing the curves for ruthenium, nickel, tungsten, zinc, iron, lead, copper, and possibly chromium (not shown).

The established portion of the curve for ruthenium (fig. 19) suggests that this curve, with downward extension, remains to the left of the

other curves. A similar course would doubtless be taken by a curve for rhodium (not shown).

With sufficient downward extension, all the curves in figures 18 and 19 would probably reverse their curvature and approach a steep tangent at a film thickness of one atomic layer (about 1 A). In a diagram of the type shown in figure 18, the slope of the tangent probably would be 1.0, if ordinates represented the first powers of the film thickness. In the figure, this slope is indicated by the broken lines extending from the lower boundary.

At a film thickness corresponding to first-order blue, the curves in figure 19 are necessarily in the same relative positions as in figure 10. At a film thickness less than about 500 A, however, the curves in figure 19 are in very different relative positions. Silicon and 24.4-percent chromium steel, which have high resistance to oxidation at first-order blue, have low resistance at a film thickness of less than about 500 A. Copper and lead, which have relatively low resistance to oxidation at first-order blue, have high initial resistance. Ruthenium, the metal with the lowest affinity for oxygen, has the highest initial resistance to oxidation, and the resistance remains high throughout the range of interference colors. As stated in discussion of figure 10, such behavior would be expected when the affinity of a metal for oxygen is very low.

The evidence in figures 18 and 19 indicates that the initial rate of oxidation tends to be high or low according as the metal has high or low affinity for oxygen. Additional evidence, however, is needed to show whether the order of increasing affinity is the order of increasing initial rate of oxidation. The horizontal distance between the tangent to a curve at its origin, at a thickness of one atomic layer, and the asymptote finally approached by the curve evidently tends to increase with increase in the affinity of the metal for oxygen. (Compare the curves for silicon and copper in figs. 18 and 19.)

3. REASONS FOR THE COMPLEX VARIATION OF THE RATE OF OXIDATION WITH THE FILM THICKNESS

The complexity of the variation of the rate of oxidation with film thickness is shown by the reversals of the curves drawn with logarithmic coordinates in figures 18 and 19, and is strikingly revealed in diagram *A* of figure 21, in which the ordinates represent first powers of the film thickness. If all the curves in figure 21 (*A*) were extended downward far enough, they eventually would reverse their curvature. It is assumed, for reasons to be given, that they would approach a 45° tangent, as do the curves for copper and ruthenium. Such an initial slope of the curves implies an initial linear relation between film thickness and oxidation time. With upward extension, the slope of each curve decreases rapidly and traverses a minimum. The curves then approach asymptotes whose slope (0.5) is that of a quadratic parabola.

The fact that there is a minimum slope in the curves drawn with logarithmic coordinates does not mean that the rate of oxidation traverses a minimum. This is illustrated by the curves in figure 20 representing the oxidation of zinc at various temperatures. The curves in this figure, drawn with Cartesian coordinates, decrease continuously in slope. Comparison of these curves with the parabolas

in the figure, however, reveals the same complexity of form that is shown in figures 18 and 21. The possible reasons for this complexity will now be considered.

The complex variation of the rate of oxidation with film thickness evidently signifies a similarly complex variation of the rate of movement of ions and electrons through the oxide film. If the concentration of the metal ions in the film falls linearly from the value at the metal-film interface to zero at the film-air interface, the steepness of the concentration gradient would vary inversely as the film thickness. The rate of oxidation at any instant, therefore, would be

$$dy/dt = D/y, \tag{6}$$

in which D is the specific diffusivity, generally assumed to be a constant. This constant depends on the oxide, on the mobility of the ions, and on the temperature. By integration, this leads to the equation of the parabolic law,

$$y^2 = 2Dt + c, \tag{7}$$

in which c is a constant of integration.

The parabolic law operates only when the film has become so thick that the rate of oxidation is controlled by the rate of diffusion through the film. Before this condition is reached, the rate of oxidation would depend somewhat on the rate of transfer of ions across the metal-film interface. The rate of transfer across this interface probably is the controlling factor immediately after the formation of a single atomic layer of oxide. Both this factor and the influence of the rate of diffusion are represented in an equation developed by Evans [5]. This equation, developed before Wagner and coworkers [1 to 4, 18, 19, 20] showed that the dry oxidation of metals is an electrochemical process, is the same in form as an equation developed by Fischbeck [6, 7] as part of a general study of the rates of reaction of solids with gases.

The equation, with the symbols altered, is

$$dy/dt = E/(W_1 + W_D). \tag{8}$$

In this equation, E is proportional to the potential of the reaction (as measured by the free energy). W_1 represents the resistance to transfer of metal ions and electrons across the metal-film interface, and W_D is the resistance to diffusion through the film.[9] The resistance W_D depends both on the film thickness and on the mean resistivity, R, of the film. Consequently,

$$W_D = Ry, \tag{9}$$

in which R is the reciprocal of the specific diffusivity, D, assumed to be constant in the derivation of the parabolic law. By substitution, eq 8 becomes

$$dy/dt = E/(W_1 + Ry). \tag{10}$$

[9] It appears unnecessary here to divide W_1 into two components representing resistances at both interfaces.

When the film is so thick that W_1 is negligible in comparison with W_D, the equation becomes

$$dy/dt = E/Ry, \tag{11}$$

the equation of a quadratic parabola. When the film is so thin that W_D is negligible in comparison with W_1, the equation becomes

$$dy/dt = E/W_1, \tag{12}$$

the equation of a straight line. Plotted with logarithmic coordinates, it would have a slope 1.0. This equation, therefore, is the basis of the assumption in figures 18 and 21 that the tangent to a curve at a film thickness of one atomic layer has a slope 1.0 or 45°.

The actual curves in a diagram of the type shown in figures 18 and 21 (*A*), however, are very different from a curve derived from eq 10. By integration eq 10 becomes

$$t = \frac{1}{E}\left(W_1 y + \frac{Ry^2}{2}\right). \tag{13}$$

This equation evidently represents the superposition of the abscissas of a straight line and a quadratic parabola. In diagram *B* of figure 21, lines 1 and 2 represent a straight line and a quadratic parabola, respectively.[10] Superposition of corresponding abscissas (not their logarithms) of curves 1 and 2 results in curve 3. This curve starts tangent to a 45° line and approaches asymptotically a line whose slope is 0.5. As the curve has no reversal, however, it is very different from the curves shown in diagram *A*. All the curves of diagram *A*, if extended far enough downward, probably would be qualitatively similar to the curves for copper and ruthenium. At the lower ends they probably would have a 45° tangent; at the upper ends, they would approach a 0.5 slope. In this respect, they resemble curve 3 of diagram *B*. Between these two slopes, however, each of the curves in diagram *A* has a reversal. (In a curve for a metal with high affinity for oxygen, such as silicon, the abscissa range between the initial 45° slope and the asymptote is very great.) To account for this great difference in form between curve 3 of diagram *B* and the curves of diagram *A*, a modification must be made in the assumptions that are the basis of curve 3 and eq 13.

Equation 13 is based on the assumption that the resistance to transfer of ions and electrons through the oxide film can be expressed as the product of the film thickness and a resistivity, *R*, independent of the film thickness. The complexity of the curves in figure 21 (*A*), however, makes it necessary to abandon the assumption of a constant resistivity. Whatever may be the interpretation in terms of fundamental factors, the variation of the rate of oxidation with the film thickness may be expressed in terms of a variation of the resistivity with the film thickness. On this assumption, the term Ry in eq 10 would become

$$\int R dy.$$

[10] The relative positions of these two lines depend on the chosen values of the constants, E, W_1, and R.

A curve representing qualitatively the probable relation between R and y is shown in figure 21 (C). The area underneath the curve, between abscissas zero and y, is

$$\int R dy.$$

The mean value, M, of R between these limits is

$$(\int R dy)/y.$$

The variation of M with y (fig. 21, C) evidently is qualitatively similar to the variation of R. From eq 10, therefore, may be derived

$$dy/dt = E/(W_1 + My). \tag{14}$$

In order that eq 14 may give a curve of the form of those shown in figure 21 (A), R (or M) must increase with y as represented qualitatively by the curve in figure 21 (C); the greater part of the increase of R must be within a relatively narrow range of y. The reversal of curvature of R is at about the same film thickness as the reversal of a curve of the type shown in figure 21 (A). Near the origin of the curve in figure 21 (C), the value of R is only about 2 percent of the asymptotic value approached after the reversal of curvature. A similar curve, except that the initial value of R is only 1 percent of the asymptotic value, has been used in the construction of curve 6 of figure 21 (B). Curve 6 is obtained by superposition of the corresponding abscissas of curves 4 and 5.

This synthetic curve is qualitatively similar to the curves in figures 18 and 21 (A). It resembles most closely the curves for ruthenium and copper in figure 21 (A). To make such a synthetic curve resemble a curve for a metal with high affinity for oxygen (such as silicon), however, the ratio of the initial value of R to the asymptotic value must be much less than 1 percent. For some metals, the ratio evidently may be of the order of 10^{-6} or less.

The resistivity of the oxide film, therefore, is not constant, but increases first at an increasing, then at a decreasing rate. After a relatively abrupt increase within a narrow range of film thickness, the resistivity approaches a constant value. Beyond this range of rapid increase of resistance, consequently, the growth of the film is approximately in accordance with the parabolic law.

In expressing the complex variation of the rate of oxidation in terms of a variation of the resistivity, there is no intention to attribute the variation of the resistivity to any particular variable, such as electrical resistance. The evidence merely indicates that a film behaves as if its resistivity to the transfer of ions and electrons varies in the manner described. The authors have found no entirely satisfactory theory to account for this variation. According to Mott [11, 12], the rate of oxidation is determined by a quantum mechanical "tunneling" of electrons up to a thickness of about 50 A; at this thickness, the tunneling is stopped by the electrostatic attraction between the metal and electrons. His theory calls for an approach to an exponential relationship at a film thickness of about 50 A at room temperature. According to Lustman and Mehl [9], however,

this theory would not satisfactorily account for the large effect of temperature on the rate of oxidation. This objection to Mott's theory is illustrated by the curves for zinc in figure 20. At 200° C, the curve becomes nearly horizontal at an air-equivalent thickness of more than 2,000 A (about 1,000 A actual thickness if corrected for index of refraction), whereas Mott's curve for aluminum at room temperature becomes nearly horizontal at only 50 A.

The curves in figure 21 (*A*) apparently give little basis for the assumption of an exponential relationship. Moreover, they give no support to the conclusion of Lustman and Mehl [9] that this region can be represented by two successive exponential curves.

It is possible that the rapid increase in resistivity within a narrow range of film thickness is due to a change of lattice structure.

The authors hope that the evidence presented in this paper will stimulate further investigation of the fundamental factors responsible for the complex variation of the rate of oxidation with the film thickness.

VIII. SUMMARY

An investigation has been made of the rate of oxidation of 18 nonferrous metals by means of the interference colors of oxide films. With eight of these metals complete diagrams were obtained; with seven metals the approximate forms and positions of the graphs were obtained for interference colors of the first order; with three metals, only the approximate positions of the graphs were obtained. A comparison is made between the results obtained with these metals and with typical steels.

The diagrams obtained with these nonferrous metals are similar to those obtained with steels [10]. For a constant film thickness, the relation between temperature and oxidation time is linear when plotted with logarithmic coordinates. The variation of the film thickness either with time at constant temperature or with temperature for constant oxidation time, when plotted with logarithmic coordinates, is represented by a reversed curve. When plotted with Cartesian coordinates, the variation of film thickness with time at constant temperature is represented by a curve without reversal; this is a complex curve becoming approximately parabolic at the upper end.

An attempt is made to correlate the forms and positions of the curves with the affinities of the metals for oxygen, with the resistances at the metal-oxide interface, and with the resistivity of the oxide film. The variation of the rate of oxidation with the film thickness is such that it may be expressed in terms of an assumed variation of the resistivity with the film thickness. This means merely that the film behaves as if its resistivity (not necessarily its electrical resistance) varies in the manner described.

IX. REFERENCES

[1] H. H. Baumback and C. Wagner, *Die elektrische Leitfähigkeit von Zinkoxyde und Cadmiumoxyd*, Z. physik. Chem. [B] **22**, 199–211 (1933).

[2] H. H. Baumback, H. Dünwald, and C. Wagner, *Leitfähigkeitsmessungen an Kupferoxyde*, Z. physik. Chem. [B], **22**, 226–230 (1933).

[3] H. Dünwald and C. Wagner, *Die Natur der elektrischen Leitfähigkeit von Kupferoxydul*, Z. physik. Chem. [B] **17**, 467–470 (1932).

[4] H. Dünwald and C. Wagner, *Untersuchungen über Fehlordnungserscheinungen in Kupferoxydul und deren Einfluss auf die elektrischen Eigenschaften*, Z. physik. Chem. [B] **22,** 212–225 (1933).
[5] U. R. Evans, *The relation between tarnishing and corrosion*, Trans. Am. Electrochem. Soc. **46,** 247–272 (1924).
[6] K. Fischbeck, *Über das Reaktionsvermogen der festen Stoffe*, Z. Elektrochemie **39,** 316–330 (1933).
[7] K. Fischbeck, L. Neundeubel, and F. Salzer-Tubingen, *Über das Reaktionsvermögen von Kristallarten*, Z. Electrochemie **40,** 517–522 (1934).
[8] K. W. Fröhlich, *Die Zunderung von reinen und von legierten Kupfer*, Z. Metallkunde **28,** 368–375 (1936).
[9] B. Lustman and R. F. Mehl, *Low temperature oxidation of single crystals of copper*, Metals Tech. **8,** T. P. 1317 (1941).
[10] D. J. McAdam, Jr., and G. W. Geil, *Rate of oxidation of steels as determined from interference colors of oxide films*, J. Research NBS **23,** 63–124 (1939) RP1221.
[11] N. F. Mott, *A theory of the formation of protective oxide films on metals*, Trans. Faraday Soc. **35,** 1175–1177 (1939).
[12] N. F. Mott, *The theory of the formation of protective oxide films on metals*, Trans. Faraday Soc. **36,** 472–483 (1940).
[13] A. M. Portevin, E. Prétet, and H. Jolivet, *Contribution to the study of the chemical resistance of various special steels*, J. Iron Steel Inst. (London) **130,** 219–277 (1934).
[14] L. E. Price, *Recent German advances in the mechanism of oxidation and tarnishing of metals*, Chemistry & Industry (J. Soc. Chem. Ind.) **15,** 769–773 (1937).
[15] E. Scheil, *Über das Zundern von Metallen und Legierungen*, Z. Metallkunde **29,** 209–214 (1937).
[16] E. Scheil and K. Kiwit, *Einfluss von Legierungs Zusätzen auf das Zundern des Eisens*, Arch. Eisenhüttenw. **9,** 405–416 (1936).
[17] W. H. J. Vernon, E. I. Akeroyd, and E. G. Stroud, *The direct oxidation of zinc*, J. Inst. Metals **6,** 253–281 (1939).
[18] C. Wagner, *Theorie der geordneten Mischphasen, III*, Z. physik. Chem. [B], **22,** 181–194 (1933).
[19] C. Wagner, *Theorie der Thermoketten von Halbleiterkombinationen*, Z. physik. Chem. [B], **22,** 195–198 (1933).
[20] C. Wagner and W. Schottky, *Theorie der geordneten Mischphasen*, Z. physik. Chem. [B], **11,** 163–210 (1930).

TABLE 1.—*Values for constants n and h, representing, respectively, the variation of oxidation time with temperature for constant film thickness, and the variation of film thickness with temperature for constant oxidation time*

Material	*n*								*h*	
	First-order—			Second-order—			Third-order blue	Fourth-order blue	Values from figures 15 and 16	$h=mn$ $(m=0.5)$
	Straw	Brown	Blue	Straw	Brown	Blue				
Nickel	25	35	36	-------	36	36	36	-------	18	18
Tungsten	25	27	28	-------	29	29	30	31	15	15
Zinc	23	29	33	-------	40	43	-------	-------	20	21.5
Lead	29	29	29	-------	-------	29	-------	-------	18	14.5
Silicon	-------	23	23	-------	23	23	23	23	11	11.5
Copper	-------	26	26	26	26	26	26	-------	16	13
Ruthenium	24	26	27	-------	-------	-------	-------	-------	-------	13.5
Vanadium	26	31	33	-------	34	35	35	-------	-------	17.5
Electrolytic iron*	30	30	31	34	36	38	40	-------	18	20
13.6% Cr steel*	32	32	32	33	33	33	-------	-------	18	16.5
24.4% Cr steel*	23	33	34	35	36	36	36	-------	22	19

* Table 2 and figures 27 and 28 of previous paper [10].

TABLE 2.—*Thermochemical and physical properties of metallic oxides*

Material	Heat of formation per gram atom of oxygen at 18° C	Entropy per gram atom of oxygen at 25° C	Free energy of formation per gram atom of oxygen			Order[a] of graphs in figure 10		Index of refraction, μ	Volume per gram atom of oxygen, V	Correction factors for position of graphs in figure 10			Melting point of—		Boiling point of metal
			At 25° C	At 427° C	At indicated temperatures	At 100 minutes	At 10^4 minutes			Factor[b] for μ	Factor[c] for V	Product of factors for μ and V	Oxide	Metal	
1	2	3	4	5	6	7	8	9	10	11	12	13	14	15	16
	kg-cal	*cal*	*kg-cal*	*kg-cal*	*kg-cal*				*cm*^{3}				°*C*	°*C*	°*C*
ZrO_2	129.0					14	15	2.2	10.8	1.00	1.03	1.03	2,700	1,900	>2,900
Al_2O_3	126.7	4.2	−125.5			5	5	1.8	8.5	0.82	0.81	0.66	2,050	658.7	1,800
V_2O_3	110.0	7.8	−104			11	9		10.3		.98	.98	1,970	1,720	3,000
SiO_2	101.7	5.0	−95.2	−86	−82(625°)	1	1	1.5	11.3	.68	1.08	.73	1,470	1,420	2,600
Ta_2O_5	99.8	6.8				7	7		10.1		0.96	.96		2,850	>4,100
MnO	96.5	14.4	−92.3			16	17	2.2	13.0	1.00	1.24	1.24	1,650	1,260	1,900
Cr_2O_3	91.0	6.5	−84.5	−78	−76(575°)	2	2	2.5	9.7	1.14	0.92	1.05	1,990	1,615	2,200
Cb_2O_5	88.4					13	14		11.9		1.13	1.13	1,520	1,950	2,900
ZnO	83.5	10.4	−76.3	−67	−69(325°)	9	8	2.0	14.5	0.91	1.38	1.26	>1,800	419.5	907
Fe_2O_3	66.2	7.2	−60.0	−53	−56(225°)	17	16	3.2	10.1	1.45	0.96	1.39	1,565	1,535	
WO_3	65.2	6.1	−58.9	−51	−53(325°)	10	11	[d]2.1	10.8	0.95	1.03	0.98	1,473	3,370	5,900
CdO	65.2	13.1	−61.4			12	12	2.5	18.5	1.14	1.76	2.00	>1,426	320.9	767
MoO_3	65.0					8	10		14.2		1.35	1.35		2,620	3,700
NiO	58.4	9.0	−51.6	−43	−44(375°)	6	6	2.2	10.0	1.00	0.95	0.95	2,090	1,452	2,900
CoO	57.5	14.5	−53.3			15	13		14.1		1.34	1.34		1,480	2,900
PbO	52.0	16.6	−44.9		−42(150°)	18	18	2.5	23.5	1.14	2.24	2.55	888	327.4	1,620
Cu_2O	42.5	24.1	−35.0			19	19	2.7	23.9	1.23	2.28	2.80	1,235	1,083	2,300
RuO_2	26.3					3	3		9.6		0.91	0.91		2,450	4,150
Rh_2O	21.0					4	4							1,985	>2,500

[a] Order according to temperature required to produce an oxide film yielding the first blue interference color.

[b] Corrected to a value of 2.2 for μ.

[c] Corrected to a value of 10.5 for V.

[d] Value for $WO_3.H_2O$.

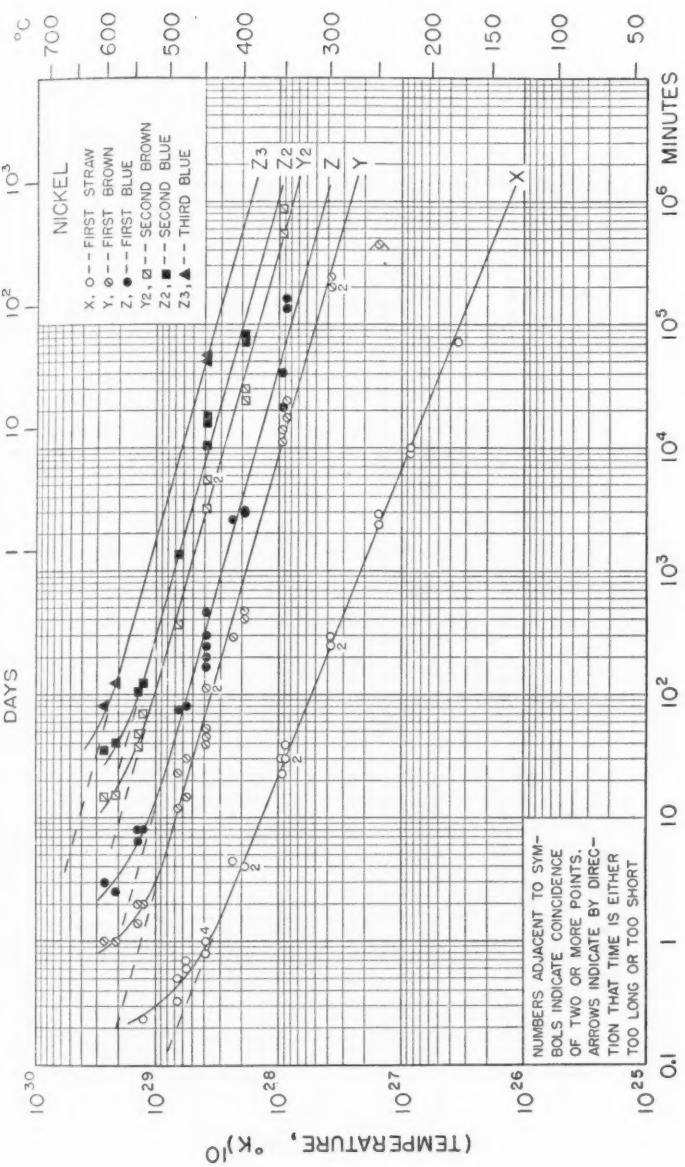
NICKEL
X, ○ -- FIRST STRAW
Y, ⊘ -- FIRST BROWN
Z, ● -- FIRST BLUE
Y2, ⊡ -- SECOND BROWN
Z2, ■ -- SECOND BLUE
Z3, ▲ -- THIRD BLUE
NUMBERS ADJACENT TO SYMBOLS INDICATE COINCIDENCE OF TWO OR MORE POINTS. ARROWS INDICATE BY DIRECTION THAT TIME IS EITHER TOO LONG OR TOO SHORT
DAYS
TIME
MINUTES
°C
(TEMPERATURE, °K)10

FIGURE 1.—*Influence of temperature on the oxidation time of nickel.*

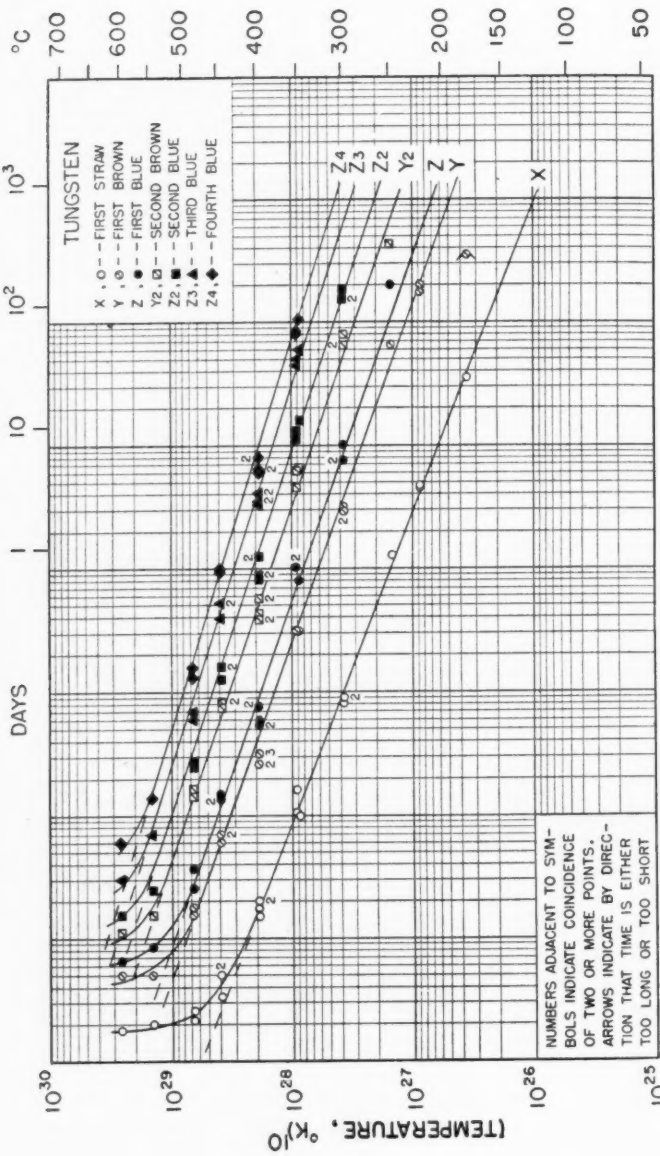

FIGURE 2.—*Influence of temperature on the oxidation time of tungsten.*

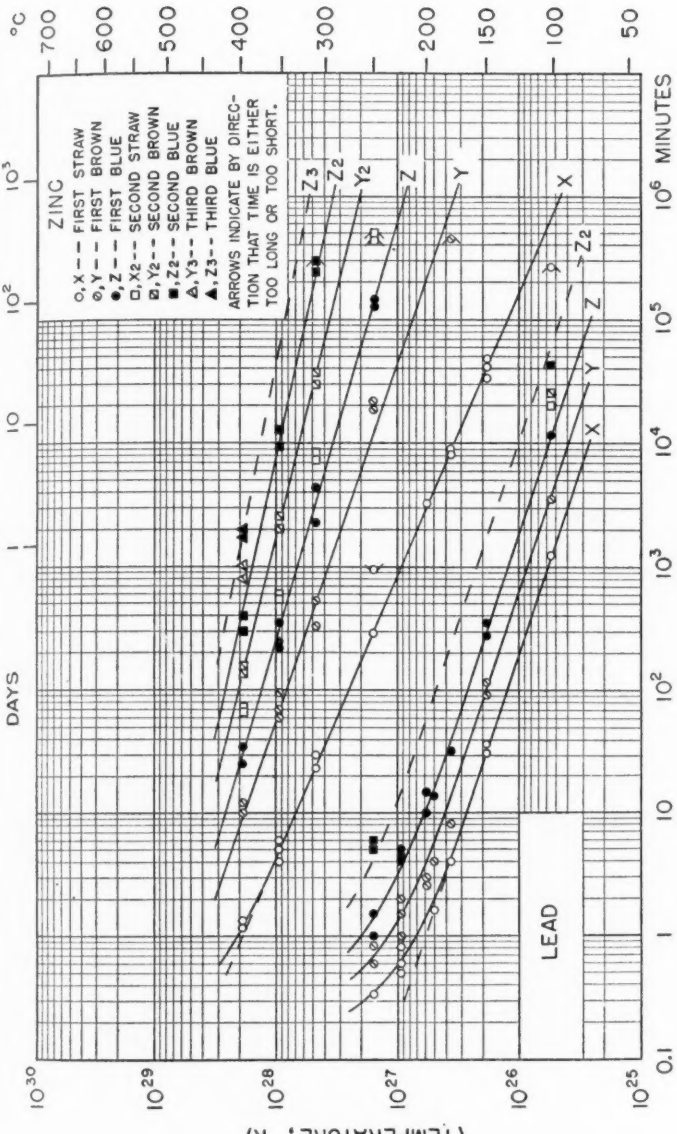

FIGURE 3.—*Influence of temperature on the oxidation time of zinc and lead.*

FIGURE 2.—*Influence of temperature on the oxidation time of tungsten.*

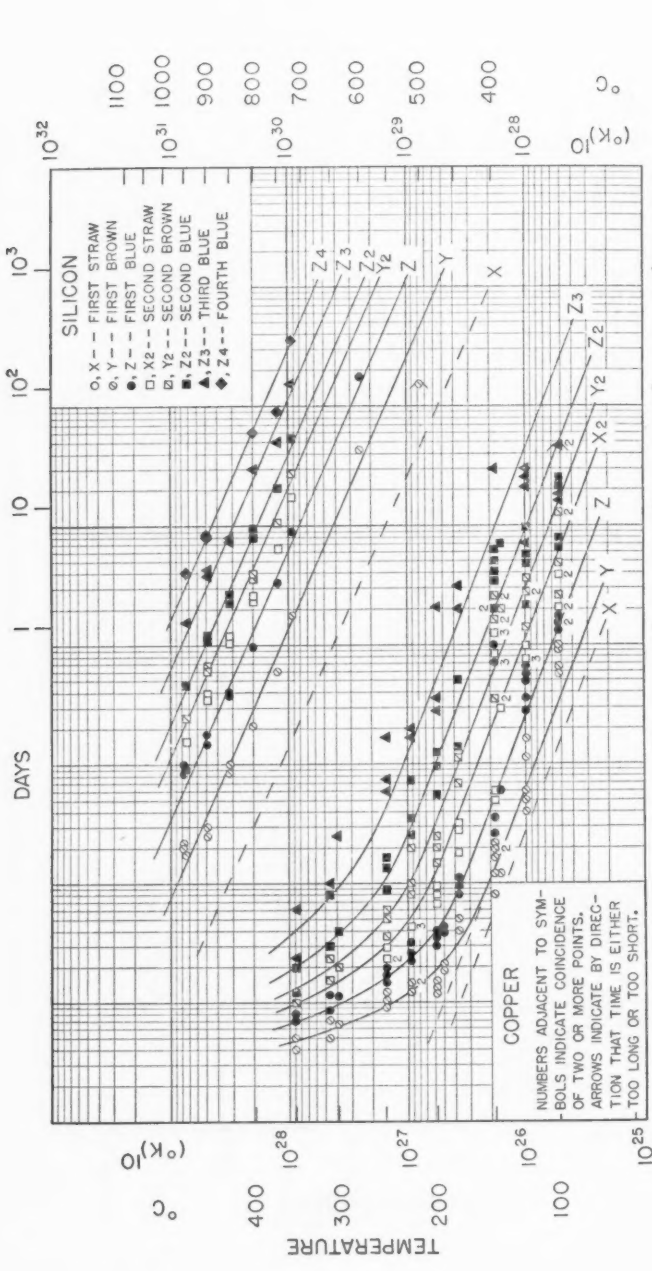

FIGURE 4.—*Influence of temperature on the oxidation time of silicon and copper.*

FIGURE 4.—*Influence of temperature on the oxidation time of silicon and copper.*

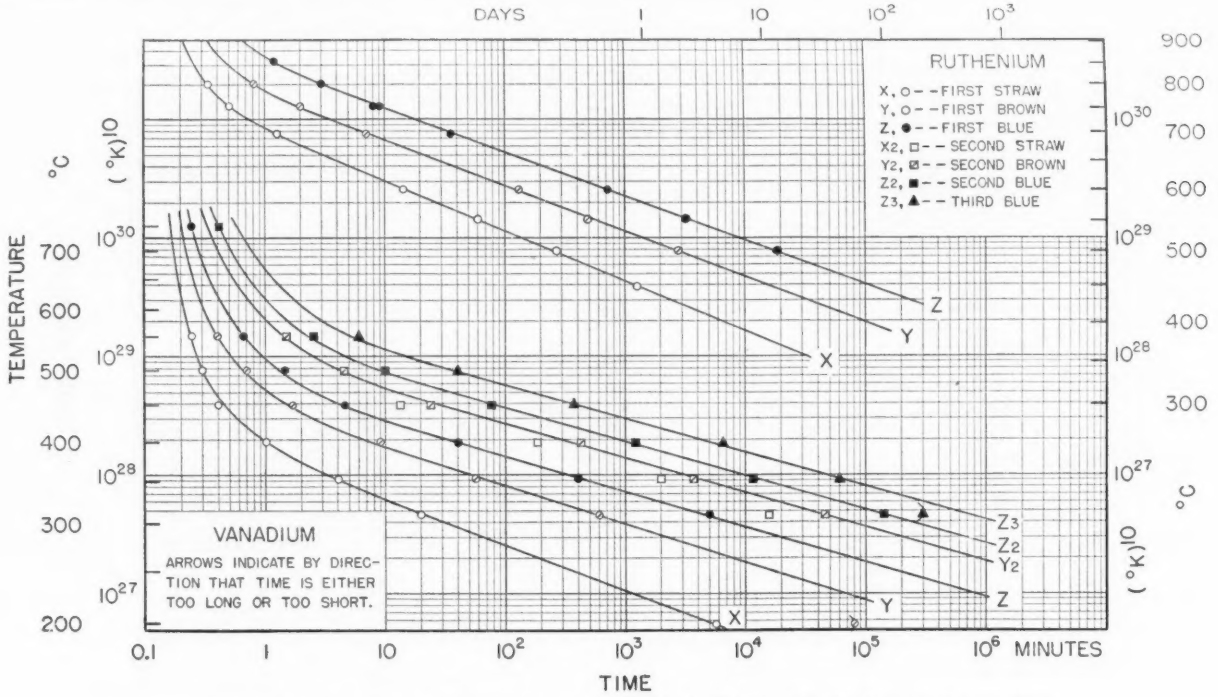

FIGURE 5.—*Influence of temperature on the oxidation time of ruthenium and vanadium.*

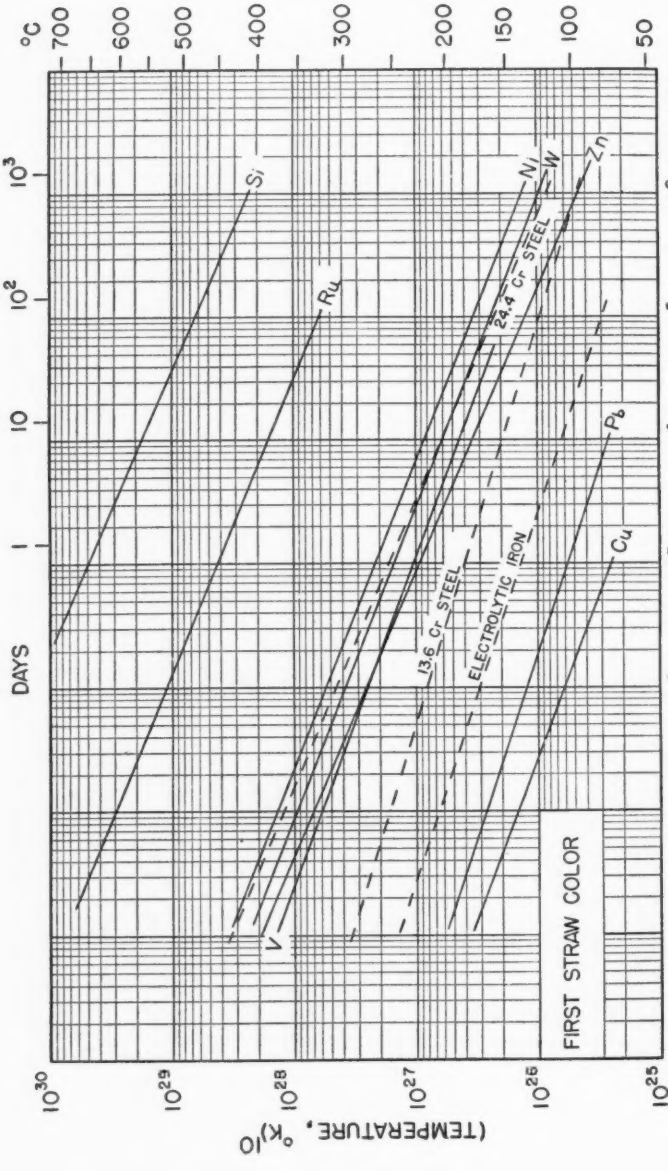

FIGURE 6.—*Influence of temperature on the oxidation time; comparison of graphs for first-order straw color.*

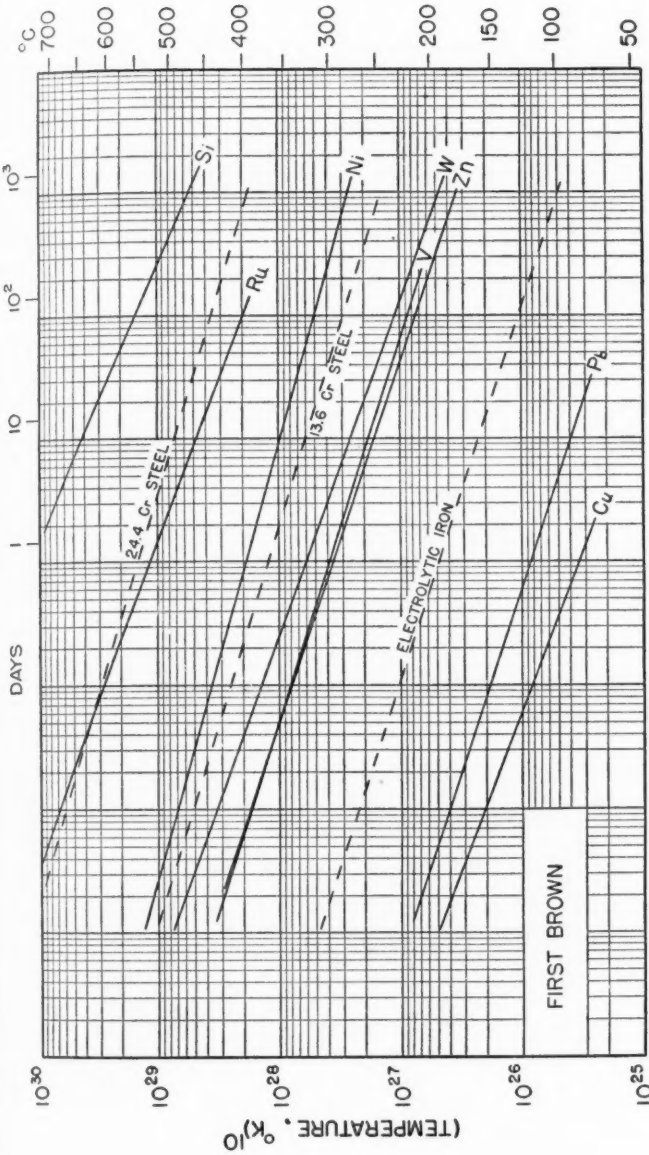

FIGURE 7.—*Influence of temperature on the oxidation time; comparison of graphs for first-order brown.*

FIGURE 6.—*Influence of temperature on the oxidation time; comparison of graphs for first-order straw color.*

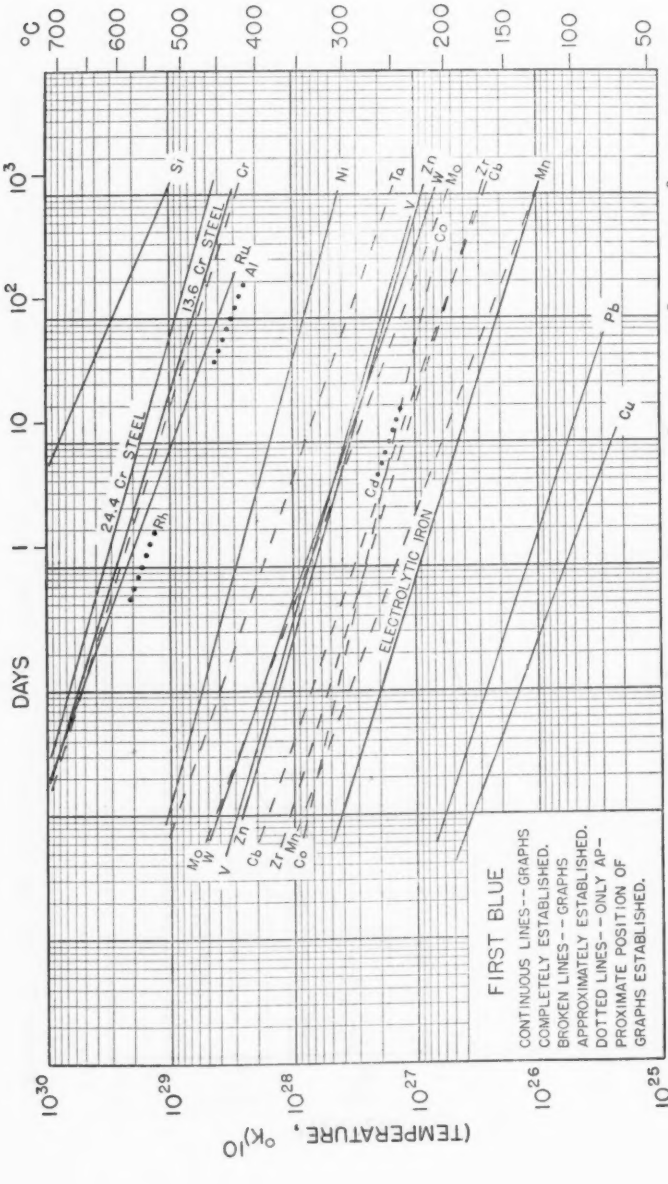

FIGURE 8.—*Influence of temperature on the oxidation time; comparison of graphs for first-order blue.*

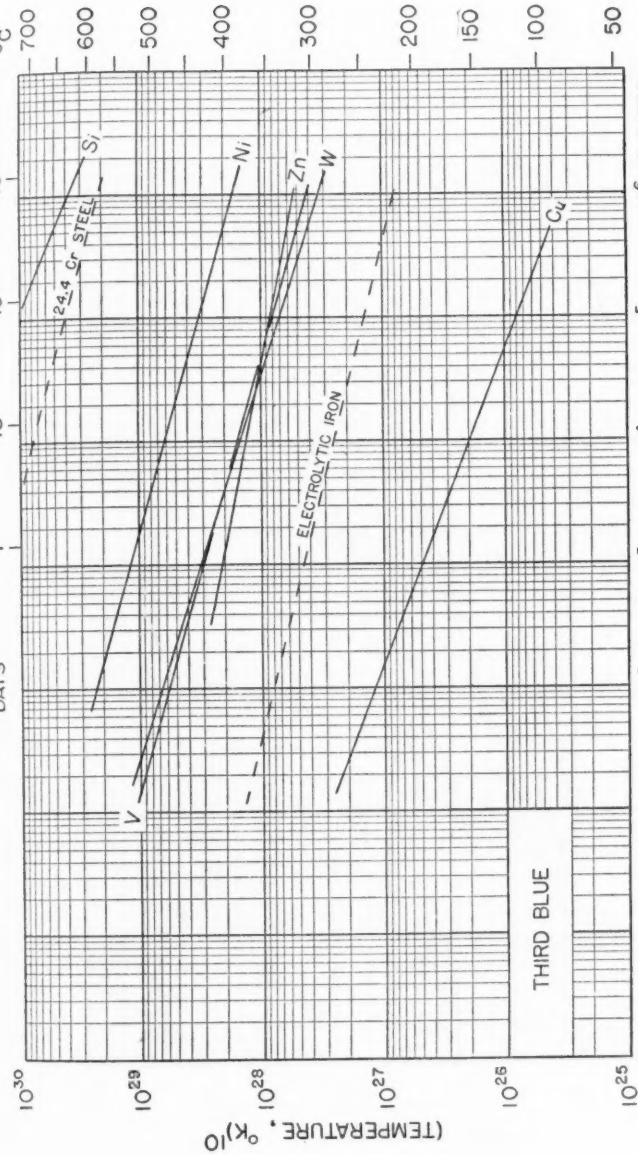

FIGURE 9.—*Influence of temperature on the oxidation time; comparison of graphs for third-order blue.*

FIGURE 8.—*Influence of temperature on the oxidation time; comparison of graphs for first-order blue.*

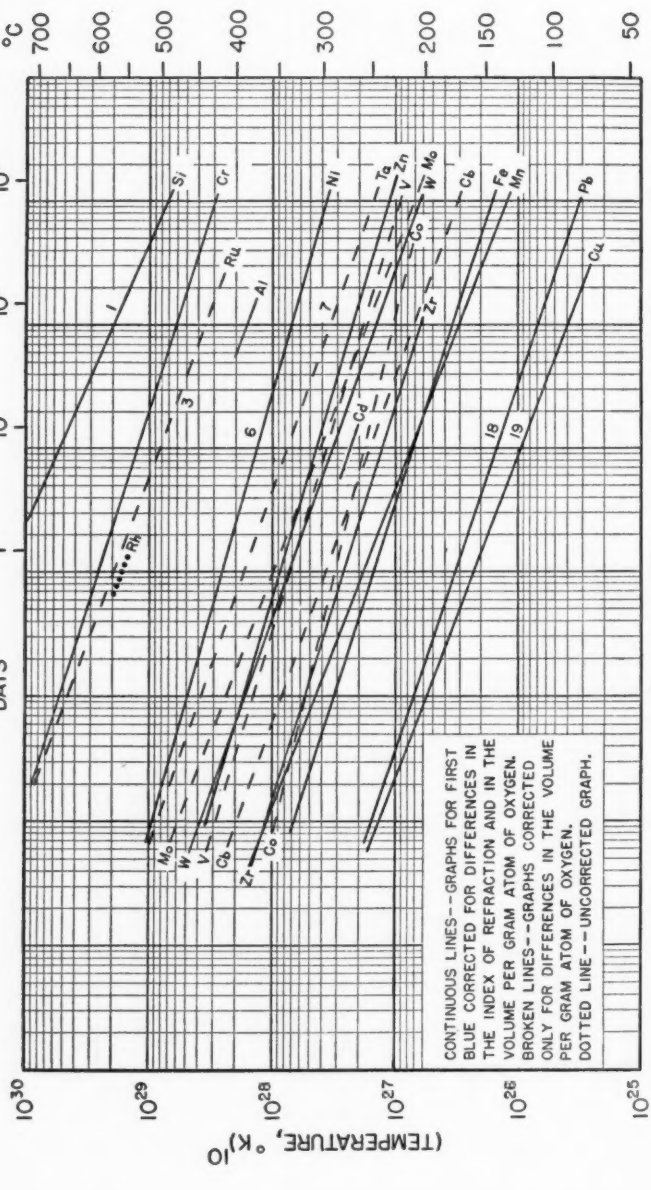

FIGURE 10.—*Influence of temperature on the oxidation time; comparison of graphs for first-order blue corrected for differences in the index of refraction and in the volume per gram atom of oxygen.*

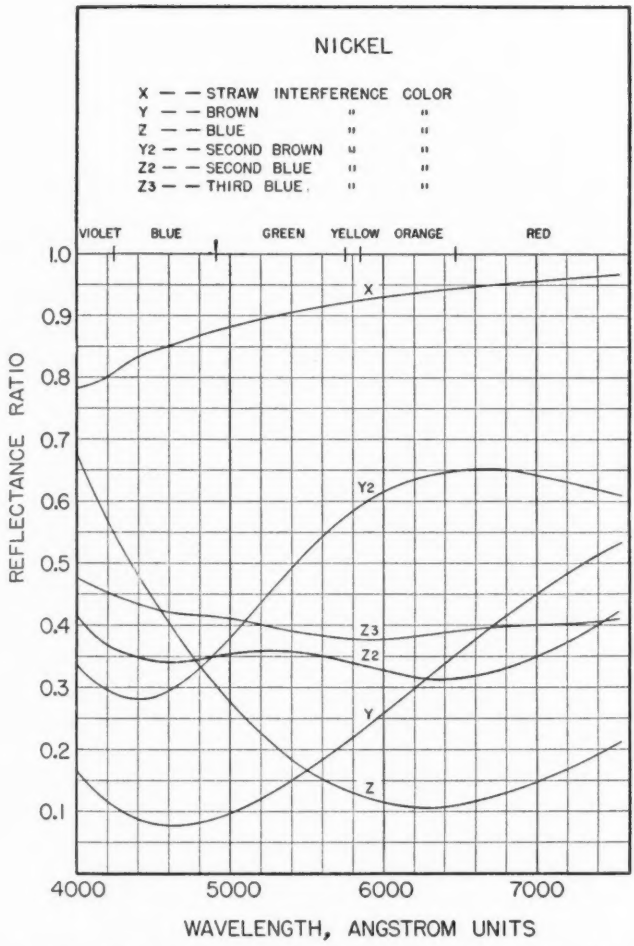

FIGURE 11.—*Variation of reflectance ratio with wavelength for interference colors on nickel.*

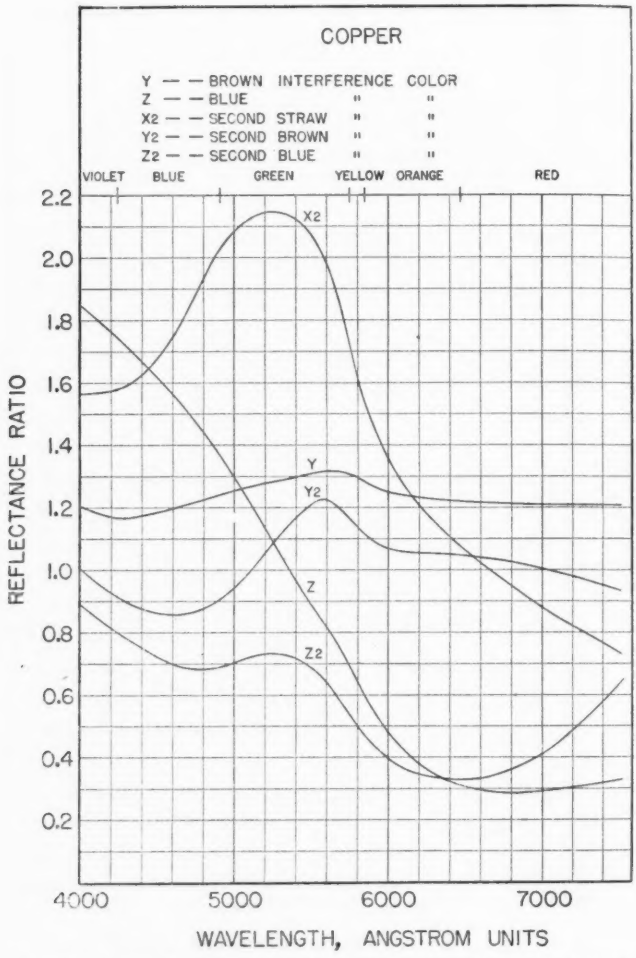

FIGURE 12.—*Variation of reflectance ratio with wavelength for interference colors on copper.*

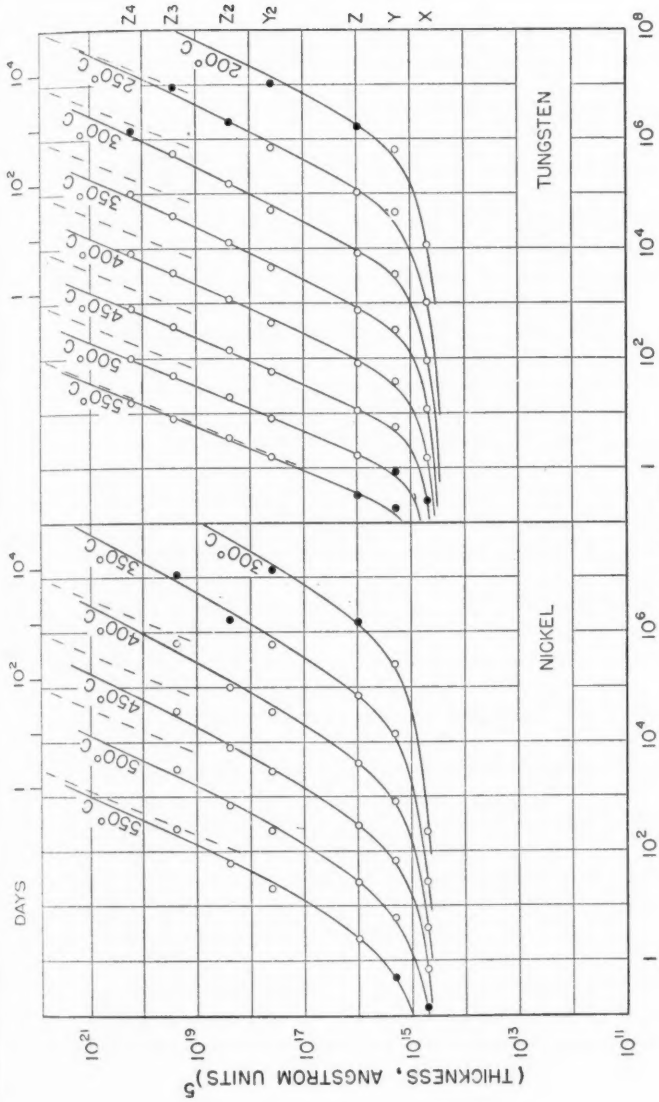

FIGURE 13.—*Variation of air-equivalent thickness of oxide film with time; nickel and tungsten.*

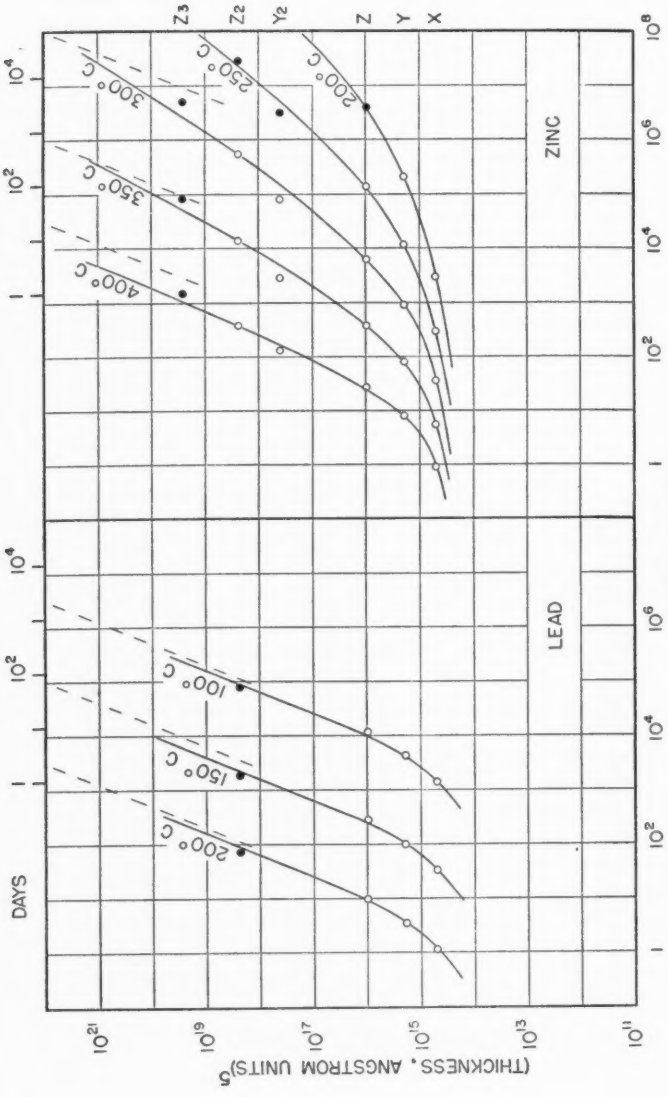

FIGURE 14.—*Variation of air-equivalent thickness of oxide film with time; lead and zinc.*

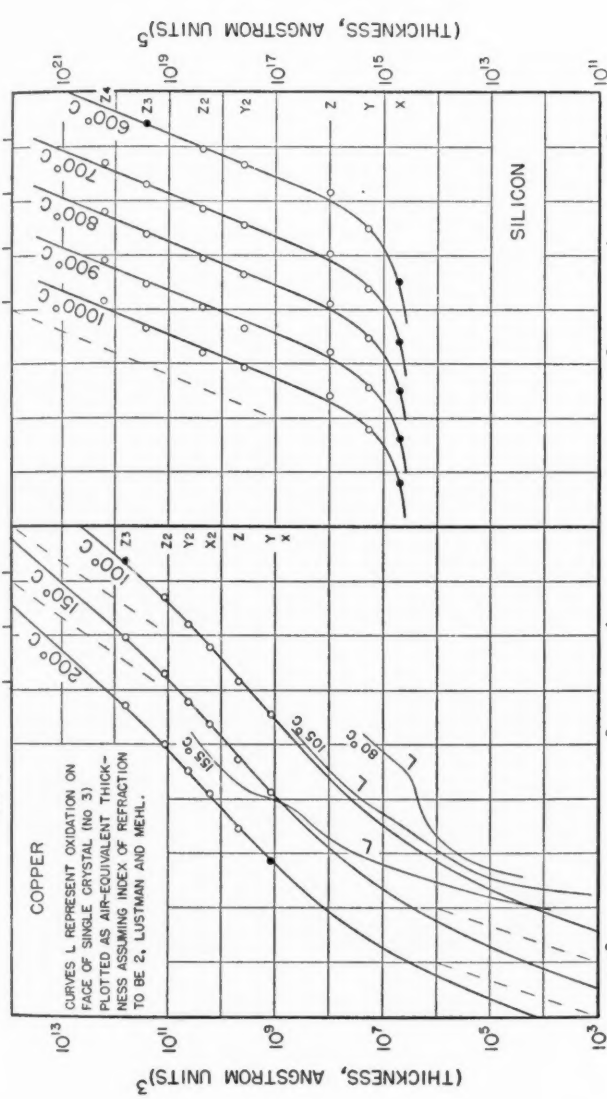
COPPER
CURVES L REPRESENT OXIDATION ON FACE OF SINGLE CRYSTAL (No 3) PLOTTED AS AIR-EQUIVALENT THICKNESS ASSUMING INDEX OF REFRACTION TO BE 2, LUSTMAN AND MEHL.
SILICON
DAYS
TIME, MINUTES
(THICKNESS, ANGSTROM UNITS)³
(THICKNESS, ANGSTROM UNITS)⁵

FIGURE 15.—*Variation of air-equivalent thickness of oxide film with time; copper and silicon.*

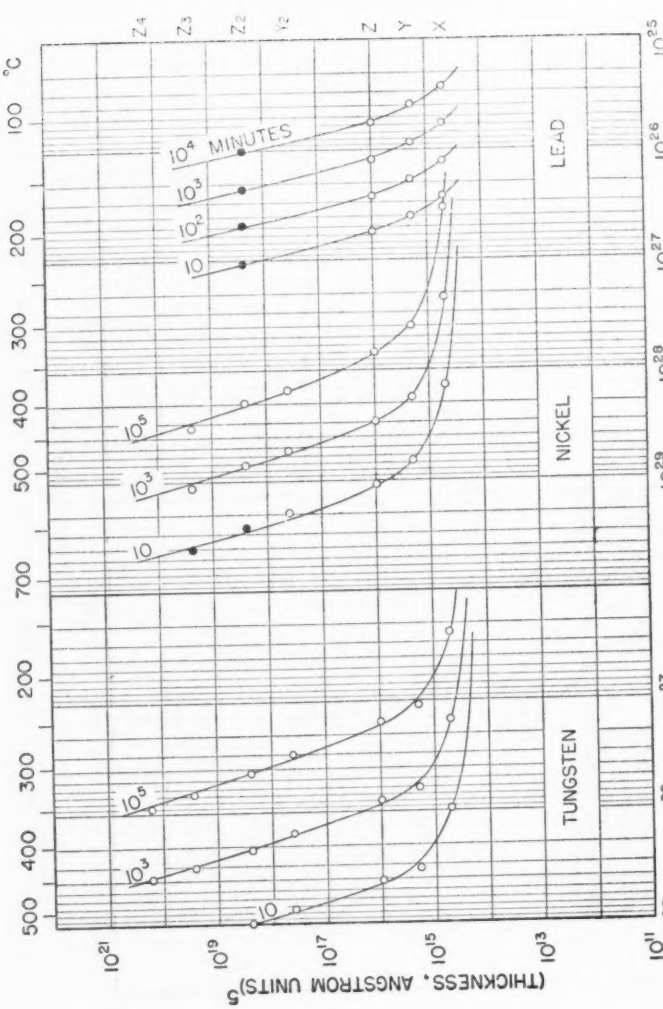

FIGURE 16.—*Variation of air-equivalent thickness of oxide film with temperature; tungsten, nickel, and lead.*

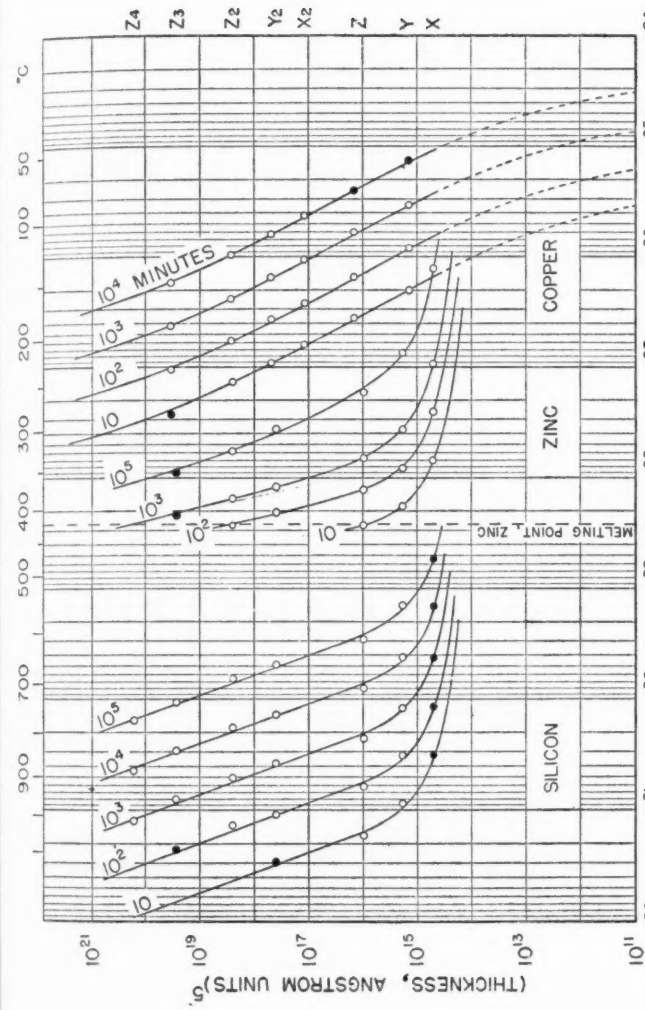

FIGURE 17.—*Variation of air-equivalent thickness of oxide film with temperature; silicon, zinc, and copper.*

FIGURE 16.—*Variation of air-equivalent thickness of oxide film with temperature; tungsten, nickel, and lead.*

451601—42——5

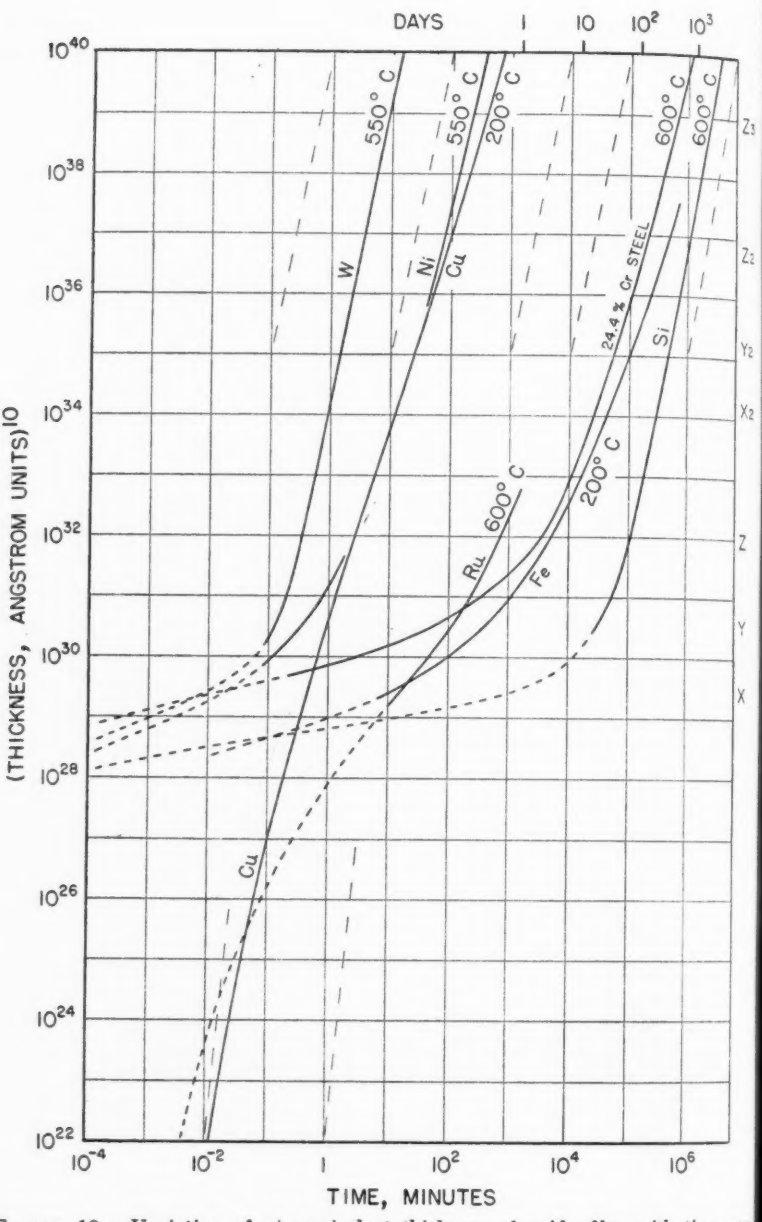

FIGURE 18.—*Variation of air-equivalent thickness of oxide film with time; comparison of curves for typical nonferrous metals and steels.*

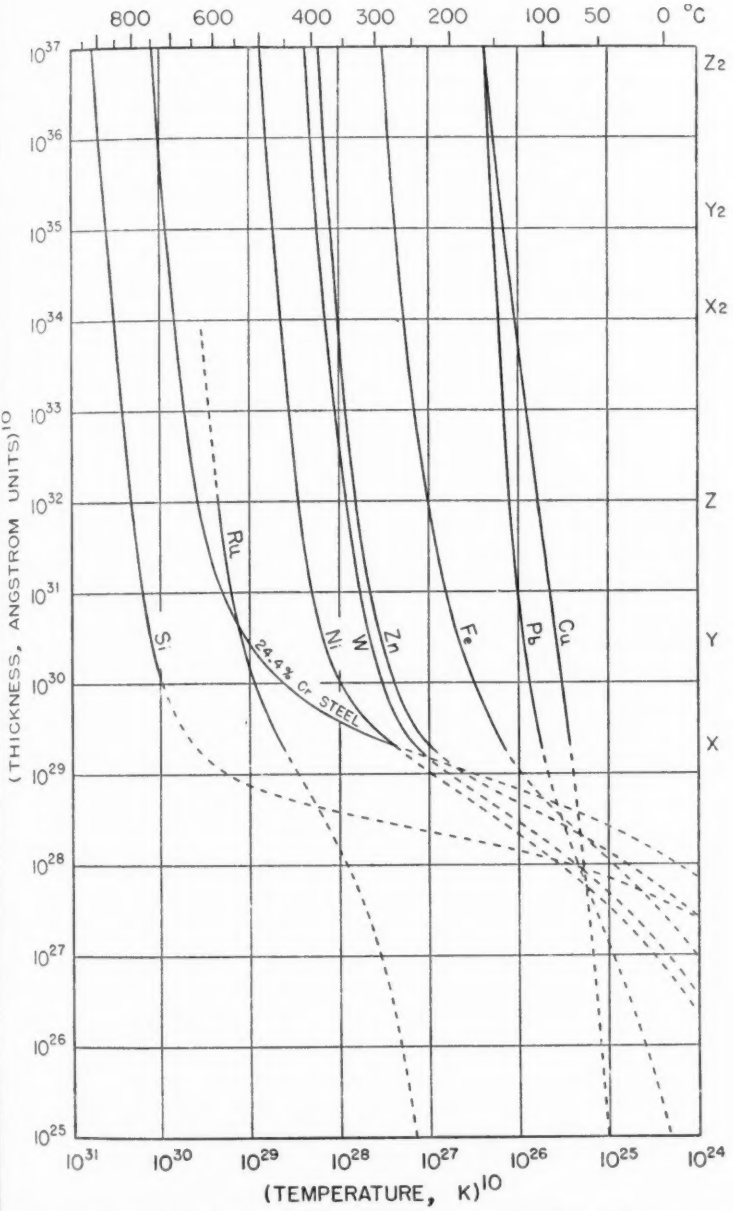

FIGURE 19.—*Variation of air-equivalent thickness of oxide film with temperature, for a constant oxidation time of 1,000 minutes; typical nonferrous metals and steels.*

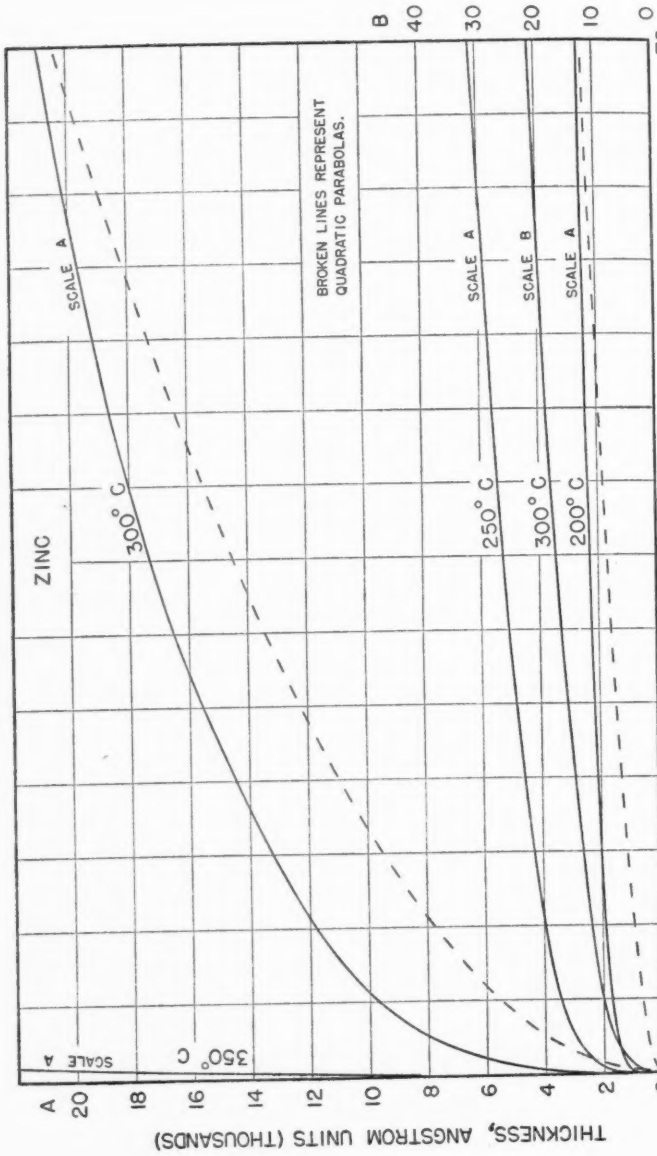

FIGURE 20.—*Variation of air-equivalent thickness of oxide film with time; typical curves for zinc.*

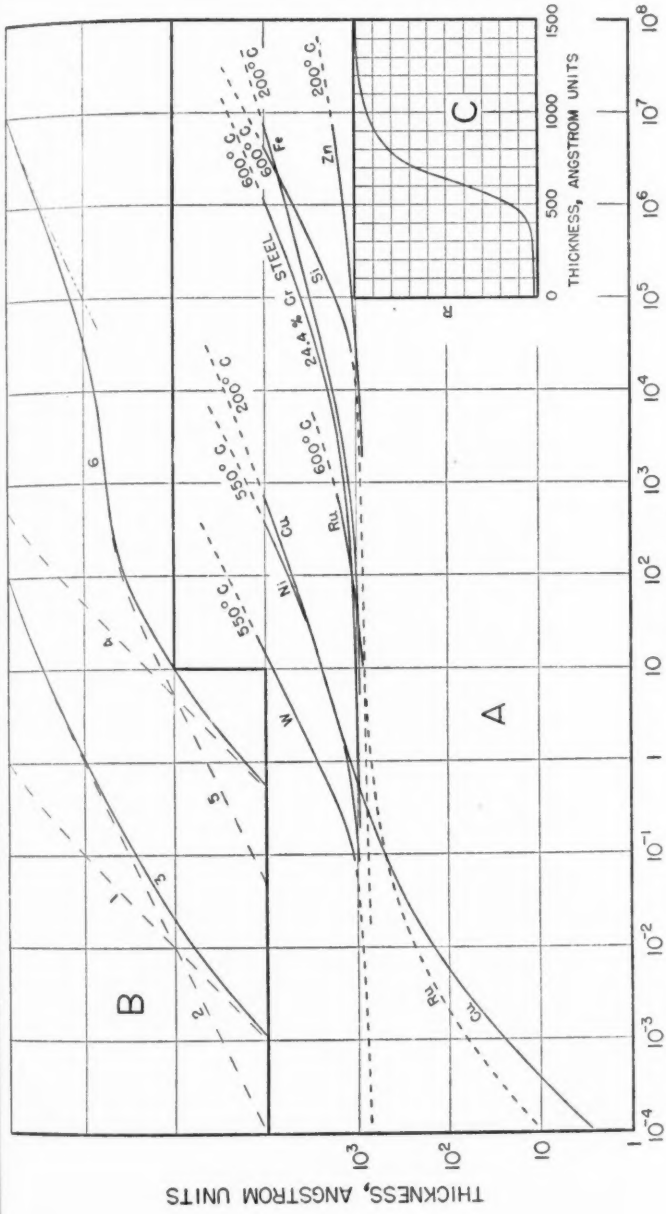

FIGURE 21.—*Actual and theoretical variation of air-equivalent thickness of oxide film with time.*

FIGURE 20.—*Variation of air-equivalent thickness of oxide film with time; typical curves for zinc.*

WASHINGTON, February 17, 1942.

U. S. Department of Commerce National Bureau of Standards

RESEARCH PAPER RP1471

Part of Journal of Research of the National Bureau of Standards, Volume 28, May 1942

IMPROVED INSTRUMENT FOR MEASURING THE AIR PERMEABILITY OF FABRICS

By Herbert F. Schiefer and Paul M. Boyland

ABSTRACT

This paper describes a new model of an instrument for the direct measurement of the air permeability of fabrics. The air, which is drawn through the fabric by a given suction, is measured with orifice-type flowmeters. The instrument is mounted in the top of a table and a new clamping device is provided, which permit measurements to be made rapidly on any part of a large piece of cloth without cutting.

The calibration and operation of the instrument are discussed. Results of measurements on two very different types of fabrics—parachute cloth and blankets—are given for several methods of clamping. A suitable method is described for which the edge leakage is negligible. The random sampling error of the average of 5 tests for air permeability is less than 5 percent approximately 9 times out of 10.

CONTENTS

	Page
I. Introduction	637
II. Description of the new instrument and its operation	637
III. Calibration	639
1. Inclined manometer	639
2. Orifices for measuring air flow	639
IV. Results	640

I. INTRODUCTION

Since publication of a description of the portable instrument for measuring air permeability of fabrics,[1] the instrument has been improved in a number of ways. It has been mounted on a table and provided with clamps which permit the testing of any part of a piece of cloth without cutting.[2] The duplicability of tests, the variability of air permeability within fabrics, and the effect of the method of clamping have been investigated. The new model is described in this paper, the calibration is discussed, and the results of work with it are given.

II. DESCRIPTION OF THE NEW INSTRUMENT AND ITS OPERATION

The instrument, before the fabric is inserted for a test, is shown in figure 1. Figure 2 shows the instrument during a test, and figure 3

[1] BS J. Research **6**, 51–58 (1931) RP261.

[2] W. H. Dietrich, chief engineer, Duplan Corporation, Hazelton, Pa., and S. W. Frazier, 953 Fifteenth Street SE., Washington, D. C., made important contributions toward the development of the table-mounted air-permeability instrument.

indicates the essential parts diagrammatically. The orifice over which the fabric is placed is mounted in the top of a table. The area of the opening is 0.0412 ft², the same as in the older model (see footnote 1). A ring weighing 3 lb and having a beveled surface with an inside diameter of 5 in. fits over a similar beveled surface of the orifice rim. The beveled ring is placed over the fabric to hold it across the orifice in a smooth condition and with a slight tension in all directions. This ring is applicable to the testing of fabrics as thick as blankets and as thin as parachute cloth. It can be dispensed with in testing fabrics which are stiff enough to remain flat when placed over the orifice.

The clamp for holding the fabric against the orifice is pivoted in its supporting frame so that it will press uniformly against the upper surface of the orifice. The frame is hinged at the back of the table and locks at the front. It can be raised to permit cloth to be drawn from a bolt across the orifice.

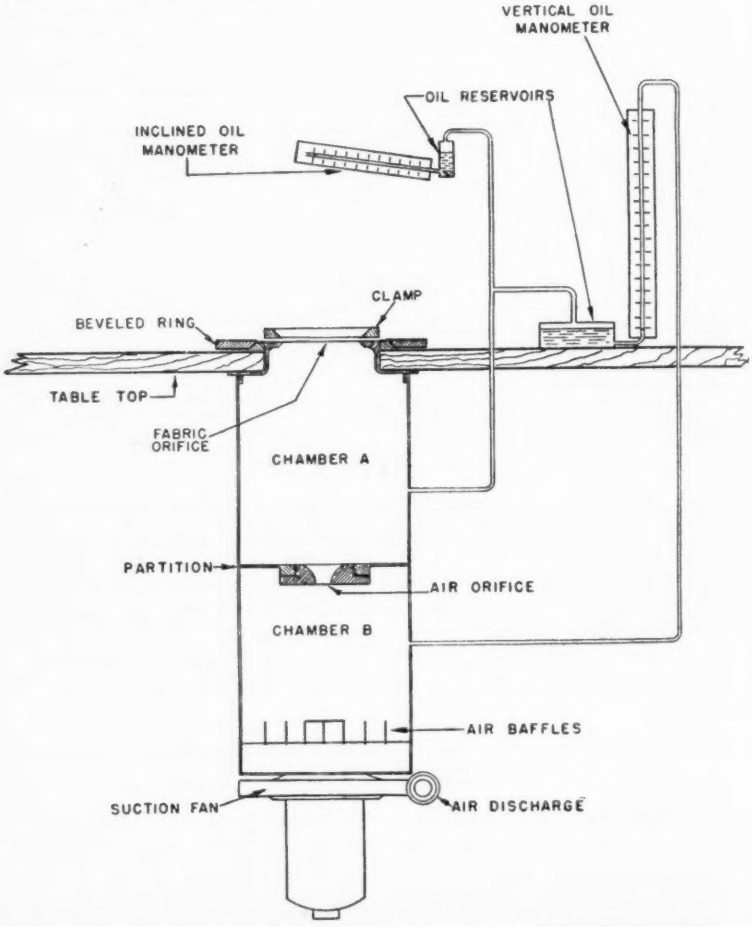

FIGURE 3.—*Schematic diagram of the air-permeability instrument.*

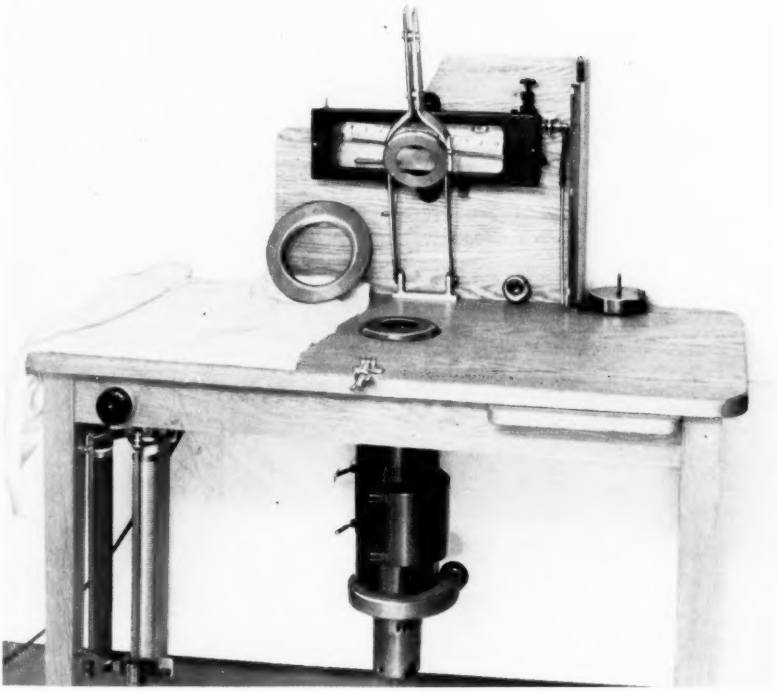

FIGURE 1.—*Air-permeability instrument.*

FIGURE 2.—*Air-permeability instrument during a test on a fabric.*

The speed of the motor which draws air through the area of fabric under test is adjusted by two rheostats, one of high resistance to obtain rapid changes in speed and one of low resistance for fine adjustment.

Manometers filled with a special oil furnished with the instrument are used to indicate the pressure drops across the fabric under test and across the orifice for measuring the air flow. The inclined manometer, which indicates the pressure drop across the fabric, is provided with leveling screws and a micrometer plunger for adjusting the meniscus to zero when no air is being drawn through the fabric. This manometer functions smoothly and dependably and is a great improvement over the water manometer formerly used, which was very sluggish in operation and had to be cleaned frequently. The vertical manometer, which indicates the pressure drop across the orifice for measuring the air flow, is connected to a reservoir having a large area compared with the cross-sectional area of the manometer so that the oil level in the reservoir remains sufficiently constant.

The amount of air flowing through a fabric under test is determined from the pressure drop indicated by the vertical manometer and the calibration of the orifice which is used. A set of nine orifices covers the range of air permeability from 1 to 700 cubic feet per minute per square foot of fabric. The orifices are easily inserted through a door opening into chamber *B* of figure 3. The door is partially open in figure 1.

The air permeability is usually measured for a pressure drop across the fabric of 0.5 in. of water, but it may be measured at any pressure drop between 0.1 and 1.0 in. of water or at a series of pressure drops between these limits. The appropriate size of orifice to use for a fabric whose approximate air permeability is not known is determined by a trial run. The pressure drop indicated by the vertical manometer should be greater than 3 in. If it is less, a smaller orifice should be used to obtain precision in the measurement.

The top of the table provides space for the excess fabric of a large piece during a test. A sliding leaf is provided for the data sheet. The manometers are mounted so that they can be read easily by the operator seated in front of the instrument.

III. CALIBRATION

1. INCLINED MANOMETER

The inclined manometer is graduated to read pressure in inches of water, one division equaling a pressure difference of 0.01 in. of water. The scale is readily readable to 0.002 in. of water. The pressures indicated by the scales of eight inclined manometers were checked against the values obtained with a sensitive differential pressure gage. The average difference of 30 comparisons, neglecting the algebraic sign, was 0.003 in. of water.

2. ORIFICES FOR MEASURING AIR FLOW

Each orifice was calibrated while in place in the instrument. In making the calibration, a given volume of air, measured by means of a calibrated gasometer, was drawn through the instrument. The pressure drop across the orifice, as indicated by the vertical manom-

eter, was maintained at a constant value during this period. The time required to discharge this volume of air, the pressure of the air at the inlet to the orifice, the pressure drop across the orifice, and the barometric pressure, temperature, and relative humidity of the air in the room were noted. This process was repeated for three additional pressure drops across the orifice. The results were computed to 70° F, 65-percent relative humidity, barometric pressure of 30 in. of Hg, and an area of 1 ft^2 of fabric. The flow of air through each orifice expressed in cubic feet per minute per square foot of fabric, was calculated for each inch of the vertical manometer scale between 1 and 15 in. The uncertainty of these values is about ± 0.5 percent.

The approximate air permeabilities which can be measured with each of the nine orifices are given in table 1. The flows through orifices of the same diameter supplied with different instruments were found to agree within about 2 percent. The values given in table 1 can be used safely for selecting the size orifice for a given air permeability range.

TABLE 1.—*Nominal sizes of the orifices and approximate air-permeability ranges of fabric*

Diameter of orifice	Air-permeability range
mm	*(cu ft/min)/sq ft*
1.0	1 to 2.5
1.4	2.5 to 4.5
2.0	4.5 to 10
3.0	10 to 20
4.0	20 to 40
6.0	40 to 100
8.0	80 to 170
11.0	160 to 320
16.0	320 to 700

Tests for air permeability should be made in a room in which the temperature and relative humidity are maintained close to 70° F and 65-percent relative humidity, respectively. The specimen should be in equilibrium with this atmosphere at the time of the test.

IV. RESULTS

The air permeabilities of three parachute cloths and of three blankets were measured in a number of locations, using the beveled ring and clamp for holding the fabric. The average of five independent measurements on the same area and the standard error are reported in table 2. The average air permeability for each material and the coefficient of variation are also given in table 2. The results of an analysis of variance of the data indicated highly significant differences with respect to location of the specimens in the fabrics. Obviously, it is advisable to test at more locations in a piece of cloth rather than to make duplicate measurements on a specimen. Using the proposed recommended practice of Committee D–13 of the American Society for Testing Materials for calculating the number of tests,[3] it follows that the random sampling error of the average of 5 tests for air permeability should not exceed 5 percent approximately 9 times out of 10.

[3] ASTM Standards on Textile Materials, p. 278–288 (October 1941).

TABLE 2.—*Air permeabilities of two types of textile fabrics*

[Cubic feet per minute per square foot of fabric for a pressure drop of 0.5 in. of water across the fabric]

Type of material	Parachute cloth			Blanket		
Material designation	I	II	III	IV	V	VI
Location number:						
1	88.2 ±1.5	83.6 ±1.3	117.6 ±0.6	61.2 ±0.1	154 ±0.8	282 ±1.0
2	77.3 ±0.9	80.7 ±0.3	119.0 ±.3	67.6 ±.1	156 ±.5	268 ±1.4
3	84.0 ±2.4	79.9 ±.9	105.6 ±.3	66.1 ±.1	140 ±.6	258 ±0.6
4	91.2 ±1.2	86.1 ±.8		64.3 ±.1	137 ±.8	283 ±.5
5	86.8 ±0.9			65.9 ±.1	140 ±.8	262 ±.9
6	94.6 ±.7					
7	100.8 ±.6					
8	90.8 ±1.0					
9	83.3 ±2.2					
Average (cu ft/min)/sq ft	88.6	82.6	114.1	65.0	145	271
Coefficient of variation, percent	8.1	3.8	6.1	3.5	5.7	3.9

The three parachute cloths, materials I, II, and III in the tables, were also tested using (a) the beveled ring without the clamp, (b) an embroidery ring with the clamp, and (c) the embroidery ring without the clamp. The three blankets, materials IV, V, and VI in the tables, were also tested using (a) the beveled ring without the clamp and (b) the clamp without the beveled ring. These materials were tested for each method of mounting at the same locations and the same number of tests were made at each location, as reported in table 2. The average of the measurements on each material for each method of mounting and the coefficient of variation in percent are given in table 3. The coefficient of variation is the number within the parentheses.

TABLE 3.—*Result showing effect of method of mounting on the air permeability*

[The average air permeability, cubic feet per minute per square foot of fabric for a pressure drop of 0.5 in of water across the fabric, is shown with the coefficient of variation in percent in parentheses]

Material designation	Method of mounting				
	Beveled ring and clamp	Beveled ring	Clamp	Embroidery ring and clamp	Embroidery ring
I	88.6 (8.1)	91.6 (9.0)		88.5 (11.3)	90.0 (11.5)
II	82.6 (3.8)	86.0 (3.4)		87.2 (5.0)	88.8 (4.5)
III	114.1 (6.1)	116.1 (4.6)		115.2 (4.9)	116.4 (5.1)
IV	65.0 (3.5)	106 (2.7)	65 (6.3)		
V	145 (5.7)	175 (4.9)	144 (5.6)		
VI	271 (3.9)	322 (3.0)	270 (4.0)		

The results on the three parachute fabrics, designations I, II, and III, were not affected significantly by the four methods of mounting. The results on the three blankets, designations IV, V, and VI, were affected significantly by the method of mounting. The air permeability was found to be over 20 percent higher when the clamp was not used. This increase was caused by air leaking through the fabric which surrounds the opening of the orifice when the clamp was not used. The edge leakage was less than 0.1 percent for blanket VI when the clamp was used.

These results show that the clamp must be used when compressible materials, such as blankets, are tested for air permeability. It is good practice to use the clamp when testing less compressible materials. The beveled ring is an aid in mounting limp fabrics. It can be used on fabrics which vary greatly in thickness. In testing stiff fabrics, which offer considerable resistance to the deformation produced by the ring, it is better to dispense with the ring and to use the clamp alone.

Several fabrics were tested on six instruments of the new model. The results obtained with the different instruments for the same fabric were within 2 percent of the average. Most of this variation is ascribable to the variation within the fabrics.

WASHINGTON, February 27, 1942.

U. S. Department of Commerce National Bureau of Standards

RESEARCH PAPER RP1472

Part of Journal of Research of the National Bureau of Standards, Volume 28, May 1942

PROPERTIES OF HIGH-PURITY IRON

By Harold E. Cleaves and John M. Hiegel

ABSTRACT

Results are recorded of new determinations of the workability, microstructure, density, and the thermal, mechanical, electrical, and magnetic properties of high-purity iron, in which the maximum amount of an individual impurity was 0.004 percent and the total of impurities in any specimen was 0.01 percent or less.

CONTENTS

	Page
I. Introduction	673
II. Hot- and cold-working characteristics	645
III. Microstructure	646
IV. Density	648
V. Thermal properties	648
1. Freezing point	648
2. Alpha-gamma transformation	649
3. Thermal expansion	653
VI. Mechanical properties	656
1. Tensile properties	656
2. Identation hardness	659
3. Modulus of elasticity	660
VII. Electrical properties	661
1. Resistivity	661
2. Temperature coefficient of resistivity	661
3. Thermal electromotive force	663
VIII. Magnetic properties	663
1. Magnetic saturation induction	664
2. Coercivity and maximum permeability	664
IX. Summary	666
X. References	667

I. INTRODUCTION

Ferrous materials, from cast iron to complex alloy steels, are essentially impure irons, and their properties are the properties of the basic material, iron, modified by the presence of alloying elements and impurities or by factors such as heat treatment and mechanical work. Throughout the history of ferrous metallurgy, knowledge of the properties of "pure iron" has been regarded as essential to an understanding of the effects of different factors on the properties of known metals and to indicate the possibilities and limitations of new alloys or combinations. The need for accurate information is greater today than ever before to meet the demands for greater reliability and for improved or new properties in ferrous materials.

Determinations of the properties of "pure iron" have been reported periodically throughout the literature of ferrous metallurgy. Each investigator was convinced that his iron was "pure iron" and that the results of his determinations were "the properties of pure iron", but the results of different investigators usually were not in agreement and frequently were widely divergent. Many of these differences may be ascribed to changing standards of what constitutes pure iron. Improved methods of analysis revealed the presence of previously unsuspected impurities, and improved testing technique showed that previously ignored amounts of impurities have surprising effects upon certain properties of the metal. For example, metallurgists know that the properties of iron are definitely affected by such small amounts as 0.001 percent of such elements as carbon, sulfur, and hydrogen, but it is only in recent years that the necessity for such precise analyses has been recognized and the procedure for making these analyses has been available. Consequently, modern high-purity irons presumably are of higher purity and certainly are of more definitely known purity than were the earlier "pure irons." The latter term should be reserved for elemental iron which is known to be free from all impurities, a material which has not yet been prepared, at least in useful amounts.

It would be expected that the quality of the products would have improved progressively in these continued attempts and that the properties of the different specimens would have come into better agreement. This occurred to some extent, but a review [1][1] of available information showed that there is still a surprising amount of uncertainty in regard to the best or most probable values for such fundamental properties as the density, electric resistivity, and thermal expansion of iron. The reversible transformation of alpha to gamma iron at a moderately elevated temperature is a characteristic of iron which is of vital importance in industrial applications because it permits controlled alteration of the properties by suitable heat treatment. When available information was reviewed in 1935, not only was there uncertainty in regard to the temperature or temperatures at which the transformation occurred during heating and and during cooling, but, in addition, there was discussion of the hypothesis that the alpha-gamma transformation was a result of the presence of impurities and would not occur in pure iron.

This uncertainty in regard to the fundamental properties of iron induced the National Bureau of Standards to prepare iron of high purity, to definitely establish its composition, and to determine its properties. The preparation of the high-purity iron by recrystallization of ferric nitrate, conversion to ferric oxide, reduction to sponge iron, and melting under hydrogen and in a vacuum was described in previous publications [2, 3]. Nineteen ingots were produced, approximately 1 pound each in weight. Careful analyses by spectrochemical and chemical methods yielded the results shown in table 1. This iron is noteworthy in the limited number of impurities whose presence could be detected. In general, nonmetallic elements constitute the major impurities; in seven of the ingots only one metallic impurity, copper, was found. The total of identified impurities ranges

[1] Figures in brackets indicate the literature references at the end of this paper.

from 0.0083 to 0.0129 percent, with 13 of the 19 ingots having a content of less than 0.010-percent total of impurities.

TABLE 1.—*Compositions of ingots of high-purity iron*

Element[1]	Ingot number								
	1	2	3	4	5	6	7	8	9
Cu	<0.002	<0.002	<0.002	<0.002	<0.002	<0.002	<0.002	<0.002	<0.002
Si	.001	.001	.003	.001	.003	001	.001	.001	nil
Be	<.001	<.001	<.001	nil	nil	<.001	nil	nil	nil
Al	nil	nil	nil	nil	<.001	nil	nil	nil	nil
C	<.001	.001	.001	.001		<.001	<.001		
S	.002$_3$	.002$_2$	.002$_6$	.001$_0$	.001$_0$	.001$_3$	.002$_1$	.001$_0$	.002$_2$
P		<.0005							
O_2	.001$_3$	.000$_3$	.000$_5$	.003$_8$	.004$_0$	.004$_5$	.002$_0$	.003$_2$	.003$_4$
N_2	.000$_1$	.000$_2$	.000$_4$	.000$_4$	.000$_2$	.000$_2$	.000$_1$	.000$_6$	.000$_9$
H_2	.000$_1$	.000$_2$	.000$_1$	.000$_2$	.000$_3$	.000$_2$	.000$_2$	.000$_2$	.000$_1$
Total of identified impurities[2]	<0.009$_3$	<0.008$_8$	<0.011$_1$	<0.009$_9$	<0.012$_9$	<0.011$_7$	<0.008$_9$	<0.008$_9$	<0.009$_8$

Element[1]	Ingot number									
	10	11	12	13	14	15	16	17	18	19
Cu	<0.002	<0.002	<0.002	<0.002	<0.002	<0.002	<0.002	<0.002	<0.002	<0.002
Si	nil	nil	.002	nil	.002	nil	nil	<.001	nil	nil
Be	nil	nil	nil	nil	nil	nil	nil	nil	nil	nil
Al	nil	nil	nil	nil	nil	<.001	nil	nil	nil	nil
C			<.001	<.001	.001				.001	<.001
S	.002$_8$	.001$_8$	.001$_2$	.002$_4$	.001$_1$	.001$_2$	.004$_1$	.002$_8$	.001$_1$	.002$_3$
P								<.0005		
O_2	.001$_9$	.004$_3$	.001$_4$	.004$_0$	.002$_0$	.001$_9$	.001$_2$	.003$_0$	.003$_4$	.004$_2$
N_2	.000$_1$	.000$_2$	.000$_3$	.000$_3$	.000$_2$	.000$_6$	.000$_1$	.000$_3$	.000$_1$	.000$_3$
H_2	.000$_1$	.000$_1$	.000$_2$	.000$_1$	.000$_1$	.000$_2$	.000$_1$	.000$_2$	.000$_3$	.000$_2$
Total of identified impurities[2]	<0.008$_4$	<0.009$_8$	<0.008$_8$	<0.010$_3$	<0.008$_9$	<0.008$_5$	<0.009$_0$	<0.010$_5$	<0.008$_3$	<0.010$_4$

[1] The arc spectrum of each ingot was examined for the presence of sensitive lines of 49 elements. Determinations of Cu, Si, Be, and Al are recorded above, the expression "nil" meaning that the amount of the impurity, if present at all, was less than the sensitivity of the analytical method. None of the following 45 elements could be identified in any of the ingots: Ag, As, Au, B, Ba, Bi, Ca, Cb, Cd, Ce, Co, Cr, Ga, Ge, Hf, Hg, In, Ir, K, Li, Mg, Mn, Mo, Na, Ni, Os, Pb, Pd, Pt, Rh, Ru, Sb, Sc, Sn, Sr, Ta, Th, Ti, Tl, U, V, W, Y, Zn, and Zr.

[2] Each total of identified impurities includes 0.001 percent of carbon and 0.0005 percent of phosphorus, although these elements were not determined for all the ingots.

The determinations of the properties of this material have been made with the cooperation of other laboratories of the Bureau and of outside agencies. The size of the ingots was not sufficient to permit determination of all the properties on any one ingot. Instead, in most cases, each property was determined on specimens of several ingots selected to include a range of compositions. The present paper summarizes these determinations and compares the results with the data available from the review of 1935 and from subsequent publications.

II. HOT- AND COLD-WORKING CHARACTERISTICS

The ingots were prepared by allowing the vacuum-melted metal to solidify and cool in the furnace. The resulting ingots all contained concealed shrinkage cavities, which sometimes extended more than half the length of the ingot, and the metal had the coarsely crystalline structure which is characteristic of slowly cooled ferrite, as is shown in figure 1. Some of the determinations of properties could be made

on specimens sawed from the ingots, but most of the determinations required rod or wire specimens.

The procedure that was adopted to convert the ingot metal into rods, with minimum wastage, was first to quarter each ingot longitudinally and grind or machine the inner surface to remove any defective material in the vicinity of the pipe. The ingot sections were then hot-forged to break up the coarsely crystalline structure and to convert the triangular cross section to a square. The specimens were heated to about 800° C in an induction furnace prior to forging and whenever annealing of the rods was necessary in the subsequent operations. Oxide scale formed during the heating was removed by pickling in hydrochloric acid which contained a commercial inhibitor. Analyses showed that this procedure did not introduce oxygen or other contamination into the metal. The forged rods were cold-rolled and swaged to rods 6 mm or less in diameter. Wire specimens were prepared by drawing small swaged rods through sapphire dies. The wires were annealed in vacuum by passing a current through the wires suspended between two electrodes. The hot- and cold-working characteristics of most of the ingots were those of a reasonably ductile metal of high purity.

No difficulty was encountered in any of the hot-working operations, and most of the specimens responded satisfactorily to cold work with occasional annealing. Certain of the rods, however, developed cracks during rolling, and this tendency was more evident in subsequent swaging. In some cases the trouble could be cured by grinding out the transverse cracks or cropping the split ends and by modifying the annealing treatment and working schedule, but in other cases the cracking persisted in spite of all precautions. The tendency to crack could not be attributed to differences in composition of the different ingots nor to differences in the hot- or cold-working procedure. Some sections from certain ingots worked satisfactorily, whereas other sections of the same ingots developed difficulties. In a few instances, more or less difficulty was encountered in working all sections of a particular ingot.

It seems probable that the difficulties experienced in working some specimens are associated with the coarse-grained structure of the furnace-cooled ingots. These difficulties might have been avoided if the ingots had been chill-cast instead of slowly solidified and slowly cooled.

Adcock and Bristow [4] reported similar difficulties in working certain samples of their high-purity iron, and attributed this brittleness to the presence of microscopic spots or cavities in the grain boundaries. Naumann [5] also found that nodules existed in the grain boundaries of steel which had been embrittled by treatment in hydrogen under pressure and at elevated temperatures. Microscopic examination of the NBS iron, as described in the next section of this report, indicated that such imperfections at the grain boundaries as were observed in the iron were caused by the polishing and etching technique.

III. MICROSTRUCTURE [2]

The preparation of specimens of high-purity iron for microscopic examination was not entirely satisfactory when the conventional

[2] The study of the microstructure was made with the cooperation of T. D. Brown, of the Division of Metallurgy of this Bureau.

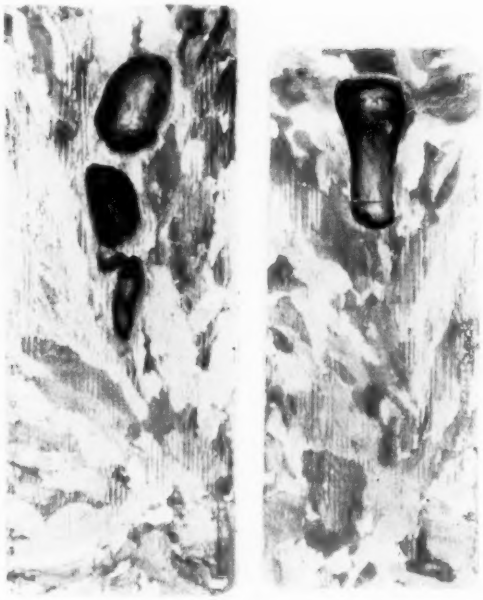

FIGURE 1.—*Macrosections of two ingots of high-purity iron, showing the concealed pipes and coarsely crystalline structure.*

Cold work from grinding caused the parallel lines. Etched with 1-percent nital. ×1.

FIGURE 2.—*Streaks on the grain boundaries of high-purity iron ground on a lap and polished with rouge.*

Etched with 1-percent nital. ×250.

UNIV. OF MICH.

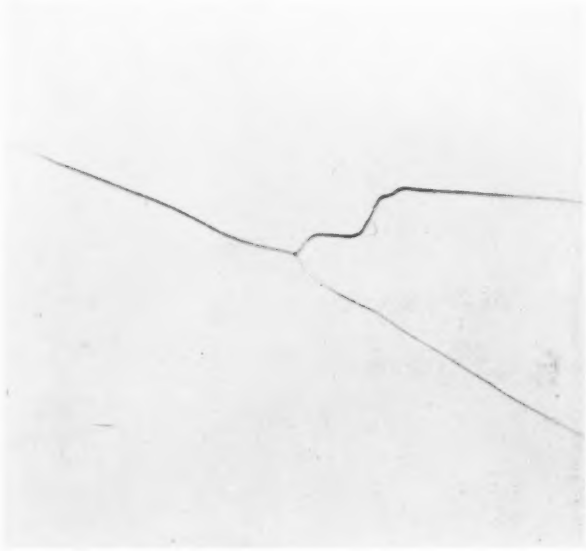

FIGURE 3.—*Specimens prepared without using any abrasive or polishing compound were free from local defects, but the surfaces were not flat.*

Etched with 1-percent nital. ×1000.

FIGURE 4.—*Large, clean grains and sharply defined, clean grain boundaries are typical of high-purity iron.*

The specimen was filed, lapped, and electrolytically polished. Etched with 1-percent nital. ×250

FIGURE 5.—*Alpha veining in high-purity iron.*
Etched with picric acid. ×100.

FIGURE 6.—*Deformation bands produced in high-purity iron by cold work.*
Etched with picric acid. ×250.

methods of grinding on paper and subsequent wet polishing were employed. The surface of the specimen invariably was marred by particles of abrasive or by the pits which remained after the abrasive was removed by the etchant. These defects were observed both within the grains and at the grain boundaries, and in appearance resembled the spots or streaks to which other writers [4, 5] attributed the brittleness of some of their specimens. The use of metal laps instead of abrasive papers resulted in improvement, although some spots remained in the grain boundaries, as is illustrated in the micrographs published by Ellinger and Acken [6]. Streaks on the grain boundaries of high-purity iron ground on a lap and polished with rouge are illustrated in figure 2. Complete freedom from these defects was achieved by eliminating all abrasives and polishing compounds, that is, when the sawed surface was smoothed with a No. 4 file and then polished electrolytically. However, such surfaces were not flat; in fact, it was frequently difficult to get enough of the field in focus at one time to make a satisfactory picture. Figure 3 shows the appearance of a specimen prepared by filing and electrolytic polishing. This unmounted specimen was polished in an acetic-anhydride–perchloric-acid electrolyte [7]. Equally good results for specimens mounted in bakelite were obtained when an orthophosphoric acid electrolyte [8] was used.

The best results, all things considered, were obtained by smoothing the specimen with a file, grinding on a lap just enough to produce a flat surface, and polishing electrolytically. Occasional pits and other surface defects resulted from this procedure, but, in general, the appearance of the high-purity iron revealed large clean grains with sharply defined, clean grain boundaries, as shown in figure 4. Comparison of figure 4 with figure 2 shows the effect, on the appearance of the same specimen, of variations in the grinding and polishing technique. These results indicate that the surface defects, particularly the defects in the grain boundaries, are caused by the grinding and polishing technique and are not inherent characteristics of this high-purity iron.

There were no definite differences in the microstructure of the different ingots which could be correlated with the variations in composition, or with the behavior in hot and cold working. Figure 4 actually represents a sample forged from ingot 16 but is typical of all the ingots.

Figure 5 illustrates alpha veining in specimens cut from the original ingots. The alpha veining must have developed when the ingot passed through the A_3 transformation in cooling from the molten state. No subsequent heat treatment was applied, and the only work on the material was the sawing of the specimen from the ingot. Alpha veining also was observed in specimens which had been worked and subsequently annealed at temperatures above A_3.

Cold working, without subsequent annealing, produced the deformation bands or worked structure illustrated in figure 6. The majority of the grains in each specimen showed an unusual amount of deformation bands, but certain grains were entirely free from strain markings. This phenomenon, together with the variation in direction and intensity of the bands, obviously is associated with differences in the orientation of different grains.

451601—42——6

Further evidence indicating the ease of permanently altering the structure of high-purity iron by work hardening is found in the parallel markings in many of the grains in figure 1. The marks follow the direction of travel of the grinding wheel across the surface and most of the grains are thus affected, but a few grains are unmarked. The depth to which this effect had penetrated was shown by the fact that repeated polishing and etching of the surface failed to produce any noticeable change in the number or appearance of the markings.

IV. DENSITY [3]

Determinations of the density of the high-purity iron were made on specimens representing different ingots and different conditions of cold work and heat treatment. Nineteen determinations ranged from 7.870 to 7.876 g/cm³ at 20° C. Observations of the density were made at room temperature, which varied from 23° to 26° C during these experiments. The observed values have been corrected to 20° C by means of the coefficient of expansion. The same range of values was obtained from 6-mm rods and from specimens of 2-mm wire. The values obtained from rods which had been swaged to 20-percent reduction in area were not altered beyond the limit of precision of the determination, ±0.002 percent, by annealing in vacuum at 870° C for 1½ hours. Likewise, surface grinding of the swaged rods, to produce true cylinders of circular cross section, did not appreciably affect the density values. Half or quarter sections of two of the ingots yielded values of 7.872 and 7.873 at 20° C, identical with the mean of all the values.

In summarizing these results, the higher values appear to be more reliable than the lower ones within this range. Concealed pipes or spongy areas would lead to low density values for the ingot material. Cracks in worked material also would result in low density values. It is concluded, therefore, that the best value for the density of high-purity iron is the mean of the 15 highest observed values, that is, 7.874 ±0.001 g/cm³ at 20° C.

A review of the literature [1] in 1935 indicated that the rounded value, 7.87, was the best approximation then available for the density of iron. Adcock and Bristow [4] subsequently reported that the density of their high-purity iron, in the annealed condition after being cold-worked, was 7.871 ±0.002 at 19° C. The new value, 7.874 ±0.001 g/cm³ at 20° C, is slightly higher than these previous values.

V. THERMAL PROPERTIES

1. FREEZING POINT [4]

Portions of ingots 3 and 15 were melted and allowed to solidify in beryllia crucibles in atmospheres of helium and hydrogen, and in vacuum. The temperatures were measured by means of an optical pyrometer sighted into a refractory black body immersed in the molten metal. Roeser and Wensel found that in vacuum the iron vapor in the line of sight absorbed about 2 percent of the light, corresponding to a reduction of 2° to 3° C. Therefore, the results obtained in

[3] The density determinations were made under the direction of E. L. Peffer, of the Weights and Measures Division of this Bureau.

[4] The freezing point determinations were made by Wm. F. Roeser and H. T. Wensel, of the Pyrometry Section of this Bureau, as described elsewhere [9].

vacuum were excluded. The values obtained in helium and in hydrogen are given in the following tabulation.

Ingot No.	Total Impurities	Freezing point	
		In helium	In hydrogen
	Percent	° *C*	° *C*
15	0. 0083	1538. 9	1537. 9
3	. 0111	1538. 7	1538. 0

The freezing point in hydrogen was about 1° C lower than the freezing point in helium, probably an effect of the solubility of hydrogen in molten iron. The variation in composition of the two ingots did not appreciably affect the freezing points, but the freezing point of pure iron probably would be slightly higher than that of the high-purity iron, which contained approximately 0.01 percent of impurities. Wensel and Roeser therefore concluded that the freezing point of pure iron would be 1,539° ± 1° C.

This figure is 4° C higher than the value selected in the review of the literature [1] in 1935. Chipman and Marshall [10] recently determined the melting point in hydrogen of a sample of carbonyl iron. The presence of impurities, such as 0.031 percent of nickel, in the carbonyl iron and the presence of hydrogen may account for the fact that Chipman and Marshall's result is 4° C lower than the value of 1,539° ± 1° C which was obtained by Roeser and Wensel.

2. ALPHA-GAMMA TRANSFORMATION [5]

The review [1] of the literature up to 1935 led to the conclusion that "the rounded value 910° C is probably the best present approximation of the temperature of the A_3 transformation of iron." At that time it appeared that the difference between Ac_3 and Ar_3 in high-purity metal, that is, the difference between the temperatures at which the transformation occurred on heating and on cooling—could be reduced to 1° or 2° C by heating and cooling at very slow rates. Yensen had proposed the hypothesis that the A_3 transformation was a function of impurities, and some support had been afforded to this hypothesis by the reported observations of A_3 temperatures appreciably higher than 910° C by Hensel and Larsen, and by Austin and Pierce.

Several determinations of the temperature of the A_3 transformation in high-purity iron have been reported since 1935. Wells, Ackley, and Mehl [11] determined the A_3 temperature in hydrogen-purified carbonyl iron, by a dilatometric method, and found that the transformation occurred at 909.5° ± 1° C. This confirmed their preliminary report, which was included in "The Metal—Iron" [1]. In the discussion of their paper, Austin reported that a pyrometric error had been discovered in the procedure employed by Austin and Pierce and that the previously reported high results should be reduced from 928° to 910° C. On the other hand, Adcock and Bristow [4] reported

[5] The determinations of the temperature of the alpha-gamma transformation were made by S. J. Rosenberg, of the Division of Metallurgy of this Bureau; by J. B. Austin, of the United States Steel Corporation Research Laboratory; and by B. A. Rogers and K. O. Stamm, of the U. S. Bureau of Mines.

that the Ac_3 transformation in their highest-purity iron began at 924° C. Esser [12] found that the temperature of the A_3 transformation increased with increasing purity, up to 932° C, and suggested that the allotropy of iron is an imposed, not an inherent, characteristic. Esser remarked that iron sufficiently pure so that A_3 and A_4 would merge, as suggested by Yensen, had not yet been obtained. Esser and Eusterbrock [13] used an improved dilatometer and found that the Ac_3 temperature in vacuum-melted electrolytic iron increased with decreasing carbon content, from 917° C for material which contained 0.01 percent of carbon, to 935° C when the carbon content was only 0.004 percent. However, other recent determinations do not substantiate these high values. Smith [14] converted ferric nitrate to metallic iron by chemical methods and found, by X-ray methods, that this material transformed at 907° to 908° C. Wangsgard [15] also used X-ray methods and found that a specimen of hydrogen-purified carbonyl iron transformed at 910.5° ± 0.6° C.

Considerable attention was devoted to the study of the alpha-gamma transformation in the high-purity iron because of this uncertainty as to the temperature at which A_3 occurs, as shown in the preceding paragraphs. Determinations by thermal analysis were made at this Bureau, and dilatometric and magnetometric determinations were made in other laboratories.

Heating and cooling curves of specimens cut from three of the ingots, Nos. 3, 6, and 18, were obtained by S. J. Rosenberg, using the method described by Scott and Freeman [16], with the following modifications: an improved temperature gradient was obtained by rewinding the furnace; the thermocouple wires were spot-welded to the specimen; inverse rate curves were computed from observations of the time-temperature relations.

The rates of heating or cooling through the transformation range varied slightly from run to run, from a minimum rate of 0.5° C per minute to a maximum of 1.2° C per minute. Within this range there was no effect of the rate of heating or cooling on the temperature of the transformation. The inverse rate curves usually were sharply defined, as is illustrated by the curves for irons 3 and 18 in figure 7. Minor irregularities in the shape of the heating curves, such as the split transformation of iron 6 (fig. 7), were occasionally encountered. The irregular behavior was confined to the first run except in the two specimens of iron 6, which exhibited irregularities in repeated runs. No correlation could be established between the irregular behavior and factors such as the composition of the ingot, the presence of mechanical strains from cold working, or the rate of heating and cooling. Furthermore, in the dilatometric determinations in other laboratories, irregularities were not observed in specimens of ingot 6, but difficulties were encountered with iron 3. Consequently, it appears that these difficulties or irregularities in both methods apply to individual samples or to individual runs, not to the ingot material or to the methods in general.

The results obtained by thermal analysis are listed in table 2. The mean of all the Ac_3 determinations is fractionally higher than 910° C, and the mean of the three determinations for iron 18, which has the lowest total of impurities of the three ingots, is 911° C. However, the data probably do not justify a more precise statement than that Ac_3 in these irons occurs at 910° C and Ar_3 at 900° C.

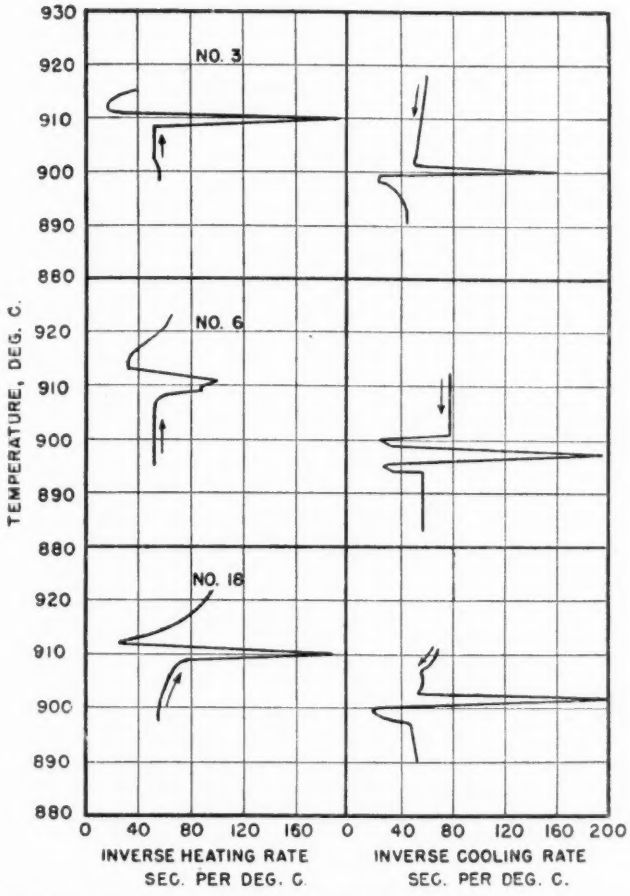

FIGURE 7.—*Inverse rate curves for A_3 in high-purity irons. (Rosenberg).*

TABLE 2.—*The A_3 temperature in high-purity iron, as determined by thermal analysis (Rosenberg)*

Ingot	Ac_3 temperature	Heating rate	Ar_3 temperature	Cooling rate
	°C	°C/min.	°C	°C/min.
3	911	0.7	900	0.8
	910	.8	900	1.0
	908	.9	900	1.0
	910	1.2	901	1.1
6	911	0.9	897	0.8
	911	1.1	898	.8
	909	1.1	900	1.0
	911	1.2	899	1.2
			900	1.2
18	911	0.5	904	0.7
	912	.8	902	1.0
	910	1.0	903	1.2
Mean of all determinations	910		900	

Dilatometric determinations of the Ac_3 temperature in specimens of rods from ingots 2, 3, 6, and 18 were made in a vacuum interferometer [17] by J. B. Austin. In the sample of ingot 2 the Ac_3 transformation started at 910° C and was completed at 918° C. A set of specimens from ingot 3 began to transform at 915° C, and the transformation was completed at 925° C. Specimens from ingot 6 began to transform at 912° C, and the transformation was completed at 918° C. A set of specimens from ingot 18 began to transform at 910° C, but there was no marked transformation until about 920° C, and the change was complete at 930° C. A second run of this set of specimens showed a relatively sharp transformation beginning at 909° C and completed at 917° C. The accuracy of these determinations was about ±2° C. The dilatometric results for ingots 2, 6, and 18 indicate a temperature of 910° ± 2° C for the beginning of the Ac_3 transformation.

The behavior of the specimens from ingot 3 is puzzling, particularly in view of the absence of any irregularities in the behavior of samples from the same ingot in the thermal-analysis determinations. Perhaps, as Austin suggested, the irregularities may result from localized segregation of impurities, silicon for example, although evidence of such segregation of impurities has not been encountered elsewhere in the study of these ingots of high-purity iron. Further indications that the irregularities pertain to individual specimens and not to the ingot from which the specimen was taken are found in the fact that ingot 6 showed irregularities in thermal analysis and not in the dilatometric determinations. Furthermore, there was no irregularity in the behavior of ingot 3 in the determinations described in the succeeding paragraphs.

The results of a magnetometric study of the A_3 transformation in samples of this high-purity iron, by B. A. Rogers and K. O. Stamm, have been reported elsewhere [18]. They found that Ac_3 occurred at 910.5° C for specimens of ingots 2, 3, and 18 and that Ar_3 occurred at 902.5° C for ingots 2 and 3 and at 902.0° C for ingot 18. In their procedure the transformation in high-purity iron was completed at a constant temperature, but with less pure iron the transformation covered a range of several degrees. Rogers and Stamm found that the rate of the Ac_3 transformation was so slow that several hours were required to complete the change from the alpha to the gamma condition. The rate of the Ar_3 transformation was perhaps three or four times that of the Ac_3 change. The presence of a small amount of oxide caused Ac_3 to begin several degrees below its normal temperature and end several degrees above it, but did not appreciably affect the Ar_3 transformation. Their data indicate that the Ac_3 transformation in this iron will complete itself at a fixed temperature, which is in the vicinity of 910.5° C, and that Ar_3 occurs at about 902.5° C.

The results obtained by the three methods are not in perfect agreement—for example, the magnetometric method shows that Ac_3 is completed at constant temperature, whereas the transformation extends over a few degrees in the thermal-analysis experiments and over a greater range in the dilatometric observations. All three methods are in agreement, however, that the Ac_3 transformation in this high-purity iron occurs at 910° to 910.5° C and that the Ar_3 transformation is about 8° C lower than Ac_3, even with very slow rates of cooling. Irregularities in a few of the determinations are

ascribed to unknown features of the individual specimen or the individual determination, rather than to the compositions of the ingots from which the specimens were taken.

3. THERMAL EXPANSION[6]

Determinations of the linear thermal expansion of high-purity iron over the temperature range from −130 to +900° C were made by P. Hidnert, using the precision-comparator type of apparatus [19]. Measurements at temperatures below 300° C were made in air, those above 300° C were made in helium. It was not practicable to cover the complete temperature range in a continuous run with a single specimen. Furthermore there was some oxidation of the specimens, in spite of the helium atmosphere, and occasionally a specimen which had been exposed to temperatures near 900° C was permanently warped. For these reasons several rods, from ingots 4 and 18, were used to cover overlapping sections of the temperature range. Attempts to protect the rods, during exposure to high temperatures, by a thin coating of electroplated gold were not entirely successful. The gold plate blistered and broke at relatively low temperatures and tended to draw up into beads or disappear altogether at higher temperatures. The best results at temperatures above 300° C were obtained from rods which had been annealed previously for 1½ hours at 870° C in vacuum.

The summary of results in table 3 includes a number of average values for temperature ranges that were covered in more than one run, and a few results of single determinations. Duplicate determinations, on heating and on cooling the same specimen, or in overlapping runs with different specimens, invariably agreed within a fraction of 1 millionth per degree centigrade. The data from table 3, plotted for the mean temperature of each interval, define the smoothly continuous curve shown in figure 8, the shape of which is in accord with the effect of temperature on other properties of iron. Particular attention was paid to the temperature range from 0 to −125° C, but no evidence was observed of the irregular behavior reported by Simon and Bergman and discussed in "The Metal—Iron" [1].

TABLE 3.—*Mean coefficient of linear thermal expansion of high-purity iron between −130° and +900° C (Hidnert)*

Temperature interval	Mean coefficient of linear thermal expansion
°C	*Millionths per °C*
−130 to −100	8.7
−100 to −75	9.5
−75 to −50	10.2
−50 to −25	10.8
−25 to 0	11.1
0 to +20	11.5$_6$
20 to 100	12.3
100 to 200	13.3
200 to 300	14.5
300 to 400	15.5
400 to 500	16.2
500 to 600	16.1$_8$
600 to 700	15.8
700 to 800	15.8
800 to 900	15.4

[6] The thermal expansion of the iron was investigated by P. Hidnert, W. B. Emerson, and J. B. Saunders, of this Bureau; by F. C. Nix and D. MacNair, of the Bell Telephone Laboratories; and by J. B. Austin, of the United States Steel Corporation Research Laboratory.

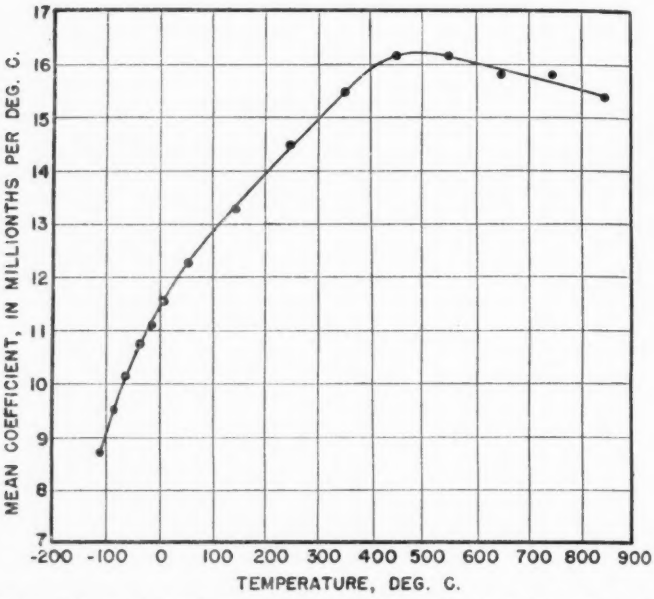

FIGURE 8.—*Linear thermal expansion of high-purity iron between −130° and +900° C (Hidnert).*

The thermal expansion of specimens of ingots 2, 6, and 18 was studied, by means of an interferometric dilatometer, by F. C. Nix and D. MacNair. Specimens 6 and 18 were used at temperatures from −180° C to room temperature, and specimens from ingot 2 were used from −180° to +680° C, as described in a recent publication [20]. The results of all three runs at low temperatures were in excellent agreement among themselves and with Hidnert's results. However, at temperatures above 0° C, the coefficient-temperature curve of Nix and MacNair shows reversals of curvature which produce divergences of almost a millionth per degree centigrade from Hidnert's results. At temperatures above 500° or 600° C such differences may be attributed to experimental difficulties at high temperatures, but a difference of 0.8×10^{-6} at 125° C is not so simply explained.

Nix and MacNair [20] suggest that these irregularities are evidence of the beginning of the Curie transition at temperatures of about 0° C, but there is no evidence of these irregularities in Hidnert's data. Hidnert's use of mean coefficients would tend to smooth out slight irregularities in his curve but would not eliminate reversals of the magnitude observed by Nix and MacNair. Similar reversals in curvature, but at higher temperatures, existed in the results of Austin and Pierce [21,] and slight reversals in curvature occurred between 40° and 200° C in the recent results of Esser and Eusterbrock [13]. Some observations of thermal expansion by J. B. Austin in the course of his determinations of the temperature A_3 indicate a definite "plateau" at about 100° to 125° C in plots of the true coefficient of expansion of specimens of irons 2 and 18.

Additional data on the expansivity of high-purity iron in the temperature range from 25° to 250° C were obtained at the Bureau by

W. B. Emerson and by J. B. Saunders. Emerson measured the thermal expansion of iron 18 by means of the interferometric dilatometer described by Merritt [22], and Saunders applied his own interferometric procedure [23] to irons 2 and 18. The true coefficients of linear thermal expansion were derived mathematically from both sets of data to eliminate the smoothing effect which presumably exists when the mean coefficients are used.

Cubical equations computed from both sets of data satisfactorily expressed the linear thermal expansion of the iron, as was shown by agreement, within the experimental error, of the observed values and the values computed from the equations. The true coefficients of linear thermal expansion were obtained by differentiation of these equations. Similar computations were made for Hidnert's data for the temperature range 25° to 250° C; but an equation was not derived for the entire temperature range covered by Hidnert's data, as the equations required would be too complex to be useful.

TABLE 4.—*True coefficient of linear thermal expansion of high-purity iron between 25° and 250° C*

Temperature	Iron 2 (Saunders)	Iron 18 (Saunders)	Iron 18 (Emerson)	Iron 18 (Hidnert)
° C	*millionths per ° C*	*millionths per ° C*	*millionths per ° C*	*millionths per ° C*
25	11.58	11.58	11.97	11.90
50	11.93	11.93	12.23	12.18
75	12.27	12.29	12.49	12.48
100	12.61	12.64	12.74	12.78
125	12.94	12.97	13.00	13.08
150	13.27	13.30	13.26	13.37
175	13.59	13.62	13.51	13.67
200	13.91	13.93	13.78	13.97
225	14.21	14.24	14.03	14.26
250	14.50	14.54	14.29	14.56

The true coefficients thus computed from the observations of Emerson, Saunders, and Hidnert are listed in table 4. All are in good agreement, as is shown in figure 9, although the plot of Saunders,

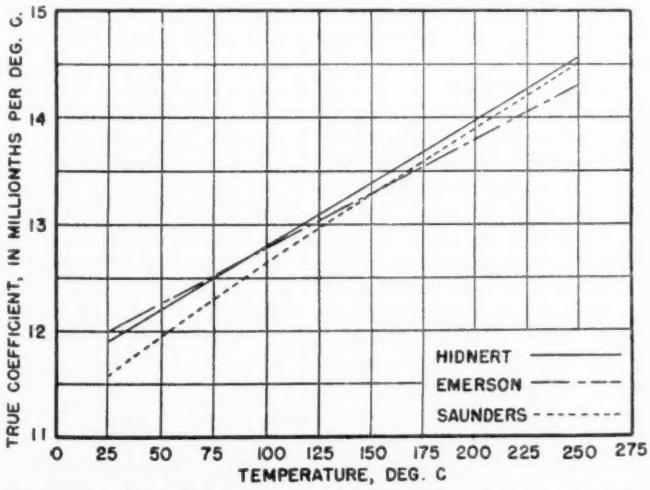

FIGURE 9.—*Linear thermal expansion of high-purity iron between room temperature and +250° C (Hidnert, Saunders, Emerson).*

results shows some curvature whereas Hidnert's and Emerson's results are almost linear. In none of these runs is there any evidence of irregularities.

The data obtained at the Bureau and by Nix and MacNair indicate that the coefficient of linear thermal expansion of this iron at 20° C is $11.7 \pm 0.2 \times 10^{-6}$ per degree centigrade. The thermal expansion at low temperatures, where the data are in good agreement, is essentially as indicated by the mean coefficients obtained by Hidnert. The expansivity of the iron at high temperatures is not satisfactorily established by the data available.

VI. MECHANICAL PROPERTIES

1. TENSILE PROPERTIES [7]

The yield point of high-purity iron is of particular interest in view of the suggestion that it is a function of impurities and that pure iron, like the nonferrous metals, will not have a yield point.

The yield point in metals has been variously defined, from the load at which a "drop of the beam" was obtained, to the more modern definition that it is "the stress at which a marked increase in strain occurs without an increase in stress" [24]. The stress-strain curve presented by Adcock and Bristow [4] did not exhibit an increase in strain without an increase in stress, hence their conclusion that their iron did not have a yield point. In the present investigation, only a limited number of rods was available and it was desired to obtain other values as well as the yield point from each specimen. Consequently it was decided to study the stress-strain relations according to the ASTM definition, by means of an Amsler testing machine equipped with a Baldwin-Southwark stress-strain recorder. Rods of high-purity iron, swaged to ¼ inch in diameter with the central portion of each rod further reduced about 0.004 inch by grinding, were used and, for comparison, specimens of electrolytic iron. The electrolytic iron had a definite yield point, as was shown by the drop in the beam when pulled on the Riehle testing machine and by the horizontal section, where strain increased without increase in stress, on the stress-strain curves obtained with the Amsler machine. In general, the level at which the horizontal section occurred was progressively lowered by annealing, as is indicated by the curves in figure 10, which represent three different annealing treatments.

The stress-strain curves for the high-purity iron also had horizontal sections, which, in general, were more pronounced than those for the electrolytic iron. The curves in figure 11 show these horizontal sections and also illustrate the range of values which resulted from different annealing treatments. Some of the high-purity specimens, particularly those in the partly annealed condition, also showed a drop in stress at the yield point, which is directly equivalent to the drop of the beam in the Riehle test. This effect is illustrated by curve *A* in figure 11, and to a lesser extent by curve *B*. The effect of annealing on the level of the yield point was greater for the high-purity iron than for the electrolytic iron. In the fully annealed condition the yield points for the high-purity iron were lower than for the electrolytic iron, but in the partially annealed condition the reverse was true.

[7] The tensile properties were determined with the cooperation of G. F. Wohlgemuth, of the Metallurgical Division of this Bureau.

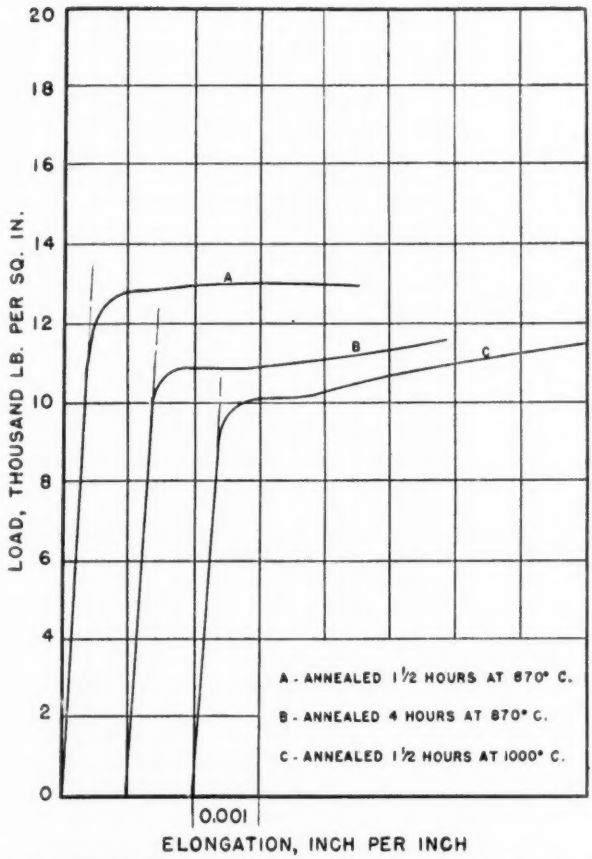

FIGURE 10.—*Stress-strain curves of vacuum-melted electrolytic iron in tension.*

In all cases the initial portion of the stress-strain curve was a straight line and the knee in the curve was relatively sharp. These features, together with the horizontal sections of the stress-strain curves, demonstrate that a yield point, according to the ASTM definition, is exhibited by fully annealed and partially annealed high-purity irons. When such definite indications of a yield point are obtained from iron which contains only a 0.01-percent total of impurities, it hardly seems probable that the yield point would disappear completely if all the impurities were eliminated.

The data for the tensile properties of the high-purity iron are summarized in table 5. The high-purity iron is weaker and more ductile than the electrolytic iron, and these differences are particularly noticeable when both materials are in the fully annealed condition. The tensile strengths of the fully annealed high-purity iron ranged from 27,700 to 29,900 lb/in^2 as compared with 35,300 to 35,700 lb/in^2 for the electrolytic iron after similar heat treatment. Differences in the grain size before and after the specimens were annealed undoubt-

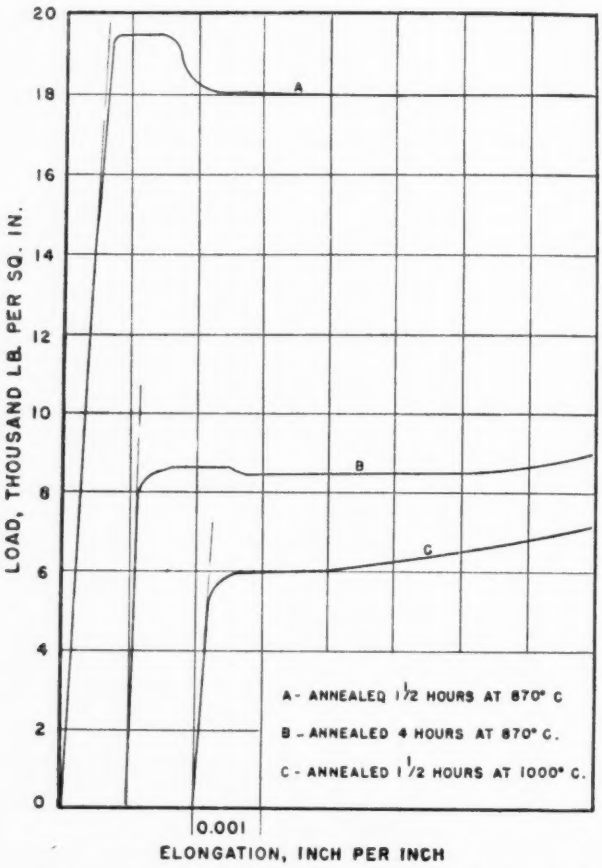

FIGURE 11.—*The presence of a "yield point" in high-purity iron is demonstrated by the shape of the stress-strain curves.*

edly affected their tensile properties. The electrolytic iron was moderately coarse-grained, according to microscopic observations, and this is also indicated by the slightly roughened surface of the fractured tensile specimens, as illustrated at the top of figure 12. The grains in the high-purity iron were much larger, according to microscopic observations. This caused a pronounced roughening of the surface of most of the tensile specimens of the high-purity iron, as illustrated at the bottom of figure 12.

Adcock and Bristow [4] reported values ranging from 20,400 to 26,700 lb/in^2 for the tensile strength of their high-purity iron. They did not specify the previous heat treatment, but the description of the fractured edge of the specimen which broke at the low value of 20,400 pounds suggests that this rod was essentially monocrystalline in the area of fracture.

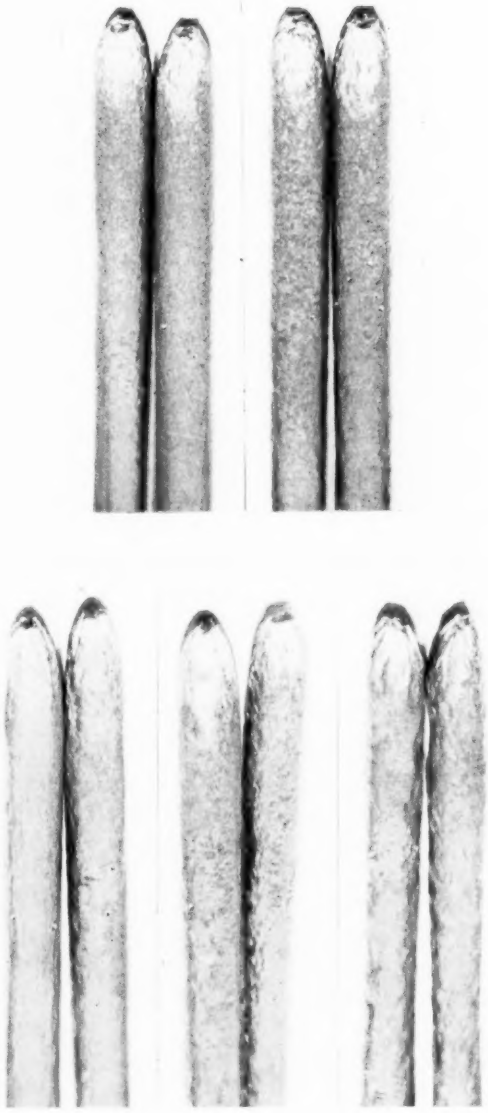

FIGURE 12.—*Appearance of the surface indicated the grain size of fractured tensile specimens.*

The two specimens at the top are electrolytic iron; the three at the bottom are high-purity iron.

TABLE 5.—*Tensile properties of high-purity iron and vacuum-melted electrolytic iron*

Annealing treatment		Number of specimens tested	Ultimate tensile strength	Yield strength at 0.2-percent offset	Reduction in area	Elongation in 2 inches
Temp.	Time					
High-purity iron						
° *C*	*Hours*		*lb/in²*	*lb/in²*	%	%
870	1½	4	29,500 to 36,500	12,500 to 18,600	81 to 91	37 to 42
870	4	2	28,500 to 29,700	8,100 to 8,600	85 to 94	36 to 46
1,000	1½	3	27,700 to 29,900	6,000 to 7,800	91 to 93	36 to 41
Vacuum-melted electrolytic iron						
870	1½	7	35,500 to 36,500	9,600 to 12,900	76 to 83	32 to 38
870	4	2	34,700 to 35,300	11,100 to 12,700	85 to 86	33
1,000	1½	2	35,300 to 35,700	10,200 to 10,500	80 to 81	31 to 32

The yield strengths of our high-purity iron, for 0.2-percent elongation in 2 inches, ranged from 25 to 50 percent of the ultimate tensile strength. The reduction in area was greater than 90 percent for the fully annealed material and was somewhat lower for the incompletely annealed specimens. The values for the elongation in 2 inches ranged from 35 to 45 percent, with little difference between the fully annealed and the partially annealed specimens.

2. INDENTATION HARDNESS

Brinell indentations, with a $\frac{1}{16}$-inch ball and 15-kg load, on the surface of furnace-cooled ingot 4 yielded results which ranged from 46 to 51 BHN, with an occasional value as low as 43 or as high as 58. The average of all the determinations was 49 BHN. Fully annealed material also was available in the form of rods ½ inch in diameter, which had been annealed for 1¼ hours at 1,000° C. Hardness determinations on the ends of these rods, with a Vickers diamond-pyramid indenter under a load of 15 kg, ranged from 46 to 54, with an average value of 49 VN. These results indicate that the indentation hardness number of fully annealed high-purity iron is about 49 in either Brinell or Vickers units. Almost identical values were obtained by Adcock and Bristow [4] from their best iron after annealing for 2 hours at 950° C.

The high-purity iron hardens readily even under light working, as was demonstrated by the Brinell numbers obtained from the polished faces of the split ingots shown in figure 1. The ingots were sawed, the surface was flattened by grinding, and was then polished and etched. After this treatment, the Brinell numbers varied widely from grain to grain, presumably reflecting the response of different orientations to the sawing, grinding, and polishing. The average of a number of determinations with a $\frac{1}{16}$-inch ball and 15-kg load was 79 BHN, which is considerably higher than the average (49 BHN) of determinations on unworked surfaces of the same ingot. Cold work by swaging produced still higher hardness numbers. Rods which had been reduced about 20 percent by swaging yielded Brinell numbers between 95 and 120. When these rods were annealed at 870° C, the Brinell number was reduced to about 85 in 1½ hours and to about

60 in 4 hours, but full annealing was obtained only when the rods were heated above the A_3 point.

3. MODULUS OF ELASTICITY[8]

The modulus of elasticity of high-purity iron and of vacuum-melted electrolytic iron was determined from simultaneous stress-strain and stress-set curves, with progressively increasing loads, as described by McAdam and Mebs [25]. The results obtained from four swaged rods, representing three ingots of high-purity iron, ranged from 27.2 to 29.5 million pounds per square inch, as recorded in table 6. Annealing the rods for 1½ hours at 870° C raised the value for the modulus slightly in some cases and definitely in others. The mean value from the four rods was increased from 28.2 to 28.9 by annealing. The precision of a single determination by this method was about ±0.5 million pounds per square inch, as is shown by the values 27.2 and 28.1 obtained from duplicate rods of the same material.

TABLE 6.—*Modulus of elasticity of high-purity iron and electrolytic iron*

Ingot	Modulus of elasticity	
	Cold-worked	Annealed 1½ hours at 870° C
High-purity iron		
	lb/in²×10⁻⁶	*lb/in²×10⁻⁶*
12	27.9	27.9
18	27.2	27.9
18a	28.1	28.7
19	29.5	30.0
Electrolytic iron		
1	30.0	31.0
2	29.5	30.5
3	29.8	29.7
3a	29.8	----------

The results from four rods of electrolytic iron, as recorded in table 6, show that the elastic modulus of this material is higher than that of the high-purity iron by at least one million pounds. Annealing at 870° C also tended to increase the modulus of the electrolytic iron. The determinations on the electrolytic iron are uniformly higher and the four determinations are more closely grouped than for the corresponding determinations on the high-purity iron. These differences may be associated with two obvious differences in the two groups of specimens: (1) the total of impurities in the electrolytic iron, about 0.04 percent, is greater; and (2) the grain size is appreciably greater in the high-purity iron.

Consideration of these data and the results reported by Adcock and Bristow [4] leads to the conclusion that Young's modulus for high-purity iron is approximately 28.5 ±0.5 million pounds per square inch.

[8] The determinations of the modulus of elasticity were made with the cooperation of R. W. Mebs, of the Metallurgical Division of this Bureau.

VII. ELECTRICAL PROPERTIES

1. RESISTIVITY[9]

The resistivities of specimens from six of the high-purity iron ingots were determined by the double-bridge method. The specimens, 2 mm in diameter and about 1 meter long, were annealed in vacuum for 15 minutes at 850° C. Two were reannealed at 850° C for 1 hour with no appreciable change in the resistivity. The results are recorded in table 7.

These values for resistivity are the lowest that have been obtained for high-purity iron at this Bureau and are somewhat below the rounded value 9.8 microhm-cm selected as the resistivity of "pure" iron at 20° C from the results available up to 1935 [1]. Since then Adcock and Bristow [4] reported 9.84 and 9.88 microhm-cm at 20° C for the resistivity of the purest iron prepared at the National Physical Laboratory, and values of 9.90, 9.40, and 9.75 for less pure irons. These latter two results are in conflict with the usually accepted belief that a decrease in resistivity accompanies an increase in purity in a metal.

TABLE 7.—*Electrical properties of high-purity iron*

Ingot	Total impurities	Electrical resistivity at 20° C (Thomas and Cooter)	Fundamental coefficient 0° to 100° C (Wensel and Roeser)	Thermal electromotive force against platinum at 100° C (Dahl)
	%	*Microhm-cm*	*Ohms per °C per ohm at 0° C*	*Microvolts*
2	<0.0085	9.69	0.00652	1981
7	<.0089	9.72	.00650	1976
14	<.0089	9.71	.00652	1982
11	<.0098	9.70	.00652	1981
19	<.0106	9.72	.00650	1978
6	<.0117	9.71	.00652	1983
Average		9.71	.00651	1980

No correlation could be made between the values for resistivity and the amounts of total or individual impurities in our irons.

2. TEMPERATURE COEFFICIENT OF RESISTIVITY[10]

The temperature coefficient of electrical resistivity over the temperature range 0° to 100° C, $(R_{100}-R_0)/100\ R_0$, usually termed the fundamental temperature coefficient, has been considered to be a measure of the purity of a metal, the higher the purity the higher the coefficient; but Wensel and Roeser found that the fundamental coefficient of resistivity of iron was appreciably affected by the prior thermal history of the specimens. In experiments with some of the preliminary products of high-purity iron, they found, as shown in figure 13, that the fundamental coefficient of wires 0.5 mm in diameter increased with increasing temperature of annealing up to 600° C, remained approximately constant for annealing temperatures between

[9] The determinations of electrical resistivity were made by J. L. Thomas and I. L. Cooter, of the Electrical Division of this Bureau.

[10] The determinations of the temperature coefficient of resistivity were made by Wm. F. Roeser, of the Heat and Power Division of this Bureau.

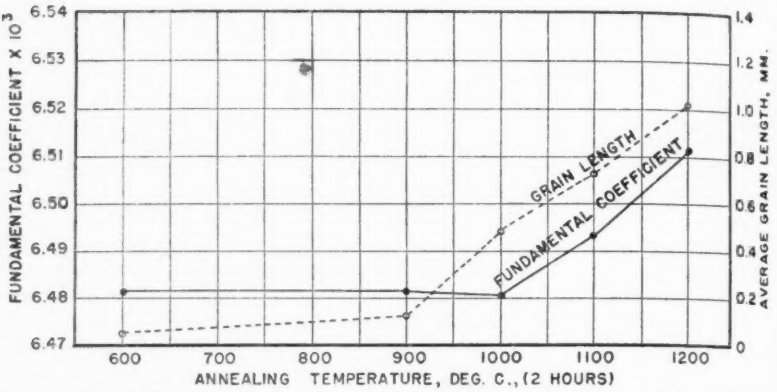

FIGURE 13.—*Relation between annealing temperature, grain size, and fundamental coefficient of resistivity* $(R_{100}-R_0)/100R_0$, *of high-purity iron wire 0.5 mm in diameter) Wensel and Roeser.*

600° and 1,000° C, and again increased with increasing temperatures of annealing above 1,000° C. Microscopic studies indicated that this final rise in the fundamental coefficient was associated with increases in the grain size when the iron was annealed at temperatures above A_3, although the data in figure 13 show that annealing at 1,000° C increased the grain size without affecting the coefficient. The effect of the annealing temperature on the fundamental coefficient was exaggerated when wires of smaller diameter were used, and with 0.2-mm wire reproducible results could not be obtained even in the 600° to 1,000° C range. Certain portions of the finer wires consisted of single crystals, and it is probable that the large grain size in proportion to the diameter of the wire was the cause of the erratic results.

The data indicate that when reproducible values for the fundamental coefficient are desired, for the purpose of comparing purity, the specimens should be annealed at a temperature between 600° and 1,000° C. For this reason determinations of the fundamental coefficient of the high-purity irons were made on wire specimens 0.5 mm in diameter which had been annealed for 2 hours at 800° C in vacuum. The values recorded in table 7 show that the fundamental coefficients of specimens of six of the high-purity ingots ranged from 0.00650 to 0.00652, with an average value of 0.00651 ohm per 0/° C per ohm at 0° C. The variations within this range could not be correlated with the compositions of the ingots nor with the resistivity data from other specimens of the same ingots.

This value, 0.00651, is in agreement with the value 0.00648 which may be computed from the data reported by Adcock and Bristow [4] for the resistivity of their best iron. Three higher values for the fundamental temperature coefficient of resistivity of iron are found in the literature: 0.00657 and 0.00821, reported by Meyer [26] in 1911; and 0.00657, reported by Holborn [27] in 1919. Meyer's results are cited in the International Critical Tables, but there are indications that his temperature and resistance measurements were erroneous. Meyer's resistance measurements on "Kahlbaum's nitrate iron," from which the high coefficient 0.00821 was derived, differ appreciably from the closely grouped results of other investigators who

used the same material. Holborn's value of 0.00657 is the highest of four values obtained on a specimen of "Kahlbaum's nitrate iron" annealed at 500° C for several minutes, the other values being 0.00643, 0.00638, and 0.00635. Determinations of the temperature coefficients at temperatures up to 511° C were alternated with the determinations of the fundamental coefficient. In view of Roeser's observation, the variation in values may have resulted from the varying temperatures to which the specimen was heated. Holborn's highest value, 0.00657, was not reproducible and probably applied only to a particular specimen which had been subjected to unusual heat treatment.

It appears, therefore, that 0.00651 is the highest reproducible value that has been obtained for the fundamental coefficient of resistivity of high-purity iron. Higher values can be obtained by annealing the specimens at higher temperatures, but the results are not easily reproducible. The temperature coefficient of resistivity may be used as an index of the purity of different specimens of iron which have received the same heat treatment, and the optimum conditions for the heat treatment of iron, to produce the maximum reproducible coefficients, are annealing for 2 hours or more at about 800° C in vacuum.

3. THERMAL ELECTROMOTIVE FORCE [11]

Observations in the Heat and Power Division of this Bureau indicated that the thermal electromotive force of iron against platinum could be correlated with the fundamental coefficient of resistivity, both increasing with purity. The thermal electromotive force of iron against platinum, then, also would serve as an indication of comparative purity. Values for the thermal electromotive force are comparable only when obtained at identical temperatures; hence the readily reproducible temperatures 100° and 0° C were used for the hot and cold junctions during the work in which the correlation between the thermal electromotive force and the temperature coefficient was obtained.

Determinations of the thermal electromotive force against the Bureau's platinum standard, Pt 27, for the fundamental temperature interval 0° to 100° C were made with specimens of the same wires, 0.5 mm in diameter and previously annealed for 2 hours at 800° C in vacuum, which had been used for the resistivity determinations. The results ranged from 1,976 to 1,983 microvolts, as shown in table 7, with no apparent correlation between the variations in the thermal electromotive force and variations in the impurities or other properties except the fundamental coefficient of resistivity.

Values of 1837 microvolts for basic open-hearth iron with a 0.17-percent total of impurities and 1966 microvolts for electrolytic iron with an 0.018-percent total of impurities have been recorded. The values from the high-purity iron, with about 0.01-percent total of impurities, are higher than the value for electrolytic iron and appreciably higher than the value for open-hearth iron.

VIII. MAGNETIC PROPERTIES

The magnetic properties of iron may be classed in two groups: (1) the magnetic saturation induction and the Curie point, which

[11] The measurements of thermal electromotive force were made by A. I. Dahl, of the Heat and Power Division of this Bureau.

are characteristics of the element and are not influenced by its condition and only slightly by impurities; and (2) permeability, hysteresis loss, coercivity, remanence, and similar properties which are greatly affected by mechanical and thermal treatment of the specimen and by impurities. Determinations of properties in both groups were made on specimens of our high-purity iron.

1. MAGNETIC SATURATION INDUCTION[12]

Swaged bars one-quarter inch in diameter, prepared from eight of the ingots, were ground to a circular, uniform diameter of 6 mm and then were cut to lengths of 8 cm. After determinations had been made on the bars in the cold-worked condition, two of them were annealed in vacuum, one at 870° C for 1 hour and the other at 1,020° C for 1 hour. Redeterminations of the saturation induction showed that the change in both cases was insignificant, that is, well within the limits of experimental error. Sanford and Bennett applied corrections to the data for (1) nonuniformity of area of the samples, (2) delayed impulse, and (3) impurities. The total of these corrections in each case was about 0.05 kilogauss, and 80 percent of this was the correction for delayed impulse. The correction for impurities was only 0.004 kilogauss, which is less than the probable error in magnetic measurements of the order of 21 kilogausses.

TABLE 8.—*Corrected values for the magnetic saturation induction of high-purity iron at 25° C, based upon a density of 7.874 g/cm³ (Sanford and Bennett)*

Ingot	Saturation induction
	Kilogausses
3	21.576
3 [a]	21.573
6	21.584
7	21.575
8	21.591
8 [b]	21.590
12	21.593
13	21.568
14	21.562
18	21.569
Mean	21.578

[a] Annealed 1 hour at 870° C.
[b] Annealed 1 hour at 1,020° C.

The corrected values for saturation intensity are listed in table 8. These values are in good agreement with the most reliable of the previous determinations [29], [30], [31], [32], according to Sanford and Bennett. They state that "It seems safe to conclude, therefore, that the saturation value for pure iron at 25° C and based upon a density of 7.874 g/cm³ is 21.58 $\pm$0.01 kilogausses."

2. COERCIVITY AND MAXIMUM PERMEABILITY[13]

Specimens for these determinations were prepared by cold-rolling sections of four of the high-purity ingots to sheets from which were cut rings 1⅛ inches in outside diameter, 1⅝ inch in inside diameter,

[12] The determinations of magnetic saturation induction were made by R. L. Sanford and E. G. Bennett, of the Electrical Division of this Bureau, as described eleswhere [28].
[13] These properties were determined by P. P. Cioffi, of the Bell Telephone Laboratories.

and 0.062 inch thick. Before determining the magnetic properties of the specimens, they were subjected to four different heat treatments which were designed to obtain different combinations of relief from mechanical strains, recrystallization effects, and elimination of nonmetallic impurities through the action of hydrogen at high temperatures.

The results recorded in table 9 show that prolonged annealing at high temperatures, where recrystallization was complete and elimination of nonmetallic impurities by hydrogen probably occurred, produced better magnetic properties than were obtained from duplicate specimens which had received only a strain-relieving anneal at low temperatures. The beneficial effect of annealing at intermediate temperatures sometimes is neutralized by other factors, perhaps by structural differences, such as preferred orientation. There is no apparent relation between purity and permeability or coercive force.

The highest maximum permeability, 88,400, was obtained on a specimen of ingot 4 annealed at 1,450° C. This specimen had a coercive force of 0.045 oersted, a residual induction of 11,830 gausses and a hysteresis loss of 150 ergs per cubic centimeter per cycle, all for a B_{max} of 15,080 gausses.

TABLE 9—*Maximum permeability and coercive force of NBS high-purity iron (Cioffi)*

Heat treatment (in hydrogen)	Iron 4	Iron 12	Iron 14	Iron 18
Maximum permeability				
18 hours at 880° C	68,100	69,100	18,400	25,600
4 hours at 1,200° C 18 hours at 880° C	49,700	62,300	36,800	44,100
20 hours at 1,200° C 18 hours at 880° C	47,500	69,500	61,400	61,100
18 hours at 1,450° C 18 hours at 880° C	88,400	87,600	65,400	80,100
Coercive force (B_{max} about 15,500)				
	Oersted	*Oersted*	*Oersted*	*Oersted*
18 hours at 880° C	0.0946	0.0931	0.130	0.260
4 hours at 1,200° C 18 hours at 880° C	.094	.0961	.0961	.0946
20 hours at 1,200° C 18 hours at 880° C	.109	.0848	.0863	.080
18 hours at 1,450° C 18 hours at 880° C	.0450	.0526	.0481	.0535

A comparative evaluation of these results is impossible because these properties are properties of the specimen, not of the material, and are pronouncedly affected by factors such as the shape and size of the specimen, the previous thermal and mechanical treatment, the structure, including the size and orientation of the grains, and the condition under which the determination is made. Adcock and Bristow [4] reported values ranging from 14,360 to 31,400 for the maximum permeability and 0.115 to 0.271 oersted for the coercive force of their high-purity iron. The variation in magnetic properties

and the lack of correlation with purity were similar to those encountered in the present work. These properties of high-purity iron are superior to those of ordinary magnetic iron, which, according to Cioffi, has a maximum permeability of about 7,000 and a coercive force of about 1.0 oersted. However, the values for maximum permeability obtained from our high-purity iron and from that of Adcock and Bristow are far from being the highest that have been reported for iron. Maximum permeabilities in excess of 200,000 were obtained from thicker specimens of polycrystalline iron by Cioffi [33] and by Yensen and Ziegler [34]. Even higher values have been obtained from single crystals of iron—for example, Cioffi and Boothby [35] obtained a maximum permeability of 1,450,000 in the direction of the cubic axis of a single crystal of "hydrogen-purified" carbonyl iron.

The results obtained from the high-purity irons confirm the belief that such magnetic properties as permeability and coercivity are influenced by factors other than purity, and hence are not satisfactory criteria of purity in iron.

IX. SUMMARY

The results of the determinations of properties of the Bureau's high-purity iron (0.01-percent total of impurities) may be summarized as follows:

Density at 20° C	7.874 ±0.001 g/cm³.
Freezing point	1,539° ±1° C.
Ac_3 transformation	910° to 910.5° C.
Ar_3 transformation	about 8° C lower than Ac_3.
Coefficient of linear thermal expansion at 20° C	11. 7±0.2×10⁻⁶/° C.
Ultimate tensile strength, fully annealed condition	28,000 to 30,000 lb/in².
Yield strength, 0.2% offset	6,000 to 8,000 lb/in².
Reduction in area	more than 90%.
Vickers or Brinell hardness, fully annealed condition	49 ±3.
Modulus of elasticity	27.2 to 30.0×10⁶ lb/in².
Electrical resistivity at 20° C	9.71 ±0.01 microhm-cm.
Temperature coefficient of resistivity, $(R_{100}-R_0)/100R_0$	0.00651 ±0.00001.
Thermal electromotive force against NBS platinum standard Pt 27 at 0° and 100° C	1,980 ±3 microvolts.
Magnetic saturation induction	21.58 ±0.01 kilogausses.
Highest values obtained for maximum permeability	88,400.
Lowest value obtained for coercive force (B_{max}=15,080)	0.045 oersted.

The effect of variations in the amounts of individual or total impurities, within the range of composition of these ingots, was less than the experimental error of the determinations that were made. Variations in the composition of this high-purity material could not be correlated with variations in the results of any of these determinations.

The authors acknowledge their indebtedness to the many workers at the Bureau and elsewhere, as indicated in the text, who contributed to this determination of the properties of high-purity iron.

X. REFERENCES

[1] H. E. Cleaves and J. G. Thompson, The Metal—Iron (McGraw-Hill Book Company, New York, N. Y., 1935).
[2] H. E. Cleaves and J. G. Thompson, J. Research NBS **18,** 595 (1937) RP996.
[3] J. G. Thompson and H. E. Cleaves, J. Research NBS **23,** 163 (1939) RP1226.
[4] F. Adcock and C. A. Bristow, Proc. Royal Soc. (London)[A] **153,** 172(1935–36).
[5] F. K. Naumann, Tech. Mitt. Krupp **1,** 207 (1938).
[6] G. A. Ellinger and J. S. Acken, Trans. Am. Soc. Metals **27,** 382 (1939).
[7] G. F. Meyer, G. D. Rahrer, and J. R. Vilella, Metals & Alloys **13,** 424 (1941).
[8] W. C. Elmore, J. Applied Physics **10,** 724 (1939).
[9] Wm. F. Roeser and H. T. Wensel, J. Research NBS **26,** 273 (1941) RP1375.
[10] J. Chipman and S. Marshall, Temperature, Its Measurement and Control, p. 958 (Reinhold Publishing Corporation, New York, N. Y., 1941).
[11] C. Wells, R. A. Ackley, and R. F. Mehl, Trans. Am. Soc. Metals **24,** 46 (1936).
[12] H. Esser, J. Iron & Steel Inst. (London), Carnegie Schol. Mem. **25,** 213 (1936). Discussion, J. Iron Steel Inst. (London) **135,** 421 (1937).
[13] H. Esser and H. Eusterbrock, Arch. Eisenhüttenw. **14,** 341 (1941).
[14] S. D. Smith, Trans. Am. Soc. Metals **26,** 255 (1938).
[15] A. P. Wangsgard, Trans. Am. Soc. Metals (1941) (Preprint).
[16] H. Scott and J. R. Freeman, Jr., BS Sci. Papers **15,** 317 (1919–20) S348.
[17] J. B. Austin, Physics **3,** 240 (1932).
[18] B. A. Rogers and K. O. Stamm, Am. Inst. Min. Met. Engrs., Tech. Pub. No. 1388, Metals, Tech. (October 1941).
[19] W. Souder and P. Hidnert, BS Sci. Pap. **21,** 1 (1926–27) S524.
[20] F. C. Nix and D. MacNair, Phys. Rev. **60,** 597 (1941).
[21] J. B. Austin and R. H. Pierce, Jr., Trans. Am. Soc. Metals **22,** 447 (1934).
[22] G. E. Merritt, BS J. Research **10,** 59 (1933) RP515.
[23] J. B. Saunders, J. Research NBS **23,** 179 (1939) RP1227.
[24] Am. Soc. Testing Materials, Standards, pt. 1, Metals, p. 761 (1939).
[25] D. J. McAdam, Jr. and R. W. Mebs, NACA Tech. Report No. 670 (1939).
[26] A. R. Meyer, Verhandl. Deut. Physik. Ges. **13,** 680 (1911).
[27] L. Holborn, Ann. Physik [4], **59,** 145 (1919).
[28] R. L. Sanford and E. G. Bennett, J. Research NBS **26,** 1 (1941) RP1354.
[29] W. Steinhaus, A. Kussman, and E. Schoen, Physik. Z. **38,** 777 (1937).
[30] E. Gumlich, Wiss. Abhandl. physik. tech. Reichsanstalt **4,** 267 (1918).
[31] K. Honda and S. Kaya, Sci. Rept., Tohoku Imp. Univ., Sendai, [1] **15,** 721 (1926).
[32] P. Weiss and R. Forrer, Ann. Phys. **12,** 279 (1929).
[33] P. P. Cioffi, Phys. Rev. **45,** 742 (1934).
[34] T. D. Yensen and N. A. Ziegler, Trans. Am. Soc. Metals, **23,** 556 (1935).
[35] P. P. Cioffi and O. L. Boothby, Phys. Rev. **55,** 673 (1939).

WASHINGTON, February 5, 1942.

○